SCATTER, DIFFRACTION AND THE SPIKING PERIOD OF A RUBY LASER

THE EFFECTS OF SCATTER AND DIFFRACTION ON THE OSCILLATION PERIOD OF A RUBY LASER

By

JOHN PAUL VAN NEST, B.Sc.

A Thesis

Submitted to the Faculty of Graduate Studies

in Partial Fulfilment of the Requirements

for the Degree

Master of Science

McMaster University

May 1964

MASTER OF SCIENCE (1964) McMASTER UNIVERSITY
(Physics) Hamilton, Ontario.

TITLE: The Effect of Scatter and Diffraction on the Oscillation Period of a Ruby Laser

AUTHOR: John Paul Van Nest, B.Sc. (McMaster University)

SUPERVISOR: Dr. C. K. Campbell

NUMBER OF PAGES: vii, 142

SCOPE AND CONTENTS:

Following the introduction to the field of lasers and the theories of laser oscillations in the light output, it is pointed out that calculations involving existing theories yield oscillation periods in excess of the period observed for our crystal. To account for this disagreement, the thesis proposes the inclusion of the additional loss terms of scatter and diffraction, augmenting the transmission loss. The theory of Birnbaum, Stocker and Welles (BSW1) is extended to include these additional loss mechanisms and the oscillation period predicted, using the measured values of these parameters, is in good agreement with the observed oscillation period.

ACKNOWLEDGEMENTS

I take pleasure in this opportunity to acknowledge my indebtedness to my supervisor, Dr. C. K. Campbell, for his instruction, guidance and encouragement throughout the duration of this thesis project.

A further expression of thanks is extended to Mr. Derwyn Johnson, Mr. John Moss, and Mr. George Walmsley for many helpful discussions.

I am particularly grateful to Mr. Johnson for his introduction of experimental techniques to me and to Mr. Walmsley for his many improvements on the Vacuum Coating Unit.

Finally, I express my sincere appreciation to Mrs. T. C. Densmore for her many hours of untiring patience in the typing of this manuscript.

TABLE OF CONTENTS

CHAPTER I

A THEORETICAL INTRODUCTION TO THE THESIS

Section Number		Page Number
I	Interaction of Radiation and Matter	1
II	Optical Masers	5
1.1	Spontaneous Emission	6
1.2	Stimulated Emission	7
1.3	The Laser Cavity	8
1.4	Pumping Considerations	16
1.5	Laser Materials	18
1.6	The Ruby Laser	23
1.7	Dynamic Description of Maser Action	24
1.8	Transmission Losses	26
III	Maser Oscillation Theory	31
1.9	The Theory of Statz and deMars - 1960 (Sd1)	31
1.10	The Theory of Statz, Luck, Shafer, Ciftan - 1961 (SLSC1)	40
1.11	The Theory of Bostick, O'Connor - Feb. 1962 (BO1)	41
1.12	The Theory of Dunsmuir - 1961 (D1)	44
1.13	The Theory of Galanin, Leontovich, Sviridenkov and Chizhikova - 1962 (GLSC1)	48
1.14	The Theory of Birnbaum, Stocker and Welles - 1963 (BSW1)	49

CHAPTER II

COMMENTS ON THE THEORY

2.1	A Further Method of Deriving Maiman's Gain Equation	52
2.2	The Derivation of the Coupled Rate Equations of Statz and deMars (Sd1)	54
2.3	The Problem of the Period of Oscillation	55
2.4	Comments on the Stimulated Emission Probability Parameter B_s of Dunsmuir	58
2.5	Comments on the Stimulated Emission Probability Parameter b of Galanin et al.	60
2.6	A Derivation of the Revised Rate Equations of Birnbaum et al.	63
2.7	The Calculation of τ', the Effective Fluorescent Lifetime	66

TABLE OF CONTENTS (CONTINUED)

2.8	A Consideration of Scatter as a Loss Parameter	68
2.9	A Consideration of Diffraction as a Loss Parameter	72
2.10	The Modulation Period of a Ruby Laser	76

CHAPTER III

EXPERIMENTAL TECHNIQUES

3.1	Metallic Film Deposition	77
3.2	Reflectivity Measurements	81
3.3	Laser Crystal Holders	86
3.4	Temperature Control	90
3.5	Power Measurement	95
3.6	Detection of Laser Action	96
3.7	The Structure of the Laser Output	97
3.8	The Determination of Oscillation Threshold	102
3.9	Period Determination	113
3.10	Measurements of the Scatter Loss for Our Ruby Crystal	122
3.11	A Measurement of the Diffraction Loss	128

CHAPTER IV

CONCLUSIONS AND RECOMMENDATIONS

4.1	The Effect of Scatter and Diffraction on the Period Determination of our Ruby Crystal	131
4.2	Recommendations	137

REFERENCES 139

LIST OF ILLUSTRATIONS

Figure Number		Page Number
1.1	A Schematic Illustration of the Processes of Absorption, Fluorescent Emission and Stimulated Emission	4
1.2	Two Possible Standing Wave (Axial Mode) Patterns in a Laser Crystal	10
1.3	An Illustration of Several Cavity Resonances Within a Fluorescent Spectrum. Illustrated on One Cavity Resonance Are a Few High Order Spherical Modes	12
1.4	A Schematic Illustration of Successive Reflections of an Off-Axial Mode	14
1.5	Schematics Illustrating the Two-, Three-, and Four-Level Maser Systems	20
1.6	A Schematic Illustrating the Thermalizing of a Resonance Line. τ_4 Represents Spin-Lattice Relaxation to the Ground State	38
1.7	Computor Solutions to Dunsmuir's Rate Equations	47
2.1	A Definition of the Amplitude of an Electromagnetic Wave in a Laser Cavity of Reflectivity R_1, R_2	53
3.1	An Edwards 12E3 Vacuum Coating Unit	79
3.2	A Strong-Type Reflectometer	83
3.3	Reflectivity Versus Transmission for Silver, After Kuhn and Wilson (KW1)	87
3.4	A Triple-Jacket Crystal Holder	88
3.5	A Double-Jacket Crystal Holder	88
3.6	The Heater Used for Cooling the Laser Crystal	92
3.7	The Electrical Circuit Associated with the Heater	94
3.8	Format of the Experimental Conditions Associated with Each Photograph	98
3.9	Laser Action Close to Threshold	98
3.10a	Trace for the Laser Crystal Out of the Holder	99
3.10b	Trace with the Laser Crystal In the Holder	99
3.11	Laser Oscillations on Expanded and Normal Scales	101
3.12	Regular Spikes Close to Threshold	101
3.13	A Test of Reproducibility of Initial Time of Laser Action and of the Period	101
3.14	A Typical Spiking Pattern Well Above Threshold	103
3.15	Over-all Laser Action Well Above Threshold	103
3.16	Over-all Laser Action Close to Threshold	103

LIST OF ILLUSTRATIONS (CONTINUED)

3.17	An Illustration of the Difficulty in Measuring Thresholds at Low Temperatures	105
3.18	The First Plot of Threshold Versus Temperature	106
3.19	Laser Oscillation on an Expanded Scale with the Differentiating Circuit	108
3.20	An Improved Threshold Curve Obtained with the Aid of a Pulse Height Analyzer	110
3.21	A Threshold Curve for R_1=99.5% and R_2=98.7%	111
3.22	Theoretical Threshold Plots for Certain f values, After D'Haenens and Asawa	112
3.23	A Schematic of the Laser Detection System	114
3.24	A Threshold Curve Using a Beckman Universal Timer	115
3.25	A Plot of Period Versus Voltage Using the Beckman Universal Timer	117
3.26	The Output Between the Discriminator and the Counter	118
3.27	A Comparison of the Number of Laser Spikes and Those Counted by the Timer	120
3.28	A Comparison of the Laser Output and the Counter Input	120
3.29	Evidence of an Erroneous Period Determination as Calculated from the Timer	120
3.30	A Threshold Curve for R_1=99.3%, R_2=86.2%	121
3.31	A Typical Plot of the Period Versus the Power Above Threshold	123
3.32	A Typical Plot of the Period Versus the Temperature	123
3.33	The Traces from Which Scatter Can Be Measured (a) Noise (b) Crystal In the System (c) Crystal Out of the System	127
3.34	A Threshold Curve to Determine the Diffraction Loss: R_1=99.3%, R_2=99.2%, r_1=0.993	130
3.35	A Threshold Curve to Determine the Diffraction Loss: R_1=99.3%, R_2=80.4%, r_2=0.893	130
4.1	An Illustration of the Experimental Period for Our Ruby Laser 2% Above Threshold, r=0.925	133

CHAPTER I

THEORETICAL INTRODUCTION TO THE THESIS

I INTERACTION OF RADIATION AND MATTER

Laser is an acronym for light amplification by stimulated emission of radiation. The term optical maser is now striving for recognition in place of laser, so that one may then speak of maser properties, referring to both the microwave and optical regions of the spectrum. Maser, in this context, is an acronym for molecular amplification by stimulated emission of radiation. We shall use the terms laser and optical maser interchangeably, but the term "maser" will always refer to the above context.

The maser principle originated in 1916, but historically one must go back to 1900 when Max Planck renounced Classical physics in the assertion that energy is emitted by matter in quanta. With this assumption he was able to predict the experimentally observed frequency distribution for the energy density ρ_ν emitted from a "black body",

$$\rho_\nu = \frac{8\pi h\nu^3}{c^3} \frac{1}{\exp(h\nu/kT) - 1}, \qquad 1.1$$

where $\frac{8\pi\nu^2\delta\nu}{c^3}$ is the number of modes between ν and $\nu + \delta\nu$ per unit volume. In 1905, Einstein made a bold step in the assertion that light itself was made up of quanta, $h\nu$,

called photons. He used this hypothesis to predict correctly the photoelectric effect. The next important step was made by Bohr in 1913 in predicting the spectroscopically observed discreteness of the hydrogen atoms on the basis of Planck's quantum of action "h". Bohr proposed stationary states for electrons in an atom and asserted that energy transfers between states (known as atomic energy levels) could only occur as quantum jumps. Thus absorption of electromagnetic radiation by an atom may occur only for a frequency of radiation satisfying the condition

$$h\nu_{12} = |E_1 - E_2| , \qquad 1.2$$

where E_1, E_2 are two energy levels, the lower of the two being E_1. Similarly, emission of electromagnetic radiation may occur only at a discrete frequency given by

$$h\nu_{21} = E_2 - E_1 . \qquad 1.3$$

By quantizing the angular momentum, which is equivalent to asserting the existence of a stationary state, Bohr was able to predict the energy levels in the hydrogen atom and hence predict the discrete frequencies ν_{21} for the emission spectrum of hydrogen.

The picture then was that of an atom with discrete energy levels, all other energies being forbidden. For a system of atoms in a steady state condition, the population of each state, N_1 and N_2, is given by the Boltzmann distribution

$$\begin{aligned} N_1 &\propto \exp[-E_1/kT] \\ N_2 &\propto \exp[-E_2/kT] . \end{aligned} \qquad 1.4$$

Now Einstein, in 1916, combined this new concept of quantum jumps with the Classical concept of statistics to describe transitions; that is, he postulated that a probability was associated with each transition. For a transition up from level 1 to level 2 (an absorption) this probability varies with the radiation density ρ_ν at the transition frequency ν_{12} and the proportionality constant, known as Einstein's absorption coefficient, is B_{12}. Hence, the probability of one atom absorbing a photon of frequency ν_{12} is $B_{12}\rho_\nu$ per second. If there are N_1 atoms in the lower state 1, then the number of absorptions per second is $N_1 B_{12} \rho_\nu$. When considering transitions down from level 2 to level 1 (emission or de-excitation), Einstein had first to consider a term known experimentally as fluorescent emission. This term is independent of the electromagnetic radiation interacting with an atom; hence the probability of an atom emitting spontaneously in one second is given by a constant, denoted by A_{21}. The number of atoms then emitting spontaneously in one second is $N_2 A_{21}$. Einstein also found it necessary, as demonstrated below, to introduce another mode of de-excitation which is dependent upon the radiation density ρ_ν. This term is then called stimulated or induced emission; the number of atoms de-exciting by this mode per second is $N_2 B_{21} \rho_\nu$. These processes are schematically represented in figure 1.1. Einstein further enunciated the principle of detailed balance: electromagnetic energy has an equal probability of inducing emission

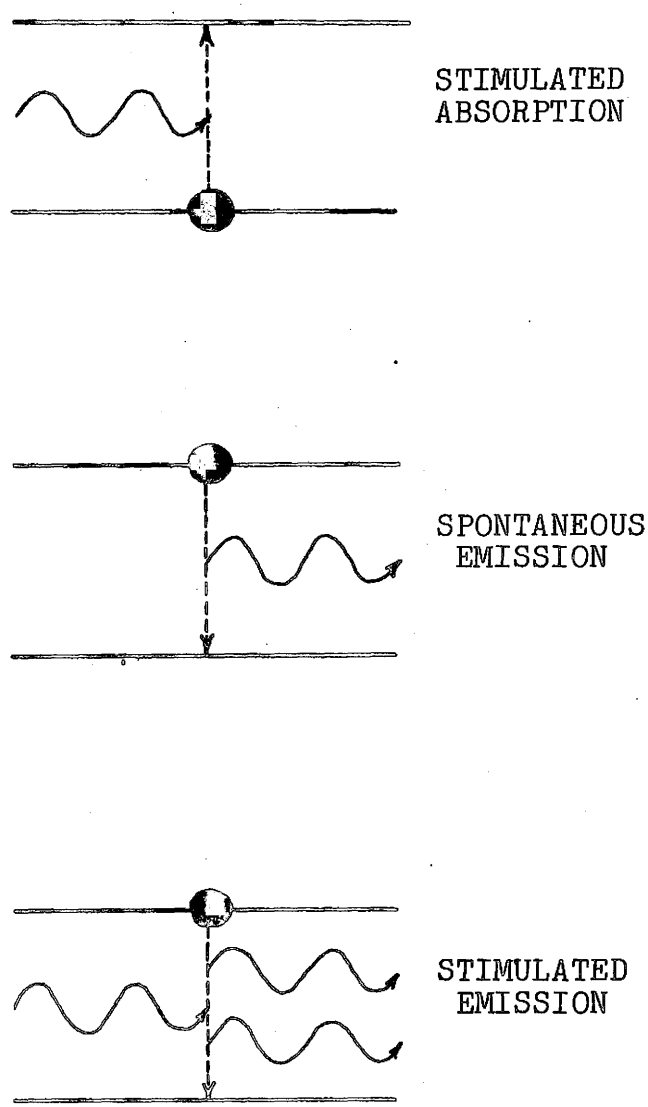

FIGURE 1.1

A SCHEMATIC ILLUSTRATION OF THE PROCESSES OF ABSORPTION, FLUORESCENT EMISSION AND STIMULATED EMISSION

and absorption. Therefore,

$$B_{12}\rho_\nu = B_{21}\rho_\nu$$

and

$$B_{12} = B_{21} \equiv B .$$

In equilibrium, matter may not gain any net energy from an electromagnetic field. Therefore, the number of upward transitions is equal to the number of downward transitions in one second and

$$N_1 B_{12}\rho_\nu = N_2 R_{21} + N_2 B_{21}\rho_\nu . \qquad 1.5$$

From equations 1.5 and 1.4 we have

$$\frac{N_2}{N_1} = \frac{B_{12}\rho_\nu}{R_{21} + B_{21}\rho_\nu} = \exp\left[-\frac{E_2 - E_1}{kT}\right] . \qquad 1.6$$

Further, from equation 1.2,

$$\frac{B\rho_\nu}{R + B\rho_\nu} = \exp\left[-\frac{h\nu}{kT}\right] . \qquad 1.7$$

Thus

$$\rho_\nu = \frac{R}{B}\,\frac{1}{\exp(+h\nu/kT) - 1} . \qquad 1.8$$

Comparing equations 1.1 and 1.8, one sees that the latter has the same form as Planck's radiation law; this was taken as justification of the term induced or stimulated emission introduced by Einstein. Hence,

$$\frac{R}{B} = \frac{8\pi h\nu^3}{c^3} . \qquad 1.9$$

II OPTICAL MASERS

Because of the technological and theoretical divergence

of infrared and optical masers from microwave masers, we shall bypass the development of microwave masers and begin with a discussion of the possibilities of masers at optical and infrared frequencies (ST1).

1.1 Spontaneous Emission:

As pointed out, the probability of spontaneous emission is independent of the radiation density. Further, spontaneously emitted photons are random in direction, and have a random phase relationship to one another since the time of emission is statistical. This term is represented by the Einstein coefficient A, which is the probability per second of an atom emitting a photon, but may also be represented by a characteristic time τ, called the spontaneous lifetime such that,

$$R = 1/\tau. \qquad 1.10$$

Directly associated with the finitude of τ is the linewidth of the excited energy level. The Uncertainty Principle gives the relationship

$$\Delta E \, \Delta t \geq \frac{\hbar}{2}, \qquad 1.11$$

where the energy of the excited atoms (those in level 2) has an uncertainty ΔE and where the time of emission of photons of energy E has an uncertainty Δt. Hence, associated with ΔE, there exists an uncertainty $\Delta \nu$ in the frequency of the spontaneously emitted photon. This gives rise to the natural linewidth of an excited energy level about a transition

frequency ν_{21}. In addition, other mechanisms responsible for line-broadening in solid state lasers are the interaction of vibrations with electronic levels (temperature broadening) and the effects of strains and defects. (L1)

It should be noted that when gases are considered, the effects of Doppler shift and collisions with other molecules and the walls must be included; the former broadens the linewidth directly, the latter may produce transitions to the lower state shortening the lifetime and, in this way, broadening the linewidth.

1.2 Stimulated Emission:

Now, consider stimulated emission. Let a photon of frequency ν_s within the resonance linewidth $\Delta\nu$ interact with an atom of energy, $h\nu_s$, above the ground state. This photon will stimulate the atom to emit a photon with the following properties:

1) its frequency is also ν_s,
2) its phase is the same as that of the stimulating photon,
3) its direction is the same as that of the stimulating photon.

Now consider an assembly of N excited atoms; place this system into a lossless cavity: one that will contain all of the electromagnetic energy. Let one atom de-excite spontaneously, liberating a photon at frequency ν_s. This

photon will interact with other atoms of energy E_s above the ground state, causing them to emit photons. The number of photons at frequency ν_s multiplies at the expense of excited atoms of energy E_s, leading one to expect that this emission would tend to "eat-a-hole" in the resonance spectrum. This is far from the case, particularly for the optical maser. There always exist relaxation processes within the resonance line which feed the energy level E_s. This thermalizing process is due to the influence of lattice vibrations and is of the order of 10^{-12} seconds. Therefore, Tang, Statz and deMars (TSd1) state that "it seems impossible to eat-a-hole into a temperature broadened line".

Thus, in the lossless cavity above, one really has the transition corresponding to E_s being fed by the rest of the resonance line, maintaining stimulated emission, and in addition, one has spontaneous emissions depleting the line. The resultant electromagnetic spectrum in the cavity is composed of a background spectrum over a frequency $\Delta\nu$ with a large peak at ν_s, representing the stimulated photons emitted.

1.3 The Laser Cavity:

Let us carry on to consider now a real (lossy) optical maser cavity. This was first discussed by Schawlow and Townes (ST1) in 1958. For the purposes of discussion, consider a cylindrical crystal of length ℓ with both end-

surfaces flat, parallel, and highly silvered. Note that for the microwave maser, it is possible to build a single mode cavity, the length of which is a small, integral number of wavelengths. Normal optical cavity resonators however, have physical dimensions which are very large compared to optical wavelengths and thus it is possible for many oscillation modes to be simultaneously excited. By the term mode or cavity resonance, one refers to a particular axial standing wave pattern; one differs from another by one more or one less node, so that each axial mode refers to a different wavelength and hence to a different frequency. (See figure 1.2.) The picture of a plane wave travelling the length of the crystal and reflected back and forth many times also has merits. For our purposes we will use the plane-wave approach or the standing-wave approach as merits greater understanding. This is also the case in the literature.

Consider therefore, a cavity which will support many axial modes, and in particular those modes whose frequencies are near the maser frequency ν_s. From the discussion of a resonant cavity, it follows that the wavelength of the axial modes is given by

$$n\lambda = 2l \qquad 1.12$$

for standing waves and "n" takes on integral values. Therefore, the frequency of the cavity resonances is given by

$$\nu = \frac{nv}{2l}, \qquad 1.13$$

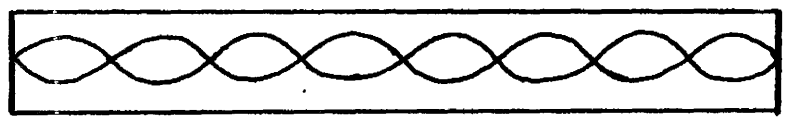

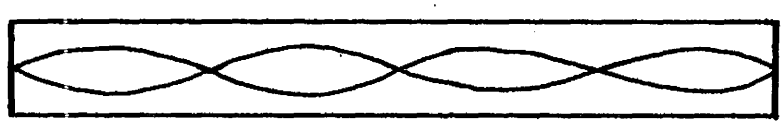

FIGURE 1.2

TWO POSSIBLE STANDING WAVE (AXIAL MODE) PATTERNS IN A LASER CRYSTAL

where "v" is the velocity of light in the cavity. For $\ell \approx 5$ centimeters, a typical value, the separation of cavity resonances (longitudinal modes) is

$$\frac{v}{2\ell} \approx 3 \times 10^9 \text{ cps} \approx 0.1 \text{ cm}^{-1}. \qquad 1.14$$

Thus a large number of longitudinal modes may be supported within a normal fluorescent linewidth. (See figure 1.3.) As the temperature is lowered, the fluorescent linewidth is decreased. Schawlow and Townes (ST1) state that for ruby at 300°K, $\Delta\nu$ is 11 cm^{-1} and at 77°K, $\Delta\nu$ is 0.2 cm^{-1}. Therefore the number of oscillating modes decreases and the threshold for each mode is more easily attained because more atoms are available for the excitation of a particular mode. In addition, there are many transverse or spherical modes at small intervals on the high frequency side of each longitudinal mode as illustrated in figure 1.3. These have been observed by Abella and Townes. (AT1)

The frequency of the cavity modes is "pulled" by the narrowing spectral line. Linear frequency pulling theory predicts that the oscillation frequency is determined by the linewidths of the cavity and fluorescent spectrum, $\Delta\nu_c$ and $\Delta\nu_m$ centred about frequencies ν_c and ν_m. Quantitatively,

$$\nu_{osc} = \frac{Q_c + Q_m}{Q_c/\nu_c + Q_m/\nu_m}, \qquad 1.15$$

where Q_c is the cavity quality factor,

Q_m is the fluorescence quality factor.

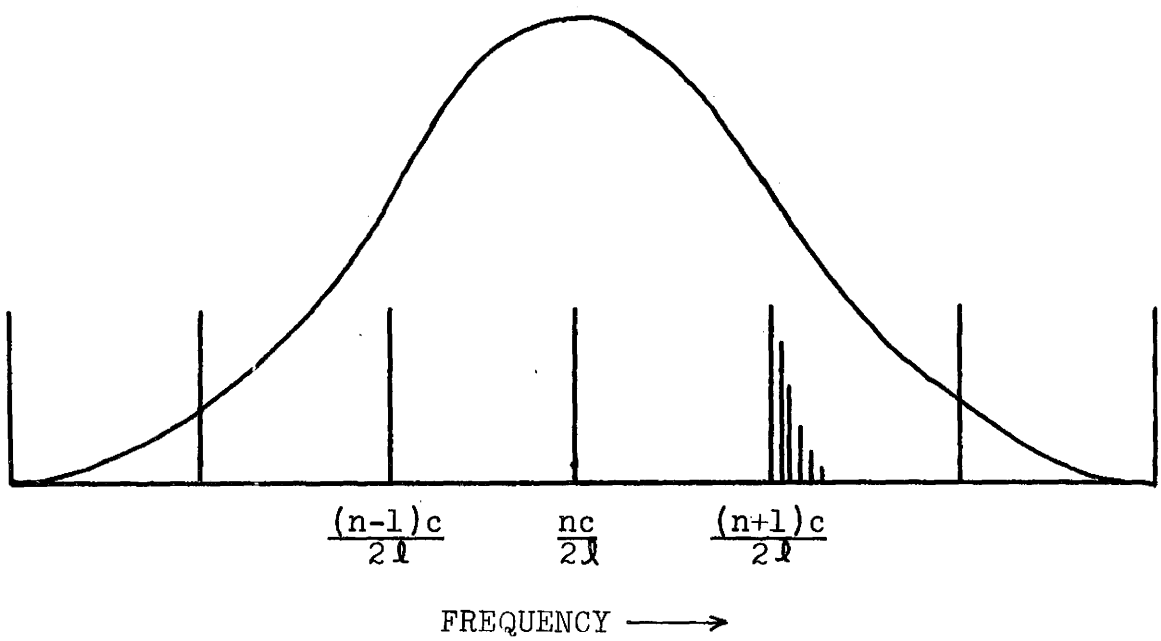

FIGURE 1.3

AN ILLUSTRATION OF SEVERAL CAVITY RESONANCES WITHIN A FLUORESCENT SPECTRUM. ILLUSTRATED ON ONE CAVITY RESONANCE ARE A FEW HIGH ORDER SPHERICAL MODES.

Q is defined as $\nu/\Delta\nu$. If the fluorescent spectrum is broad, $\Delta\nu_m$ is large. Hence Q_m is small and

$$\nu_{osc} \approx \frac{Q_c}{Q_c/\nu_c} = \nu_c . \qquad 1.16$$

But as the fluorescent spectrum narrows, ν_{osc} is pulled from ν_c towards ν_m. This theory applies to homogeneously broadened lines (temperature broadened), and hence may not apply to our own crystal, ruby, where broadening due to strain is reported to be quite effective (McM1); the fact still remains however, that the oscillation frequency is affected by the fluorescent linewidth. Furthermore, the onset of stimulated emission effectively reduces the linewidth from $\Delta\nu_m$, contributing to pulling the oscillation frequency.

From the preceding discussion, it is seen that the number of participating axial modes can be decreased by shortening the crystal and by lowering the temperature, reducing the fluorescent linewidth. However, there are many off-axial modes not yet considered, which must be discriminated against. This is, in part, done by the cavity. If a resonant cavity is to have a low loss (a high Q) in a particular mode, this propagating electromagnetic wave within the cavity must undergo many internal reflections. The modes then with the lowest loss are those propagating in an axial direction; with off-axial modes, such as illustrated in figure 1.4, the number of reflections within the cavity is

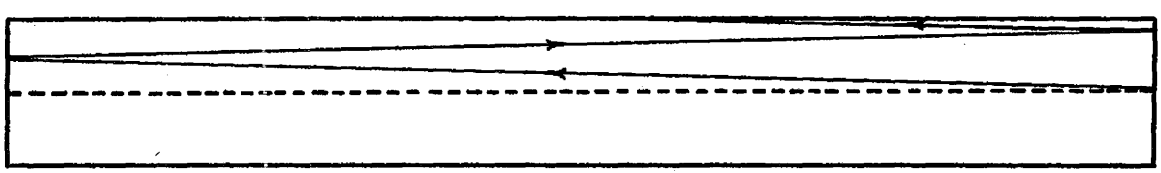

FIGURE 1.4

A SCHEMATIC ILLUSTRATION OF SUCCESSIVE REFLECTIONS OF AN OFF-AXIAL MODE.

greatly reduced. This factor makes these off-axial modes lossy (low Q) and hence sustaining oscillation in these modes is difficult. Diffraction, which occurs on every reflection, will tend to disperse even the axial waves, so that this effect further increases the losses of off-axial modes.

Now the optical cavity end-walls should not be totally reflecting if the stored electromagnetic energy is to be usefully employed. In practice one end is made as close to a 100% reflecting surface as possible, while the other end is made partially transmitting. The result is that some energy escapes from the cavity on every reflection. If R_1, R_2 are the reflection coefficients for both end-faces, the mean reflectivity of the cavity is given as

$$r = \sqrt{R_1 R_2}\,, \qquad 1.17$$

and the cavity loss per pass, L, as shown by Maiman (M2), is

$$L = \frac{1 - r}{\alpha_0 l}\,. \qquad 1.18$$

We shall return to these parameters in section 1.8.

From the above discussion, one can readily appreciate the stringent requirements of parallelism and flatness on the maser crystal end-faces. Standard requirements are parallelism to less than 6 seconds of arc and flatness to $\lambda/4$ with a highly polished surface.

1.4 Pumping Considerations:

Up to this point we have tacitly assumed a prepared system of N excited atoms. Let us now consider the means by which the system is prepared. An atom may be excited by an interaction with electromagnetic energy of frequency ν where the energy difference between the initial state and some excited state is $h\nu$. If this frequency is in the optical range, then one refers to this process of absorption of light by an atomic system as optical pumping.

One may adopt either of two approaches to optical pumping. Because only energy of $h\nu$ may be absorbed, one could attempt to pump a narrow spectral region extending over the frequency ν. Although this method would lead to a high spectral efficiency (the number of coherent photons produced for an energy input), limitations exist in the availability of sources with high powers within this narrow spectral region at the proper frequency ν. This approach is typified by the use of low pressure gas discharges.

The other approach utilizes sources with very high powers in a broad spectral region. The spectral efficiency is now quite low as much light energy is not absorbed by the atoms. Nevertheless, the amount of absorption achieved by these sources (high pressure gas discharges) is considerably greater than that achieved by the previous approach.

The requirement on the pump is in general rather demanding; it must supply enough intensity within the absorption

bandwidth so that more atoms are pumped into the upper level of the two lasing energy levels than are in the lower level. Once this situation, referred to as an inverted population, is established, the probability that a photon of energy $h\nu$ will interact with an atom in the upper state is greater than the probability that it will interact with an atom in the terminal state. This is the criterion for laser action, namely the system emits rather than absorbs energy. To be more precise, the rate of population of the upper level must be sufficient to offset the rate of loss of these excited atoms to lower states while maintaining simultaneously an inverted population. In many cases (see section 1.5), the terminal level of laser action is the ground state. Hence, the pump must excite more than one-half of the participating atoms into the upper level in order to produce an inverted population. This is a severe requirement.

The type of pump employed in this thesis was a General Electric Xenon FT-524 flashtube. This helical flashtube is clearly well suited for the cylindrical geometry of the laser crystal. The crystal is positioned coaxially with the flashtube and a cylindrical reflector enclosing the flashtube. Geometry is particularly important if one is to achieve a uniform energy density within the crystal. Obviously the pump need not itself be coherent; it simply prepares the system. Then, if a coherent wave is incident along the axis of the crystal, stimulated emission will ensue, the photons

travelling in phase along the axis; the incoming wave will be greatly amplified in the output, the input characteristics of phase and direction being preserved. This is the maser amplifier. Where the system is triggered by a spontaneous photon, the maser is a source of electromagnetic energy, oscillating at a frequency of $\sim 10^{14}$ cps. This is the maser oscillator.

1.5 Laser Materials:

Laser materials has been the subject of much recent intensive investigation in an effort to extend the frequencies that are possible with optical masers. Most optical masers operate at present in the near infrared and in the red range. As noted in equation 1.9, A/B increases as ν^3; hence, as one attempts to produce optical masers at higher and higher frequencies, the noise (spontaneous emission) increases. For this reason attempts to shorten the operating wavelength of a laser become more and more difficult.

The active atoms (participating atoms) are always diluted in a host crystal to minimize line-broadening due to the interaction of the participating atoms. Further, the host material should have a low thermal expansion coefficient. If the crystal expands with the heating due to the pump and thermal relaxations (phonon transitions), two adverse effects may result: the length of the cavity may change, inducing a shift in the longitudinal modes, and the strains produced

may also induce other modes to oscillate. The host material must also be transparent to the optical frequencies of the pump and the laser emission. It must be easily machined and polished and must be rigid. The crystalline fields should be low and the active material must not be allowed to migrate easily within the host lattice. As the thesis will exemplify, the crystal must have low strain and uniform qualities, and scattering centres (foreign particles, gaseous inclusions, or changes in refractive index) must be minimized.

The active material should have a long lifetime associated with the spontaneous decay from the upper state of the maser levels to the terminal state. One reason is that, for a long lifetime, the level is sharp, and hence, fewer longitudinal modes will be excited. Secondly, for a long lifetime the spontaneous decay rate is reduced and so the noise due to spontaneous emission will likewise be reduced. Coupled to these reasons is the fact that with reduced losses, threshold will be more easily attained.

Let us now consider the different sets of energy levels of the active material possible: the two-level maser, the three-level maser, and the four-level maser. Figure 1.5 illustrates the energy levels under consideration.

The two-level maser consists of a ground state and one excited state. If one is to use such a system as an amplifier, one must separate in space or time the pumping process and the amplifying process. Spatial separation is

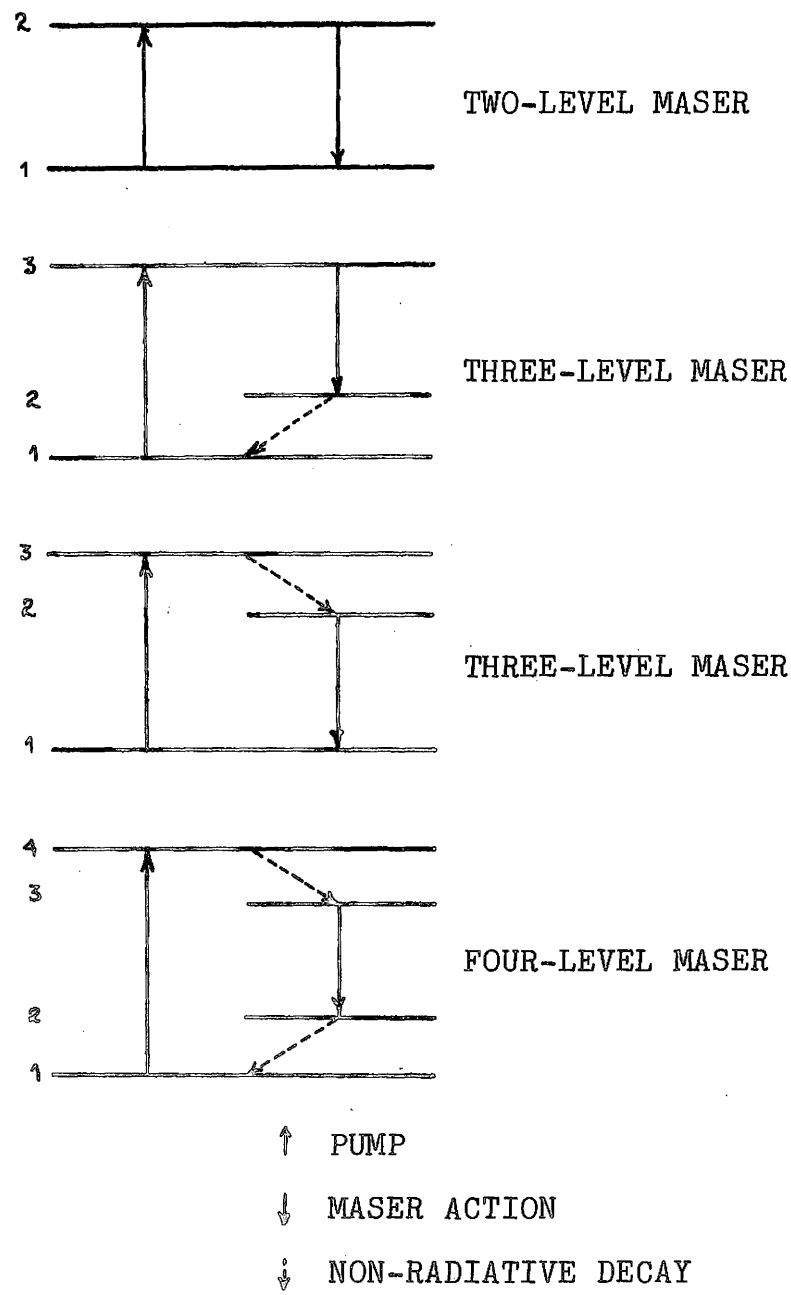

FIGURE 1.5

SCHEMATICS ILLUSTRATING THE TWO-, THREE-, AND FOUR-LEVEL MASER SYSTEMS

achieved by pumping the system outside of the maser cavity and then injecting it into the maser circuitry. Time separation refers to the same circuit pumping the system as that used to amplify the signal, leading to intermittent operation. Microwave masers employing spin-inversion are an example of a two-level system. On the other hand, the two-level optical maser is difficult on two accounts. If we pump at frequency ν , where

$$h\nu_{12} = |E_1 - E_2| \qquad 1.2$$

then our pump will also be stimulating emission because of the high energy density ρ_ν at ν , the maser frequency. Secondly much of the energy within the spectrum of the pump would not be used because only a narrow bandwidth of the pump (that within $\Delta\nu$) would be effective; on the other hand, we have already seen that it is desirable to have $\Delta\nu$ small. Hence a population inversion is difficult to achieve and maintain with a two-level system.

The three-level maser has a two-fold advantage over the two-level maser. Here the pumping is carried out between energy levels designated as 1 and 3. Then maser action may take place between levels 3 and 2 with a fast non-radiative decay from levels 2 to 1. Such a decay is a phonon-assisted decay where the energy is coupled to the lattice by a phonon. Hence, the time for the process is of the order of the lattice vibrations. The second alternative is for a fast non-radiative decay from 3 to 2 with maser action between levels 2 and 1.

Both have their advantages. In the former case, the terminal state (the lower of the maser levels - in this case, level 2) is empty, or nearly so, and so achieving a population inversion is not too difficult. Also the fast decay from level 2 to level 1 removes atoms from level 2 so that the population N_2 is always small, keeping the population inversion as large as possible. But if τ is to be long, level 3, the pumping level must be sharp, reducing the spectral efficiency. The latter case has the advantage that level 3 may be quite broad and hence lead to higher spectral efficiencies. Now level 2 may be sharp. The disadvantage of course is that one now has to pump more than half the atoms from the ground state 1 into level 3 and hence to level 2 so that a population inversion exists between levels 2 and 1.

The four-level maser combines the advantages of both three-level configurations. Here the pump operates between energy levels 1 and 4. Atoms in level 4 decay rapidly to level 3 by a phonon-assisted transition. Maser action takes place between levels 3 and 2 and a fast non-radiative transition to the ground state depopulates the terminal level - level 2. Here level 4 may be quite broad for efficient pumping and level 3 quite sharp for a long τ. Level 2 may be very nearly depopulated at steady-state so that a population inversion is easily achieved. Finally, atoms do not build up in the terminal state to decrease the population inversion. Materials exhibiting these properties are found

in the rare earth and actinide series of elements. Transitions occur between electronic levels of the inner electrons. These are shielded from any crystalline fields which are a source of line-broadening and so the levels are quite sharp. Further, the host material may now be heavily doped and dopings of 1% are standard for these materials.

1.6 The Ruby Laser:

The material first used in solid state optical masers was ruby, a three-level system with the ground state as the terminal state of the maser line. The host material for ruby is Al_2O_3. The Cr^{3+} ions substitutionally replace the Al^{3+} ions in the octahedral holes in the hexagonal close-packed structure of Al_2O_3. The pump band is a broad band in the green centred at ~ 5600Å, supplemented by another broad pump band at 4100Å. The former level is a $^4F_2$, the latter a $^4F_1$ level. A metastable level, designated ^2E, lies below these pump bands. The transition from the lower level of this doublet to the terminal level is referred to as the R_1 line (6943Å) and from the upper level the R_2 line (6929Å). These are both sharp transitions to the ground state $^4A_2$. Decay from level 2 has been shown to be about 4.3 milliseconds at $77^{\circ}K$ and further, this radiative lifetime gives an absorption coefficient of 11 cm^{-1} in good agreement with a direct measurement of this parameter. Therefore, one can say that this lifetime of 4.3 milliseconds is predominantly radiative,

that is, due to spontaneous emission (M1). If S_{ji} is the decay rate from level j to i per unit time (including both radiative and non-radiative transitions), then here $S_{21} \approx A_{21}$, the Einstein coefficient for spontaneous (radiative) emission and thermal modes play a minor role in this transition. Maiman (M1) has shown further that $S_{32} \approx 2 \times 10^{7}$ sec $^{-1}$ is predominantly non-radiative. This decay time is $\tilde{\tau}_{32} \approx 0.05 \times 10^{-6}$ seconds which is very fast compared to the spontaneous decay from level 2 to 1, $\tilde{\tau} = 4.3$ milliseconds. S_{32} is also shown to be much larger than S_{31} since the fluorescent efficiency, the ratio of the number of fluorescent quanta emitted to the number of pump photons absorbed, is close to 1. Thus, by far the majority of excited atoms decay to the ground state through level 2 as compared to the number decaying directly to 1 from 3.

1.7 Dynamic Description of Maser Action:

Recalling the processes of absorption, spontaneous emission and stimulated emission, one may set up equations governing the populations of energy levels 1, 2 and 3 for ruby, where N_1, N_2 and N_3 are the number of Cr^{3+} ions in states 1, 2 and 3. Thus

$$\begin{aligned} \frac{dN_3}{dt} &= W_{13} N_1 - (S_{31} + W_{31} + S_{32}) N_3 , \\ \frac{dN_2}{dt} &= S_{32} N_3 + W_{12} N_1 - (S_{21} + W_{21}) N_2 , \\ N_0 &= N_1 + N_2 + N_3 , \end{aligned} \qquad 1.19$$

where W_{ij} is the probability per second of absorption of energy inducing a transition from level i to level j,

S_{ji} is the probability per second of a transition (radiative or non-radiative) from level j to level i.

From the discussion for ruby (section 1.6), the following assumptions are valid:

1) S_{31}, W_{31} are very small compared to S_{32},
2) S_{21} is purely radiative $\approx A_{21}$,
3) the energy separations of levels 2 and 3 are large so that at equilibrium, the Boltzmann distribution gives $N_2 = N_3 = 0$.

Assumption (3) is certainly valid for ruby where, for example, λ is 7×10^{-5} centimeters, T is about $300^{\circ}K$:

$$\frac{N_2}{N_1} = \exp\left[-\frac{h\nu}{kT}\right] = \exp(-68) = 0 . \qquad 1.20$$

Solving equation 1.19 one gets

$$\frac{N_2}{N_1} = \frac{W_{13}\left(\frac{S_{32}}{W_{31} + S_{31} + S_{32}}\right) + W_{12}}{A_{21} + W_{21}} \qquad 1.21$$

$$\approx \frac{W_{13} + W_{12}}{A_{21} + W_{21}} . \qquad 1.22$$

Then

$$N_2 = \frac{W_{13} + W_{12}}{A_{21} + W_{21}} (N_0 - N_2) . \qquad 1.23$$

This assumes S_{32} is so large that the population N_3 is very

small at any instant, that is $N_3 \ll N_1, N_2$.

Therefore

$$\frac{N_2}{N_0} = \frac{W_{13} + W_{21}}{A_{21} + W_{21} + W_{31} + W_{12}} . \qquad 1.24$$

Similarly

$$\frac{N_1}{N_0} = \frac{A_{21} + W_{21}}{A_{21} + W_{21} + W_{13} + W_{12}} . \qquad 1.25$$

Therefore,

$$\frac{N_2 - N_1}{N_0} = \frac{W_{13} - A_{21}}{A_{21} + W_{13} + 2W_{12}} \qquad 1.26$$

assuming $W_{12} = W_{21}$. For laser action to occur, we have already shown (section 1.4) that N_2 must be greater than N_1, so that

$$W_{13} > A_{21} .$$

In fact, we must also consider losses in setting up such a criterion for oscillation:

$$W_{13} > A_{21} + \text{losses} .$$

1.8 Transmission Losses:

Let us designate the absorption coefficient as $\alpha\ cm^{-1}$ Hence, an electromagnetic wave propagating along a laser crystal axis is attenuated by a factor

$$\exp(-\alpha l) . \qquad 1.27$$

The value of α will depend in general upon the number of atoms in the ground state i, N_i, and the number in an excited state j, N_j, where α refers to the transition $i \rightarrow j$, α_{ij}. The

absorption coefficient is then

$$\alpha_{ij} = (N_i - N_j)\,\sigma_{ij}, \qquad 1.28$$

where σ_{ij} is the cross-section for absorption $i \rightarrow j$. If $N_j > N_i$, α_{ij} is negative, and rather than absorption, amplification occurs according to

$$\exp(+|\alpha_{ij}|\,l). \qquad 1.29$$

This is called negative absorption. To achieve a high degree of amplification l must be long. The same effective l may be obtained using a shorter crystal with highly reflecting end-plates. Thus on each pass plus reflection, the amplitude of the electromagnetic wave is changed by $\exp(-\alpha l)r$ where r is the mean reflection coefficient. The term $\exp(-\alpha l)$ is associated with a gain while r is associated with a loss. We, therefore, require for coherent oscillation

$$\exp(-\alpha l)\,r \simeq 1. \qquad 1.30$$

For $-\alpha l \ll 1$, as is usually the case, $(1 + \alpha l) \simeq r$ or

$$-\alpha l \simeq 1 - r. \qquad 1.31$$

Then, from equation 1.28,

$$N_2 - N_1 = \frac{1 - r}{\sigma_{12} l}. \qquad 1.32$$

σ_{12}, if measured at low powers, is given by

$$\sigma_{12} = \alpha_0 / N_0, \qquad 1.33$$

where α_0 is this absorption coefficient measured at low powers. Then equation 1.32 becomes

$$\frac{N_2 - N_1}{N_0} = \frac{1 - r}{\alpha_0 \ell} . \qquad 1.34$$

Now since, for maser action to take place, $N_2 \geq N_1$, then $N_1 / N_0 \approx \frac{1}{2}$ and equation 1.34 becomes

$$\frac{N_2}{N_0} = \frac{N_1}{N_0} + \frac{1 - r}{\alpha_0 \ell}$$

$$\approx \frac{N_1}{N_0} + 2 \frac{N_1}{N_0} \frac{1 - r}{\alpha_0 \ell} ,$$

or

$$\frac{N_2}{N_1} \approx 1 + 2 \frac{1 - r}{\alpha_0 \ell} , \qquad 1.35$$

which agrees with Maiman's result (M2). This result states that an equal number of atoms in the upper state as in the lower state is not sufficient to maintain laser oscillation. An additional number are required to overcome this loss term of

$$\frac{2 (1 - r)}{\alpha_0 \ell} .$$

Let us now introduce the concept of the Q of a cavity. Cavity Q is defined by

$$Q = \frac{\omega W}{P} , \qquad 1.36$$

where ω is the angular frequency at which the energy is stored in the cavity,

W is the stored energy in the cavity per unit time,

P is the energy lost from the cavity per unit time.

This equation shows that for small losses in the cavity, Q is high.

For an isolated cavity, the energy decays according to

$$P \equiv -\frac{dW}{dt} = \frac{\omega W}{Q}, \qquad 1.37$$

and

$$W = \exp\left(-\frac{\omega t}{Q}\right). \qquad 1.38$$

Define $$Q = \omega \tau, \qquad 1.39$$

where τ is the decay time constant of energy in the cavity. Hence,

$$W = \exp\left[-\frac{t}{\tau}\right]. \qquad 1.40$$

For an unloaded cavity (no external losses), then the total cavity Q is defined as

$$\frac{1}{Q_T} = \frac{1}{Q_0}. \qquad 1.41$$

For a loaded cavity, where Q_c represents the coupling of energy to an external system, total Q is given by

$$\frac{1}{Q_T} = \frac{1}{Q_0} + \frac{1}{Q_c}. \qquad 1.42$$

For a material in the cavity, Q_m represents the energy of the cavity coupled to the material. Therefore, for normal absorption, Q_m is positive and

$$\frac{1}{Q_T} = \frac{1}{Q_0} + \frac{1}{Q_c} + \frac{1}{Q_m}. \qquad 1.43$$

However for a population inversion in the material, the material feeds energy into the cavity and Q_m is negative.

$$\frac{1}{Q_T} = \frac{1}{Q_o} + \frac{1}{Q_c} - \frac{1}{|Q_m|}. \qquad 1.44$$

For oscillation, therefore

$$\frac{1}{|Q_m|} \geq \frac{1}{Q_o} + \frac{1}{Q_c}. \qquad 1.45$$

For amplification, Q_m must be larger and the requirement is

$$\frac{1}{|Q_m|} \geq \frac{1}{Q_o}. \qquad 1.46$$

With this introduction to cavity Q, we can now derive the oscillation condition in another fashion. The rate of loss of energy in a cavity of length l, where the only loss mechanism is an external coupling loss through the partially transmitting end-walls, is

$$\beta = \frac{v}{l}(1-r), \qquad 1.47$$

where v is the velocity of light along the axis of the crystal and is given by

$$v = c/\sqrt{\varepsilon}, \qquad 1.48$$

Here c is the velocity of light in a vacuum and ε is the dielectric constant of the medium. The characteristic time associated with this loss is then defined as

$$\tau = \frac{l\sqrt{\varepsilon}}{c(1-r)}. \qquad 1.49$$

Therefore

$$Q_c = \omega\tau = \frac{2\pi}{\lambda}\,\frac{\ell\sqrt{\varepsilon}}{\phi(1-r)}. \qquad 1.50$$

The material Q is given as (M2)

$$Q_m = \frac{2\pi\sqrt{\varepsilon}}{\lambda\alpha}. \qquad 1.51$$

Therefore for oscillation to just begin,

$$\frac{-1}{|Q_m|} = \frac{1}{Q_c}, \qquad 1.52$$

which yields on substitution

$$-\alpha\ell = 1 - r. \qquad 1.31$$

III MASER OSCILLATION THEORY

For optical masers the light output from a pulsed ruby laser is typically an oscillation phenomenon. The period of this oscillation, henceforth denoted as the modulation period T_M is typically of the order of five microseconds. It is the main concern of this thesis to predict this period obtained experimentally.

1.9 The Theory of Statz and deMars - 1960 (Sd1):

The first quantitative attempt to explain these oscillations in microwave masers was made by Statz and deMars. A brief discussion of microwave masers will be necessary to understand the terminology used in these equations.

Under a magnetic field, electron spin degeneracy is removed so that an electron with its spin up may be in a higher energy state than that with its spin down. Hence, an atom with an unpaired electron may have a resultant spin (corresponding to a ground state or an excited state) of $\pm\frac{1}{2}$. Atoms with two valence electrons may have spins of 1, 0 or -1 depending on the relative orientation of each electron spin. The frequency corresponding to the energy gap between such levels is typically in the microwave region. If a population inversion can then be produced between two spin energy levels, then maser action is possible. With a spin $\frac{1}{2}$ material, a two-level maser is possible; with a spin 1 material, a three-level maser is possible.

The mode of spontaneous emission at microwave frequencies has a low probability of occurence. On the other hand, the probability of other modes of relaxation is considerably higher. Spin-lattice relaxation refers to the energy lost by the spin system to the normal vibrational modes of a crystal lattice in an attempt to equalize the energies associated with each. The time associated with this de-excitation is designated τ_4. The spin-spin relaxation acts to destroy the internal coherence of the emitted energy without changing the energy of the spins. This occurs through the interaction of spins; each spin may be likened to a bar magnet, precessing about a magnetic field H. M_1, the magnetic dipole moment of one, may be resolved into a DC

component and an oscillating component, the latter rotating at the Larmour frequency ω_L. M_2 may be likewise resolved. The DC component of M_2 produces an effective DC field at M_1, altering ω_L. If this altered frequency is close to the frequency of the oscillating component of M_2 at M_1, a transition may be induced. This mode of de-excitation broadens the linewidth and the time associated with this mode is designated $\tilde{\tau}_s$. The effect of crystalline electric fields produces an effective electric field on the electrons which may shift the spin energy levels by differing amounts, further broadening the linewidth. (V1)

Of concern also are transitions within a resonance line. As mentioned in section 1.2 for optical masers, lattice vibrations are responsible for "thermalizing" the resonance lines. However, in the microwave case, the predominant process is that of cross-relaxation, propounded by Bloembergen, Shapiro, Phersan, and Artmann (BSPA1). This is a "flip-flop" phenomenon where the spins "flip" from the excited to the ground state and "flop" back up to the excited state "almost instantaneously". Energy in this process is "nearly conserved", and hence, the spin state is essentially mobile throughout the linewidth. This process tends to maintain the line shape so that if N_s, the number of spins at the maser frequency, is depleted faster than other portions of the linewidth, this narrow region will tend to be fed by the rest of the line.

Statz and deMars developed phenomenological rate

equations for maser action:

$$\frac{dP}{dt} = -\frac{\omega P}{Q_L} \qquad 1.53$$

$$\frac{1}{Q_L} = \frac{1}{Q_0} + \frac{1}{Q_e} - Cn \triangleq \frac{1}{Q} - Cn \qquad 1.54$$

$$\frac{dn}{dt} = -\frac{n - n_1}{\tau_L} - DnP, \qquad 1.55$$

where P is the energy stored in the cavity at the maser frequency,

Q_L is the quality factor of the cavity,

n is the population inversion of participating atoms,

Q_0 includes the wall losses and dielectric absorption in the active material,

τ_L is the spin-lattice relaxation time,

Q_e is associated with the electromagnetic energy losses coupled outside the cavity,

n_1 is the equilibrium population inversion with the the pump on,

D is the proportionality constant determining the rate at which spins are inverted by the cavity energy P.

Equation 1.53 is essentially that stated previously (equation 1.37) for an isolated cavity. Equation 1.54 states the dependence of the cavity Q on the different loss mechanisms, and on the population inversion term which supplies energy to the cavity. Equation 1.55 describes the change in the population inversion with time. The first term represents

the spontaneous decay of excited atoms; the second represents the loss of excited atoms due to stimulated emission.

These equations 1.53 - 1.55 may be rewritten as two coupled equations in terms of the normalized parameters π and η such that.

$$\frac{d\pi}{dT} = \frac{1}{Q}\,\pi(\eta - 1) \qquad 1.56$$

$$\frac{d\eta}{dT} = -\frac{\eta - \alpha}{\tau_0} + \frac{1-\alpha}{\tau_0}\,\eta\pi, \qquad 1.57$$

where $\pi = \frac{P}{P_0}$, $\eta = \frac{n}{n_0}$, $\tau_0 = \omega\tau$, $T = \omega t$, $\alpha = \frac{n_1}{n_0}$,

and P_0 is the steady state energy, stored in a cavity under normal oscillation conditions. n_0 is the amount of level inversion required to overcome the losses associated with Q^{-1}. These equations are verified in Chapter II.

Statz and deMars then discuss how maser oscillations may arise from these equations. η increases with the pump intensity, and when $\eta = 1$, the population inversion term n just balances the term n_0. At this point the maser becomes unstable and as η increases above 1, $\frac{d\pi}{dT}$ becomes positive. Hence, emission of electromagnetic energy predominates over absorption and π increases. Now we have two competing processes: η is being augmented by the pump but simultaneously, stimulated emission is depleting the upper level.

The latter process predominates as π increases above

1 and the maser levels saturate, $\eta = 1$. At this point, the electromagnetic energy in the cavity, π , is a maximum. As η is decreased below 1, more energy is absorbed than emitted and π is reduced. π continues to decrease until "inverted spins" (those in the excited state) are produced faster by the pump than downward transitions are produced by π . Then η commences to increase again and the cycle is complete. Furthermore, this cycle will repeat itself just as long as the pump power is sufficient to invert the population, that is, produce an $\eta > 1$.

From this discussion, one can understand the effect of the parameters Q, T_o and α on T_M. If the Q of the cavity is small, then the electromagnetic energy in the cavity decays rapidly according to equation 1.38. Furthermore, if T_o, the time constant governing the recovery of the population inversion η , is large then the buildup to $\eta > 1$ is slow. Finally, if α is small, η also builds up slowly to a value in excess of 1. Hence, a large value of Q and T_o and a small value of α tend to produce a long period T_M.

Now consider the results in light of experiment. A period in agreement with experiment can be obtained by the proper choice of parameters, but are these parameters realiztic? A large value of Q ($\approx 10^5$) is quoted for the maser oscillator. If the maser oscillations or spikes are to be damped in amplitude, π must not decay into the noise level before η rises through the value 1. To ensure this, the

cavity Q must be large. Damped spikes are commonly observed in maser oscillations. Secondly, a value of 10^7 for T_o gives τ = 1.2 milliseconds for a maser frequency of 1.3 kilomega-cycles per second. The experimentally determined τ is 2.5 x 10^{-2} seconds. Therefore, T_o must be larger than 10^7 and the resultant longer rise-time leads to an even larger value of Q required for damping. Thirdly, the value of 10 for α was thought to be too large. With all these considerations, a revamping of the processes was needed.

The above problem was resolved by assuming the process of cross-relaxation as supplying spins at the maser frequency. Consider the resonance line divided into two regions:

1) spins not at the maser level - large system,

2) spins at the maser level - small system.

The oscillation pulse tends to "eat-a-hole" in the resonance line at the maser transition, and so the large system feeds the small system in an attempt to re-establish the resonance line-shape. This supply of inverted spins at the maser level increases η faster, reducing the need for a large Q. (See figure 1.6).

With this process in mind, we reformulate the equations 1.53, 1.54 and 1.55. The first two are unchanged:

$$\frac{dP}{dt} = -\frac{\omega P}{Q_L} \qquad 1.53$$

$$\frac{1}{Q_L} = \frac{1}{Q_o} + \frac{1}{Q_e} - C\eta . \qquad 1.54$$

Let S be the number of participating spins in the large

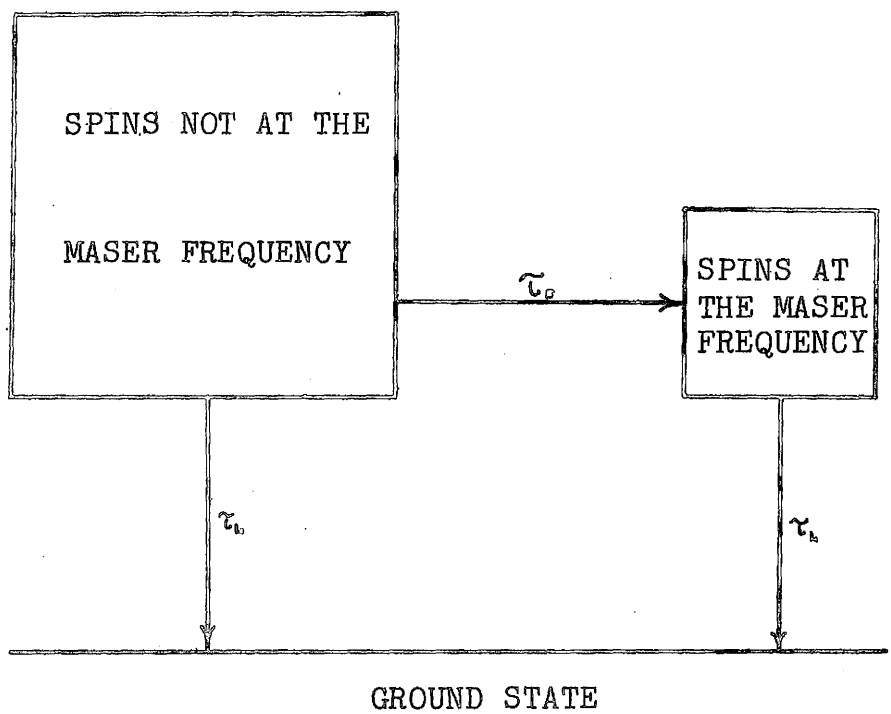

FIGURE 1.6

A SCHEMATIC ILLUSTRATING THE THERMALIZING OF A RESONANCE LINE. τ_L REPRESENTS SPIN-LATTICE RELAXATION TO THE GROUND STATE.

system,

S_1 be the number of participating spins in the small system,

n be the number of inverted spins in the small system,

N be the number of inverted spins in the large system.

For equal "spin temperatures",

$$\frac{n}{S_1} = \frac{N}{S},$$

$$n_{eq} = \frac{S_1}{S} N. \qquad 1.58$$

Therefore, the change in "n" with time is given by

$$\frac{dn}{dt} = -\frac{n - S_1/S\, N}{\tau_s} - D n P, \qquad 1.59$$

where τ_s is in particular the time constant associated with cross-relaxation. Note that

$$n < n_{eq} = S_1/S\, N.$$

Because of this "hole-eating" process, this first term is positive and represents a supply of "n" by the cross-relaxation process. The change in "N" with time is given by

$$\frac{dN}{dt} = -\frac{N - N_2}{\tau_L} + \frac{n - S_1/S\, N}{\tau_s}. \qquad 1.60$$

The first term represents spin-lattice relaxation to the lower level where N_2 is the equilibrium value for the large system. The second term represents the loss of spins to the small system by cross-relaxation. The solution of equations 1.53, 1.54, 1.59, 1.60 gives a period of several milliseconds for a $Q \sim 10^3$ which is in much better agreement with experiment.

1.10 The Theory of Statz, Luck, Shafer, Ciftan - 1961 (SLSC1):

These authors extend the equations of Statz and deMars (Sd1) to the optical maser case. Solutions are obtained by linearizing the equations about the steady state values of $\eta = \pi = 1$; that is, one substitutes $\eta = 1 + \Delta\eta$ and $\pi = 1 + \Delta\pi$:

$$\frac{d\Delta\pi}{dT} = \frac{1}{Q}(1+\Delta\pi)(1+\Delta\eta-1)$$
$$\approx \frac{1}{Q}\Delta\eta, \qquad 1.61$$

assuming $\Delta\pi \ll 1$;

and

$$\frac{d\Delta\eta}{dT} = -\frac{1+\Delta\eta-\alpha}{T_0} + \frac{1-\alpha}{T_0}(1+\Delta\pi)(1+\Delta\eta)$$
$$= -\frac{\Delta\eta}{T_0} + \frac{1-\alpha}{T_0}\left(1-1+\Delta\pi+\Delta\eta\right)$$
$$= -\frac{\Delta\eta}{T_0} + \frac{1-\alpha}{T_0}(\Delta\pi+\Delta\eta), \qquad 1.62$$

assuming $\Delta\pi\,\Delta\eta \ll \Delta\pi$ or $\Delta\eta$.

The solutions to these equations are of the form

$$\left.\begin{matrix}\Delta\pi \\ \Delta\eta\end{matrix}\right\} \propto \exp \beta T, \qquad 1.63$$

where

$$\beta = -\frac{\alpha}{2T_0} \pm \frac{1}{2}\left[\left(\frac{\alpha}{T_0}\right)^2 - \frac{4}{Q}\frac{\alpha-1}{T_0}\right]^{1/2} \qquad 1.64$$
$$\approx -\frac{\alpha}{2T_0} \pm i\left(\frac{\alpha-1}{QT_0}\right)^{1/2}, \qquad 1.65$$

assuming

$$\frac{\alpha^2}{T_0^2} \ll \frac{4}{Q}\frac{\alpha-1}{T_0}. \qquad 1.66$$

For values of $\alpha \sim 2$,

$t_0 = 5 \times 10^{-3}$ seconds,

$Q \sim 10^7$ for an optical cavity,

the predicted value of T_M is 25 microseconds. This is to be

compared with an experimental period T_M of 4.6 microseconds on the average, close to threshold.

Statz et al. attributed this discrepancy to the effects of multimode oscillations within the cavity, whereas their theory applied only to a single oscillation mode. In this respect, suppose that when the laser is pumped, the energy density is a maximum in the central region. Then, if this region is the first to attain oscillation, it will be depopulated and laser action will cease. But it is possible that now the energy density in an outer area is sufficient to make this outer area oscillate providing another light pulsation or "spike" in the output from the crystal. Spikes, thus derived, would considerably shorten the period from the predicted value above. Such multimode effects could be detected by exploring the laser end-face with a lucite light-pipe probe. Studies of the light output from various regions showed that spikes from different areas were different in amplitude; from this Statz et al. concluded that spikes from different areas of the laser were composed of different sets of modes.

1.11 The Theory of Bostick, O'Connor - Feb. 1962 (BO1):

We next turn to a theory which, along with that of Kaiser, Garrett, and Wood (KGW1), was the first enunciated in terms of readily observable parameters. The equations of Bostick and O'Connor (BO1) describe an optical cavity for a

four-level system or a system satisfying these conditions:

1) cavity losses are small (Q_L large),

2) the density of the atoms in the ground state is fixed,

3) the terminal state is empty.

Thus these rate equations which are satisfactory from a phenomenological viewpoint, may be written as

$$\dot{n} = bP - \frac{n}{\tau} - \frac{n \alpha N}{\tau} \qquad 1.67$$

$$\dot{N} = \frac{\alpha n N}{\tau} - \beta N , \qquad 1.68$$

where n is the total number of pumped ions,

N is the total number of coherent photons in the cavity.

In equation 1.67,

bP represents the rate of optical ion pumping,

n/τ represents the rate of spontaneous emission,

$\frac{\alpha n N}{\tau}$ represents the rate of stimulated emission,

In equation 1.68,

$\frac{\alpha n N}{\tau}$ represents the rate of emission of coherent photons by stimulated emission,

βN represents the rate of loss of coherent photons from the cavity.

Let the critical population of the excited states at oscillation threshold be n_o. At this threshold, therefore, $\dot{N} = 0$ so that

$$n_o = \beta \tau / \alpha . \qquad 1.69$$

To evaluate the pump power P_o at oscillation threshold, assume that the system is in equilibrium ($\dot{n} = o$) and that oscillation has not yet begun; thus equation 1.67 reduces to

$$bP_o = \frac{n_o}{\tau}, \qquad 1.70$$

or

$$P_o = n_o/b\tau. \qquad 1.71$$

Assume now that the pump power P has a value slightly above threshold such that the system is in oscillation. If we consider that an equilibrium condition exists, under the stimulus of N_o coherent photons ($\dot{n} = o$) and further, if we assume that the new equilibrium population distribution is close to the threshold distribution n_o, we have for steady state

$$o = bP - \frac{n_o}{\tau}(1 + \alpha N_o), \qquad 1.72$$

substituting for n_o and b from equations 1.69 and 1.70, one obtains

$$N_o = \frac{1}{\alpha}\left(\frac{P}{P_o} - 1\right). \qquad 1.73$$

Therefore, to linearize the solutions, set

$$n = n_o + \Delta n \quad \text{and} \quad N = N_o + \Delta N.$$

The resulting equations can be solved for ΔN of the form

$$\Delta N \approx \exp\left[\frac{-t}{T} \pm i\omega t\right], \qquad 1.74$$

where

$$T^{-1} = \frac{P}{2P_o\tau} \qquad 1.75$$

is a damping term and where

$$\omega = \left[\left(\frac{P}{P_o} - 1\right)\frac{\beta}{\tau}\right]^{1/2} \qquad 1.76$$

is an oscillatory term. The threshold density n_o is attained when

$$\frac{P}{P_o}\left[1 - \exp\left(-\frac{t}{\tau}\right)\right] = 1. \qquad 1.77$$

This equation relates the initial time of laser action "t" to the ratio P/P_o. Note that the losses here are due solely to the transmission losses at the end surfaces of the laser crystal and are given by Maiman (M2) as

$$\beta = \frac{v(1-r)}{l}, \qquad 1.47$$

where v is the velocity of light in the crystal,

r is the mean reflectivity of the crystal faces,

l is the length of the resonator.

One can also express such losses in terms of the cavity quality factor Q. In this particular system, therefore, we would have

$$Q = \frac{\omega}{\beta}. \qquad 1.78$$

The rate equations 1.67 and 1.68 have been derived from the three-level rate equations of Kaplan and Zier (KZ1) by means of the assumptions applicable to the four-level scheme.

1.12 The Theory of Dunsmuir 1961 (D1):

In several papers, another term is added to the phenomenological rate equations as a perturbation to initiate

laser action. We shall deal with these equations in the notation used by the paper under discussion.

The first is that of Dunsmuir (D1). With this perturbation included, the rate equations are

$$\frac{dn}{dt} = W - \frac{n}{\tau} - n B_s q \qquad 1.79$$

$$\frac{dq}{dt} = n B_s q - \frac{q}{t_c} + \frac{n}{P_m \tau} \qquad 1.80$$

where n is the population inversion per unit volume,

q is the total number of photons at the maser frequency,

W is the rate of supply of atoms to the upper energy level by the pump per unit volume,

$\frac{n}{\tau}$ is the rate of spontaneous emission (which is small compared to the stimulated emission term once laser action is initiated).

$nB_s q$ is the rate of stimulated emission (B_s is the Einstein coefficient per quantum per mode.),

q/t_c is the rate of loss of coherent photons from the cavity,

$\frac{n}{\tau P_m}$ is the rate of spontaneous decay per mode. This term is the perturbation initiating stimulated emission.

P_m is the number of modes within the fluorescent line and is given as

$$P_m = \frac{8\pi\nu^2}{c^3} \Delta\nu V \qquad 1.81$$

where V is the volume of the active medium. B_s is given as $1/\tau P_m$.

We can find the steady state parameters n_o, Q_o as before: for $\frac{dq}{dt} = 0$, $\frac{n}{\tau P_m}$ small and $n \approx n_o$,

then $$n_o B_s q = q/t_c , \qquad 1.82$$

and $$n_o = 1/B_s t_c . \qquad 1.83$$

Also for $\frac{dn}{dt} = 0$, $n \approx n_o$, $q = q_o$,

then $$W = n_o B_s q_o - n_o/\tau . \qquad 1.84$$

Substituting for B_s,

$$q_o = t_c W - P_m . \qquad 1.85$$

Computer solutions to these equations were found by Dunsmuir, assuming the following values of parameters:

$\tau = 5 \times 10^{-3}$ seconds,

$\Delta\nu = 8.3$ cm^{-1} $= 24.9 \times 10^{10}$ cps.,

$\nu = 4.33 \times 10^{14}$ sec^{-1},

$W = 3.5 \times 10^{21}$ mol/cm^3/sec,

$t_c = 1.6 \times 10^{-8}$ second,

$V = 1$ cm^3.

These solutions are plotted in figure 1.7 and are seen to exhibit damped oscillations. The period of the predicted oscillations decreases with time but is approximately 1.5 microsecond.

If on the other hand, one employs linearized equations which apply near steady-state, such that $\eta = n - n_o$ and $\epsilon = q - q_o$, then

$$\left.\begin{matrix}\eta \\ \epsilon\end{matrix}\right\} \propto \exp\left(-\frac{B_s q_o t}{2}\right) \sin B_s \sqrt{n_o q_o}\, t . \qquad 1.86$$

From these linearized solutions, the period is seen to be

$$\omega = B_s \sqrt{n_o q_o} , \qquad 1.87$$

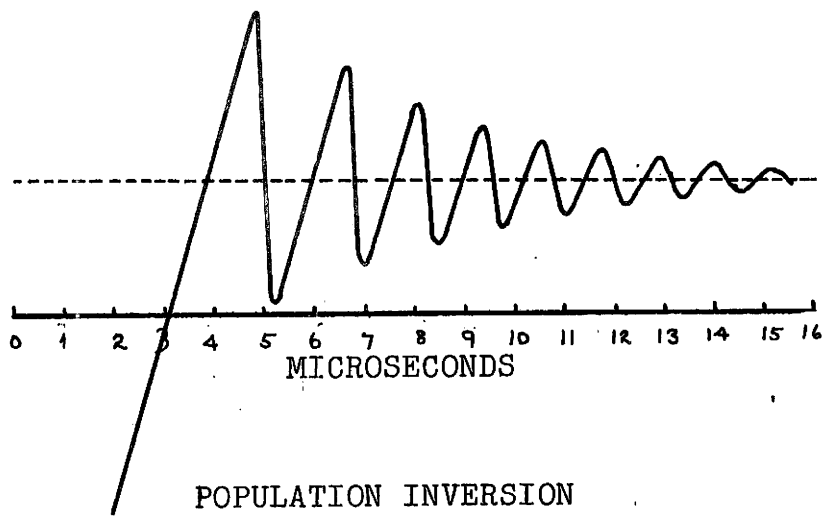

POPULATION INVERSION

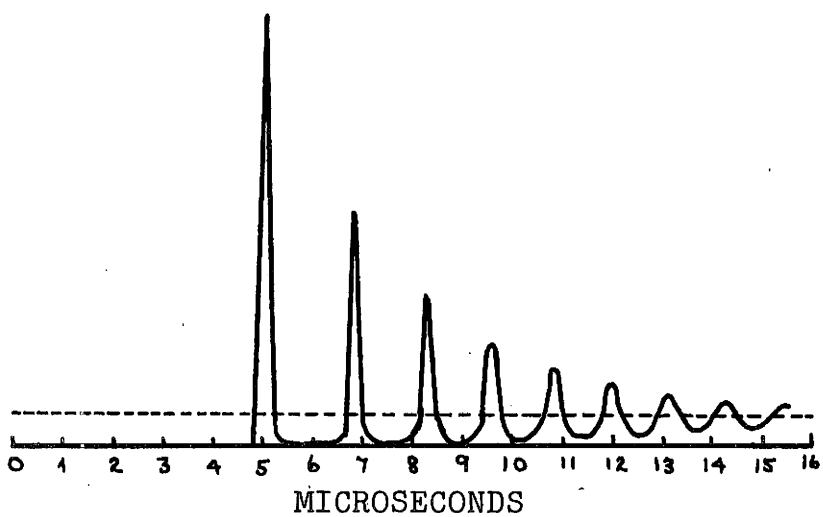

LASER EMISSION

FIGURE 1.7

COMPUTER SOLUTIONS TO DUNSMUIR'S RATE EQUATIONS

or

$$T_M \approx \frac{2\pi}{B_s\sqrt{\frac{1}{B_s t_c}\cdot W t_c}}, \qquad 1.88$$

where $P_m \ll W t_c$,

and

$$T_M \approx \frac{2\pi}{\sqrt{B_s W}}, \qquad 1.89$$

or

$$T_M \approx 2\pi\sqrt{\frac{8\pi\nu^2\Delta\nu\tau}{c^3}\frac{V}{W}}. \qquad 1.90$$

Using the above values, T_M can be calculated to be 1.6 microseconds. Hence, the linearized solution is in good agreement with the exact solution.

1.13 The Theory of Galanin, Leontovich, Sviridenkov, and Chizhikova - 1962 (GLSC1):

These authors used similar rate equations to the foregoing but assume the term for spontaneous decay to be small. Then

$$\frac{dn}{dt} = E - bnN \qquad 1.91$$

$$\frac{dN}{dt} = bnN - \frac{N}{T}, \qquad 1.92$$

where n is the population inversion,

N is the energy density expressed in terms of the number of coherent photons,

b is given as $B_E h$, where B_E is Einstein coefficient for stimulated transitions.

Here

$$b = \frac{k_0}{n_0}\frac{c}{\mu}\left(\frac{\varepsilon}{\varepsilon_{eff}}\right)^2, \qquad 1.93$$

where k_o is the absorption coefficient (cm^{-1}),

n_o is the number of Cr^{3+} ions in 1 cm^3,

μ is the index of refraction of ruby,

$\mathcal{E}$ is the intensity of mean electromagnetic field in the crystal,

$\mathcal{E}_{eff}$ is the intensity of effective electromagnetic field in the crystal,

$T = \mu l \left[c \ln 1/r\right]^{-1}$ is the mean lifetime of emission in the crystal,

E is the pump intensity (number of photons absorbed per cm^3 per second.)

More will be said later about this paper.

1.14 The Theory of Birnbaum, Stocker, and Welles - 1963 (BSW1):

A paper by Birnbaum, Stocker and Welles sets up rate equations within the framework of Bostick and O'Connor's equations, but revamped to incorporate the assumptions relevant to a three-level maser oscillating between energy levels previously designated as 2 and 1. The original equations of Bostick and O'Connor, with the perturbation term "Bn" included, are restated in the terminology used by Birnbaum et al.

$$\dot{n} = Wn_o - n/\tau - Bnp, \qquad 1.94$$

$$\dot{p} = Bnp - \beta p + Bn, \qquad 1.95$$

where $n = n_2 - n_1$ is the population inversion,

n_o is the total number of active ions,

W is the rate of excitation to the metastable state,

B is the rate of stimulated emission per coherent photon in the laser cavity,

p is the number of coherent photons in the cavity,

β is the coherent photon loss rate due to partial transmission at the cavity end-walls.

The derivation of the rate equations used by Birnbaum et al. as applied to a three-level optical maser is not given in their paper and will be deferred until section 2.6. The rate equations used are as follows:

$$\dot{n} = (n_o - n)W - \frac{n_o + n}{\tau} - 2Bnp, \qquad 1.96$$

$$\dot{p} = Bnp - \beta p + B\,\frac{n_o + n}{2}. \qquad 1.97$$

As in the previous sections, these equations may be linearized and the resulting solution for p near steady-state is

$$p = p_o \exp\left[-\tfrac{1}{2}\left(W - \tfrac{1}{\tau}\right)\frac{n_o}{n_s}\,t \pm it\left\{\beta\left(W - \tfrac{1}{\tau}\right)\frac{n_o}{n_s} - \left[\tfrac{1}{2}\left(W - \tfrac{1}{\tau}\right)\frac{n_o}{n_s}\right]^2\right\}^{1/2}\right], \qquad 1.98$$

where n_s is the steady state population inversion. At threshold, the necessary pumping rate, W_{th}, is

$$W_{th} = \frac{1}{\tau}\left(1 + 2\,\frac{n_s}{n_o}\right). \qquad 1.99$$

Just above threshold the solution for p is given as

$$p \approx p_o \exp\left[-\frac{t}{2\tau'} + i\sqrt{\frac{\beta}{\tau'}}\,t\right]. \qquad 1.100$$

The procedure used by Birnbaum et al. to test this theory was to measure the decay time of the oscillation pulses at conditions just above oscillation threshold. This decay time gives

a value for τ'. Further, if the coherent photon loss rate, β, is known, then the period of oscillation can be predicted by

$$T_M = 2\pi\sqrt{\frac{\tau'}{\beta}} \qquad 1.101$$

For a ruby crystal with highly reflecting silvered end-plates, the period predicted by the above procedure was 10 microseconds and the observed period was 13 microseconds. This agreement was considered good.

CHAPTER II

COMMENTS ON THE THEORY

2.1 A Further Method of Deriving Maimain's Gain Equation:

Let us re-examine this gain equation, derived originally by Maiman (M2), and given as equation 1.31 in this paper, namely

$$-\alpha l = 1 - r \qquad 1.31$$

In order to demonstrate the validity of equation 1.31 for a cavity with end-walls of reflectivity R_1 and R_2, consider figure 2.1. E^+ and E^- represent the amplitude of electromagnetic waves travelling to the right and left respectively. The wave travelling through the laser crystal is attenuated by an amount $\exp(-\alpha l)$ on each traverse. Therefore, we have

$$E_2^+ = E_1^+ \exp(-\alpha l) \qquad 2.1$$

$$E_1^- = E_2^- \exp(-\alpha l), \qquad 2.2$$

and

$$E_2^- = E_2^+ R_2 \qquad 2.3$$

$$E_1^+ = E_1^- R_1 . \qquad 2.4$$

From equations 2.3 and 2.4, therefore,

$$E_2^+ / E_2^- = 1/R_2 \qquad 2.5$$

$$E_1^+ / E_1^- = R_1 . \qquad 2.6$$

Dividing equation 2.1 by 2.2, one has

$$\frac{E_2^+}{E_2^-} = \frac{E_1^+}{E_1^-} \exp(-2\alpha l). \qquad 2.7$$

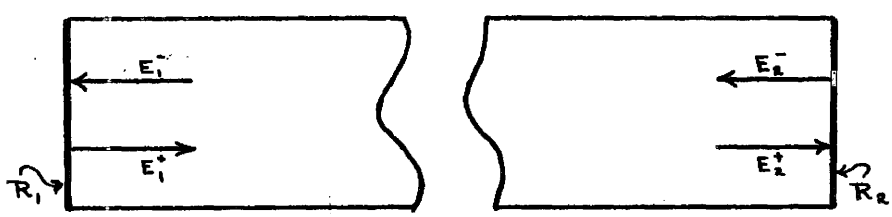

FIGURE 2.1

A DEFINITION OF THE AMPLITUDE OF AN ELECTROMAGNETIC WAVE IN A LASER CAVITY OF REFLECTIVITY R_1 AND R_2.

Substituting equations 2.5 and 2.6 into equation 2.7 gives

$$\frac{1}{R_2} = R_1 \exp(-2\alpha l) . \qquad 2.8$$

Therefore, $\exp \alpha l = \sqrt{R_1 R_2}$. 2.9

For $\alpha l \ll 1$ equation 2.9 becomes

$$1 + \alpha l = \sqrt{R_1 R_2} , \qquad 2.10$$

and $$-\alpha l = 1 - r . \qquad 1.31$$

in agreement with Maiman (M2). This approach will be used again in section 2.8.

2.2 The Derivation of the Coupled Rate Equations of Statz, and deMars (Sd1):

Equations 1.56 and 1.57, quoted from reference (Sd1), may be derived from the original rate equations in terms of the parameters defined in section 1.9:

$$\frac{dP}{dt} = -\frac{\omega P}{Q_L} \qquad 1.53$$

$$\frac{1}{Q_L} = \frac{1}{Q} - C n \qquad 1.54$$

$$\frac{dn}{dt} = -\frac{n - n_1}{\tau} - D n P . \qquad 1.55$$

Divide equation 1.53 by $P_0 \omega$, where P_0 and ω are constants.

$$\frac{d P/P_0}{d \omega t} = -\frac{\omega P}{\omega P_0 Q_L} . \qquad 2.11$$

Recalling the $P/P_0 = \pi$ and $n/n_0 = \eta$, substitute equation 1.54 into equation 2.11. Thus

$$\frac{d\pi}{d\tau} = -\frac{\pi}{Q_L} = -\frac{\pi}{Q}\left(1 - C n Q\right)$$

$$= \frac{\pi}{Q}\left(\eta C Q n_0 - 1\right) . \qquad 2.12$$

One can solve for the constant C at steady-state where $\frac{dP}{dt} = 0$ and $n = n_o$ so that from equation 1.53, $\frac{1}{Q_L} = 0$ or from equation 1.54,

$$C = 1/n_o Q . \qquad 2.13$$

Equation 2.12, therefore, reduces to

$$\frac{d\pi}{d\tau} = \frac{1}{Q} \pi (\eta - 1) . \qquad 1.56$$

One may verify equation 1.57 by the same procedure. Dividing through equation 1.55 by $n_o \omega$, one finds

$$\frac{d\eta}{d\tau} = - \frac{\eta - \alpha}{T_o} - \frac{D \eta P}{T_o} \tau \qquad 2.14$$

$$= - \frac{\eta - \alpha}{T_o} - \frac{D \eta \pi P_o}{T_o} \tau . \qquad 2.15$$

Again at steady-state, $\frac{dn}{dt} = 0$ and $n = n_o$. Therefore, from equation 1.49

$$D n_o P_o = \frac{n_o - n_1}{\tau} \qquad 2.16$$

$$D \tau P_o = 1 - \alpha , \qquad 2.17$$

and equation 2.15 becomes

$$\frac{d\eta}{d\tau} = - \frac{\eta - \alpha}{T_o} - \frac{1 - \alpha}{T_o} \eta \pi . \qquad 1.57$$

2.3 The Problem of the Period of Oscillation:

As asserted in section 1.10, the presence of "extra spikes" from a multimode cavity accounts for an experimental period smaller than a theoretical period. Statz et al. (SLSC1) observe that spikes from different areas of the laser end-face exhibit different amplitudes. From this,

these authors conclude that different sets of modes participate in the output from different areas of the laser end-face. On the basis of such reasoning, one would foresee, at sufficiently low powers, the possibility of a spike from one area without a simultaneous spike from another area, assuming that light emerging from a portion of the laser end-face was derived from the volume directly behind it. Note, however that we can also attribute such spatial variations in the laser output to light scattered from one area of the laser into other areas. Scattering can be caused by foreign particles, gaseous inclusions or inhomogeneities. The laser light can also be "steered" into another area by inhomogeneities in the index of refraction, forming light pipes. From either of these hypotheses, scattered light or light piping, one would also expect the same time-resolved spiking structure but differing amplitudes of spikes in the light emergent from various areas of the laser end-face. From the reasoning of these authors (section 1.10), one would not expect the same spiking pattern, particularly at low powers; that is, one would not expect the spikes from the outer area to bear a regular time-dependence to the spikes from the central region.

Much better experimental evidence on the correlation of spiking patterns from various areas of the laser end-face has been shown by Ready (Feb 63)(R1), who demonstrated conclusively that the spikes from different portions of the

laser were correlated in time but not in amplitude. He further observed the presence of "dark spots" on the end-face of the laser from which no light output was obtained. An increase of pump power to a value of two and one-half times the oscillation threshold value did not cause light to emit from these "dark spots". Ready argued that the existence of these "dark spots" negates scattered light as the mechanism by which the same time-resolved spiking structure is observed from different portions of the laser end-face.

On the other hand, Kaiser and Keck (KK1) point out that ruby has a rather high extinction loss (approximately 17% per pass) due mainly to scattering centres of the order of about 1 micron in diameter. As they point out, Mie theory predicts rather strong scattering of laser light by these centres. Some of these centres lying close to the end-surface could therefore scatter light emerging from the laser, producing shadows. Another possible mechanism for "dark spots" is the light piping of the laser light by changes in the index of refraction. This mechanism could "steer" light away from certain portions of the laser end-face to produce "dark spots". These possibilities, we feel, negate Ready's assertion that scattered light is not responsible for the same spiking pattern across the laser end-face.

A further result of interest in this problem of the participating modes and the spiking structure is contained

in a paper by Evtuhov and Neeland (Jul 62) (EN1). In this paper, it is reported that no simple correlation between the spiking structure and the mode structure was found. Close to threshold, a complicated mode structure could be derived from a simple spiking structure and vice versa.

In summary, then, one must conclude that the postulate of "extra spikes" proposed by Statz et al. (SLSC1) remains unverified, if not negated. As a result, it is not known why their theory yields a value for the modulation period T_M which for a given set of boundary conditions may be five times that observed. It is not yet understood how different areas oscillate so that the same spiking structure (but for the amplitude) is derived from different areas of the laser. Finally, it is not understood how the mode structure and the spiking structure are interrelated.

2.4 Comments on the Stimulated Emission Probability Parameter B_S of Dunsmuir:

The new terminology involved in the stimulated emission term nB_Sq in Dunsmuir's rate equations requires some elaboration. Consider the probability of a spontaneous decay in one mode at the laser frequency to be $1/\tau p_m$ where p_m is the number of modes (equation 1.8) and τ is the spontaneous decay time. Thus, for q coherent photons at the laser frequency in the cavity, the probability of a stimulated emission is given by $q/\tau p_m$. Therefore, if n participating atoms are in an excited

state, the number of stimulated emissions per second will be given by $nB_S q$, where $B_S = \frac{1}{\tau p_m}$ (Bl, Hl)

B_S may now be related to the Einstein coefficient B_E. Recall that the number of stimulated photons per second per unit volume is given by Einstein to be (section I)

$$B_E \rho_\nu N_j$$

Thus, the number of stimulated photons per second per unit volume not compensated for by absorption is

$$B_E \rho_\nu n , \qquad 2.18$$

where n is the population inversion, and the number in a certain mode per unit volume is given by

$$\frac{B_E \rho_\nu n}{p_m} . \qquad 2.19$$

Now this term must be equivalent to the stimulated emission term used by Dunsmuir (equation 1.79) and

$$\frac{B_E \rho_\nu n}{p_m} = n B_s q_\nu . \qquad 2.20$$

Therefore

$$\frac{B_E q_\nu h\nu n}{p_m} = n B_s q_\nu ,$$

and

$$B_s = \frac{B_E h\nu}{p_m} , \qquad 2.21$$

or B_S in Dunsmuir's notation is the Einstein coefficient per quantum per mode.

2.5 Comments on the Stimulated Emission Probability Parameter b of Galanin et al.:

One may write Dunsmuir's parameter B_S in terms of the linewidth of the laser spectrum. Let $\rho(\nu)$ be the energy density per unit frequency range per unit volume of the laser signal. Taking this unit frequency range to be the linewidth of the laser output, we, therefore, have

$$\rho = \frac{q h\nu}{\Delta\nu\, V}. \qquad 2.22$$

From equation 1.9

$$B_E = \frac{A c^3}{8\pi h \nu^3}.$$

Therefore, using equation 1.81,

$$B_E \rho = \frac{A c^3 q}{8\pi \nu^2 \Delta\nu V} \qquad 2.23$$

$$= \frac{R}{\rho_m} q$$

$$= B_S q, \qquad 2.24$$

as used by Dunsmuir.

Thus

$$\frac{B_E q h\nu}{\Delta\nu\, V} = B_S q, \qquad 2.25$$

and per unit volume B_S is given as

$$B_S = \frac{B_E h\nu}{\Delta\nu} \qquad 2.26$$

Now, since Galanin et al. (GLSC1) use as their term for stimulated emission, bnN, while Dunsmuir uses nB_Sq where N and q are equivalent, then b is equivalent to B_S and we may express equation 2.26 as

$$b = B_E h \frac{\nu}{\Delta\nu}. \qquad 2.27$$

This result is in disagreement with the result of Galanin et al. which is

$$b = B_E h. \qquad 2.28$$

Galanin et al. also give the relation

$$b = \frac{k_o}{n_o} \frac{c}{\mu} \left(\frac{\mathcal{E}}{\mathcal{E}_{eff}}\right)^2. \qquad 1.93$$

Let us consider the validity of this expression; the terms will be defined as they arise in the discussion. Further, one need not be concerned with the term $\mathcal{E}/\mathcal{E}_{eff}$ in verifying this equation, where $\mathcal{E}$ is intensity of the mean field and $\mathcal{E}_{eff}$ is the intensity of the effective field. For our purposes, set this term equal to 1.

Note that Maiman (M2) gives the rate of change of stimulated energy as

$$\frac{dW}{dt} = W_{21}\, n\, h\nu, \qquad 2.29$$

where n is again the population inversion and W is the energy = $nh\nu$, or

$$\frac{dn}{dt} = W_{21}\, n. \qquad 2.30$$

Further,

$$W_{21} = \int \frac{c\,\sigma(\nu)\rho(\nu)\,d\nu}{h\nu\sqrt{\epsilon}}, \qquad 2.31$$

where σ is the capture cross-section,

ϵ is the dielectric constant = μ^2 where μ is the index of refraction,

c is the velocity of light.

If we take the resonance line shape to be rectangular, for simplicity, then equation 2.31 becomes

$$W_{21} = \frac{c\,\sigma(\nu)\rho(\nu)\,\Delta\nu}{h\nu\mu} \qquad 2.32$$

and $\Delta\nu$ is the width of the spectrum.

Also

$$\sigma(\nu) = \frac{\pi}{2}\,\Delta\nu\,\sigma_0\,g(\nu) \qquad 2.33$$

$$\sigma(\nu_0) = \pi/2\,\Delta\nu\,\sigma_0\,g(\nu_0), \qquad 2.34$$

where

$$g(\nu) = \frac{\Delta\nu}{2\pi}\,\frac{1}{(\nu-\nu_0)^2 + \left(\frac{\Delta\nu}{2}\right)^2} \qquad 2.35$$

$$g(\nu_0) \cong \frac{\Delta\nu}{2\pi}\,\frac{4}{(\Delta\nu)^2} = \frac{2}{\pi\Delta\nu}. \qquad 2.36$$

Therefore

$$\sigma(\nu_0) = \frac{\pi}{2}\,\Delta\nu\,\sigma_0\,\frac{2}{\pi\Delta\nu} = \sigma_0, \qquad 2.37$$

and $\sigma_0 = k_0/n_0$ where k_0 is the absorption coefficient and n_0 is the total number atoms in the system. Therefore, from equation 2.32 and substituting equations 2.22 and 2.37,

$$W_{21} = c\,\frac{k_0}{n_0}\,\frac{g h\nu}{\Delta\nu}\,\Delta\nu\,\frac{1}{h\nu\mu}$$

$$= \frac{c\,g\,k_0}{n_0\,\mu}. \qquad 2.38$$

Therefore,

$$\frac{dn}{dt} = \frac{k_0}{n_0}\,\frac{c}{\mu}\,g\,n \equiv b\,g\,n. \qquad 2.39$$

and

$$b = \frac{k_0}{n_0}\,\frac{c}{\mu}. \qquad 2.40$$

One, therefore, concludes that equation 1.93

$$b = \frac{k_0}{n_0}\,\frac{c}{\mu}\left(\frac{\varepsilon}{\varepsilon_{eff}}\right)^2, \qquad 2.41$$

as used by Galanin et al. is correct while the term

$$b = B_E h \qquad 2.28$$

is incorrect and should be replaced by

$$b = B_E h\,\frac{\nu}{\Delta\nu}. \qquad 2.27$$

2.6 A Derivation of the Revised Rate Equations of Birnbaum et al. (BSW1):

The rate equations used by Birnbaum et al. to describe a three-level ruby optical maser are given as

$$\dot{n} = (n_o - n)W - \frac{n_o + n}{\tau} - 2Bnp \qquad 1.96$$

$$\dot{q} = Bnp - \beta p + B\left(\frac{n_o + n}{2}\right). \qquad 1.97$$

The various terms in equation 1.96 arise as follows:

First Term:

This term represents optical pumping in ruby. If we call n_1 and n_2 the populations of levels 1 and 2, recalling that n_3 is assumed zero (section 1.7), then

$$n_o = n_1 + n_2 \qquad 2.42$$

where n_o is the total number of participating atoms and

$$n = n_2 - n_1 \qquad 2.43$$

where n is the population iversion.

Hence,

$$n_1 = \frac{n_o - n}{2}, \qquad 2.44$$

and

$$n_2 = \frac{n_o + n}{2}. \qquad 2.45$$

The improvement in the theory is this: one is not always pumping on n_o atoms, but more accurately on n_1 atoms. Therefore, the pumping term in equation 1.94 of Bostick and O'Conner is replaced by $n_1 W$. However, this is not yet correct since one must allow for n, the population inversion, increasing by 2 for every atom pumped: that is, for n_1 decreased by 1, n_2 increases by 1 and n increases by 2. Therefore, the

pumping term is $2n_1W$ or

$$(n_0 - n)\,W. \qquad 2.46$$

Another approach is this: after pumping, the population inversion is

$$n = (n_2 + n_1 W_{12}) - (n_1 - n_1 W_{12}) \qquad 2.47$$

$$= n_2 - n_1 + 2 n_1 W_{12} \qquad 2.48$$

$$= \text{initial population inversion} + 2n_1W_{12}. \qquad 2.49$$

From 2.49 the pumping term is $2n_1W_{12}$.

Second Term:

The spontaneous emission term arises in the same way as above and is

$$2An_2 = \frac{2}{\tau}\,\frac{n_0+n}{2} = \frac{n_0+n}{\tau}. \qquad 2.50$$

Third Term:

Here one must consider stimulated emission and absorption in considering the rate of population inversion.

$$\dot{n} \equiv \frac{d}{dt}(n_2 - n_1). \qquad 2.51$$

Now

$$\frac{dn_2}{dt} = -Bn_2p + Bn_1p \qquad 2.52$$

and

$$\frac{dn_1}{dt} = Bn_2p - Bn_1p. \qquad 2.53$$

Therefore, substituting into equation 2.5

$$\dot{n} = -2Bn_2p + 2Bn_1p \qquad 2.54$$

$$= -2Bp(n_2 - n_1)$$

$$= -2Bnp. \qquad 2.55$$

The various terms in equation 1.97 arise as follows:

First Term:

Here one does not, because of the high loss rate of coherent photons through the end-walls, consider the absorption process between levels 1 and 2 as significant. Hence no factor of 2 arises as in equation 2.55 and this term is simply

$$n B p. \qquad 2.56$$

Second Term:

This term holds true for any maser cavity representing the loss rate of coherent photons from that cavity and remains

$$\beta p. \qquad 2.57$$

Third Term:

This term represents spontaneous emission from level 2 in any mode and, as such, is a source of noise. Recall, however, that this term also serves as a perturbation to start the oscillation. It is represented by

$$B n_2 = B \frac{n_0 + n}{2}. \qquad 2.58$$

This term compares with that of Dunsmuir

$$\frac{n}{\tau P_m},$$

so that

$$B \equiv B_s = \frac{1}{\tau P_m}.$$

The above reasoning justifies the equations used by Birnbaum et al., equations 1.96 and 1.97.

2.7 The Calculation of τ', the Effective Fluorescent Lifetime:

Difficulty was encountered in an attempt to follow the procedures of Birnbaum et al. First of all, our laser emission at no time consisted of a smoothly decaying series of spikes at 1% above threshold. Therefore, Birnbaum's method of measuring τ' from the decay time of the spikes could not be applied in our case. Secondly, the duration of laser action was impossible to reproduce. One reason was that our power measurement was accurate only to 2% in power; another reason was that the decay time of the laser pulse was reported (SLSC1) to be very sensitive to small non-linearities and noise effects. It was, therefore, desirable to circumvent a direct measurement of τ' and so the following procedure was derived.

Comparing the first terms of equations 1.98 and 1.100, one has

$$-\frac{1}{2\tau'} = -\frac{1}{2}\left(W-\frac{1}{\tau}\right)\frac{n_0}{n_3} \qquad 2.59$$

from which

$$\frac{1}{\tau'} = \left(W-1/\tau\right)\frac{n_0}{n_3}. \qquad 2.60$$

This definition of τ' is also verified by a comparison of the second terms of these same equations. The third term of equation 1.98 is much smaller than the second, so that

$$\beta\left(W-1/\tau\right)\frac{n_0}{n_3} \gg \left[\frac{1}{2}\left(W-1/\tau\right)\frac{n_0}{n_3}\right]^2. \qquad 2.61$$

This is a reasonable approximation in that, for a typical laser system, $\beta \sim 10^{8}$, $W \sim 1/\tau \ll 1$ and $\left(\frac{n_o}{n_s}\right)^2 \lesssim 10^{4}$.

For steady-state conditions, we assume that the population inversion close to threshold is approximately that at steady-state. In this case $\dot{n} = 0$, $n = n_o$ and p_s is assumed zero. Therefore, from equation 1.96, one can determine the threshold pumping requirement:

$$(n_o - n_s) W_{th} = \frac{n_o + n_s}{\tau} \qquad 2.62$$

Therefore,

$$W_{th} = \frac{1}{\tau} \frac{1 + n_s/n_o}{1 - n_s/n_o} \qquad 2.63$$

or

$$W_{th} \approx \frac{1}{\tau}\left(1 + 2\frac{n_s}{n_o}\right) \text{ for } \frac{n_s}{n_o} \ll 1. \qquad 2.64$$

We also have a relation for W during laser action from the definition of τ' (equation 2.60):

$$W = \frac{n_s}{n_o}\frac{1}{\tau'} + \frac{1}{\tau}. \qquad 2.65$$

Therefore,

$$\frac{W_{th}}{W} = \frac{1 + 2\, n_s/n_o}{\frac{n_s}{n_o}\frac{\tau}{\tau'} + 1} \qquad 2.66$$

and

$$\frac{\tau}{\tau'} = \frac{n_o}{n_s}\left[\left(1 + 2\frac{n_s}{n_o}\right)\frac{W}{W_{th}} - 1\right] \qquad 2.67$$

This equation gives us a measure of τ' from n_s/n_o and W/W_{th} obviating the problem of attempting to find this decay time constant τ' from the observed decay time.

For the calculation of n_s/n_o, we assume that n_s is essentially equal to the threshold population inversion.

Therefore, from equation 1.34

$$\frac{n_s}{n_o} \approx \frac{1-r}{\alpha_o l} . \qquad 2.68$$

Using equations 1.47

$$\beta = \frac{v(1-r)}{l} , \qquad 1.47$$

and 2.68 and 2.67, one can predict T_M from

$$T_M = 2\pi\sqrt{\frac{\tau'}{\beta}} . \qquad 1.101$$

Let us inquire as to the validity of equation 1.101 for the spiking period, T_M, in view of experimental observations. In this respect it is found that a discrepancy does exist between calculated and observed values for this parameter. As an example, for a given set of experimental conditions, T_M may be calculated to be in the order of 15 microseconds while the observed value may be in the order of 6 microseconds. The main consideration of the thesis will be an attempt to account for this discrepancy.

2.8 A Consideration of Scatter as a Loss Parameter:

First note that an increase in the reflection loss r produces a decrease in the period. For illustration, if r is decreased from 90% to 80%, T_M decreases from 17 microseconds to 12.5 microseconds for the same power (1% above threshold) and temperature. However, it must also be

observed that n_s/n_o increases from .02 to .05; one must further recall that equation 2.67 holds only for $n_s/n_o \ll 1$.

Secondly, a paper by Kaiser and Keck (KK1) suggests that scatter loss may be rather high. The fact that the predicted threshold may be as much as five times less than the actual value caused them to study losses other than transmission losses in laser cavities. A paper by Collins and Nelson (1961) (CN1) made a detailed study of ruby and found a loss of 30% per pass due to local imperfections and changes in the index of refraction. Kaiser and Keck studied the losses due to scattering of foreign particles or gaseous inclusions evidenced by the Tyndall effect. The size of the scattering centres in ruby is estimated to be about 1 micron in diameter. For the effective index of refraction n_1/n_2, where n_1 is the index of refraction of the scattering particles and n_2 of the matrix material, and for particles of 1 micron in diameter, radiation of wavelength $\lambda_o = 7000$ Å ($= \lambda n_2$) is scattered quite effectively. In small angle transmission measurements they found an extinction loss of 17%.

Such a high scatter loss as 30%, predicted by Collins and Nelson (CN1), would certainly enter into the period determination, augmenting the transmission loss. Let us consider a period determination for this scatter loss of 30% in addition to a transmission loss of 15% on one pass and 0% on the return pass; that is, $R_1 = 100\%$, $R_2 = 85\%$. Further, consider this scatter loss to be an effective transmission loss: that is,

the reflectivity of one end-face is $R_1 - L = (100-30)\%$; also $R_2 - L = (85-30)\%$. This is an approximation in that scatter occurs throughout the length of the crystal rather than just at the end-surfaces. Recalling the approach of section 2.1, we have

$$\begin{aligned} E_2^+ &= E_1^+ \exp(-\alpha l), \\ E_1^- &= E_2^- \exp(-\alpha l), \\ E_2^- &= E_2^+ (R_2 - L), \\ E_1^+ &= E_1^- (R_1 - L). \end{aligned} \qquad 2.69$$

Solving as before,

$$\exp \alpha l = \sqrt{(R_1-L)(R_2-L)}, \qquad 2.70$$

and

$$\alpha = \frac{\ln\sqrt{(R_1-L)(R_2-L)}}{l} \qquad 2.71$$

Since $(N_1 - N_2)\sigma_{12} = \alpha_{12}$,

then

$$N_2 - N_1 = -\frac{\ln\sqrt{(R_1-L)(R_2-L)}}{l\sigma}, \qquad 2.72$$

and

$$\frac{n_s}{n_o} \approx -\frac{\ln\sqrt{(R_1-L)(R_2-L)}}{\alpha_o l}. \qquad 2.73$$

This is the new equation for n_s/n_o when scatter loss is treated as an effective transmission loss, replacing equation 2.68. With this revision, the value of n_s/n_o is found to be too large for the approximation in equation 2.64 to hold. Therefore, the exact value of τ/τ' must be derived. It is found using equations 2.63 and 2.65 that

$$\frac{\tau}{\tau'} = \frac{n_o}{n_s}\left[\frac{1 + n_s/n_o}{1 - n_s/n_o}\,\frac{W}{W_{th}} - 1\right]. \qquad 2.74$$

Using this equation, one can evaluate τ'.

We must further examine the validity of equation 1.66 where r now implies $r = \sqrt{(R_1-L)(R_2-L)}$, rather than $\sqrt{R_1R_2}$. The term 1-r now may be rather large and so

$$\exp(-\alpha l)\, r = 1 \qquad 1.30$$

more exactly reduces to

$$-\alpha l = \ln \frac{1}{r}. \qquad 2.75$$

Therefore, the scatter and transmission losses in the cavity are given by $\ln\frac{1}{r}$ while the loss rate, β, of coherent photons from the cavity is given by

$$\beta = \frac{v}{l} \ln \frac{1}{r}. \qquad 2.76$$

As an illustrative example, using equations 2.76, 2.73, 2.74 and 1.101 for a scatter loss of 30%, an oscillation period of about 6 microseconds was obtained. This agreement is encouraging, although misleading, as further discussion will show (section 2.10).

It was stated above that scatter was considered as an effective reflectivity. More realistically, however, scatter should be considered an effective absorption coefficient since scatter, like absorption, occurs throughout the length of the crystal. Let us call the scatter loss per centimeter S. Then, the condition for high amplification (equation 1.30) becomes

$$\exp\left[-(\alpha+s)l\right] r \approx 1, \qquad 2.77$$

and $$-(\alpha+S)l = \ln 1/r, \qquad 2.78$$

or $$-\alpha l = \ln \frac{1}{r} + Sl. \qquad 2.79$$

Since, for laser action to occur, α is negative; equation 2.79 becomes

$$|\alpha| l = \ln \frac{1}{r} + Sl. \qquad 2.80$$

Again, since $(N_1-N_2)\sigma_{12}=\alpha_{12}$, using equation 2.79

$$N_2 - N_1 = \frac{\ln \frac{1}{r} + Sl}{\sigma_{12} l}, \qquad 2.81$$

and again defining $\alpha_0 = \sigma_{12} n_0$,

$$\frac{n_s}{n_0} = \frac{\ln \frac{1}{r} + Sl}{\alpha_0 l}. \qquad 2.82$$

The rate of loss of coherent photons from the cavity will now be enhanced by the scatter loss. The rate of loss due to scatter will be

$$\frac{v}{l} Sl. \qquad 2.83$$

Hence, the total loss rate will be the sum of the transmission loss and the scatter loss

$$\beta = \frac{v}{l}\left[\ln \frac{1}{r} + Sl\right]. \qquad 2.84$$

2.9 A Consideration of Diffraction as a Loss Parameter:

In a paper by Aagard (A1), it was suggested that, in addition to the scatter loss suggested above, a large diffraction loss might also exist in a laser crystal. In this respect, if laser emission, as observed in section 2.3, can emerge from the end-faces of a crystal in small diameter

light-pipes, then diffraction arising from this filimentary output may be quite large. The nebulous nature of the filaments, however, makes a theoretical treatment difficult. Aagard obviates this difficulty by the following technique: from the threshold-temperature characteristics of the laser system, a measure of the total losses during laser action may be obtained, and, knowing the values of all other losses but diffraction, one may find the diffraction loss. This was also the approach used by Collins and Nelson (CN1).

Cavity losses, Aagard states, arise from six sources:

1) walkoff,
2) lack of mirror flatness,
3) transmission losses at the end-plates,
4) absorption losses in the end-plates,
5) scatter losses,
6) diffraction from various emission light-pipes.

Walkoff occurs when a mode is induced to shift from a stable position (axial) to a less favorable position where the Q of the cavity is reduced. This loss is considered negligible for an alignment of plane mirrors to within 3 seconds of arc as Ready and Harwell (RH1) demonstrate, in that oscillation threshold is relatively unchanged for the alignment shifted over a range of 2 minutes of arc. Crystal end-faces may be ground flat enough (less than $\lambda/4$) that imperfect flatness is also a negligible loss. Trans-

mission and absorption losses in the mirror end-plates are accounted for in a measurement of the reflectivity. Scattering can be measured as described in section 3.1D. Hence, one may account for all losses but those due to diffraction.

Aagard states that for laser action to occur, the losses must be just balanced by the gain of the cavity; hence

$$\alpha l = \ln \frac{1}{\xi r} + S l . \qquad 2.85$$

(We shall call scatter loss per centimeter S rather than the β Aagard uses to avoid confusion with the cavity loss rate.) $1 - \xi$ is the diffraction loss and we call $\sqrt{R_1 R_2} = r$.

A check of our approach in section 2.8 (considering scatter as an effective absorption coefficient) is afforded by this equation 2.85. We may further extend equation 2.80 to include diffraction and derive, in our own way, equation 2.85. In considering diffraction loss as an effective reflectivity, one can see that $\mu = 1 - \xi$ and

$$r = \sqrt{[R_1 - (1-\xi)][R_2 - (1-\xi)]} , \qquad 2.86$$

For no reflection loss ($R_1 = R_2 = 1$) and no scatter loss,

$$r = \xi \text{ and } S = 0 . \qquad 2.87$$

Therefore, the diffraction loss appears as

$$\ln 1/\xi , \qquad 2.88$$

and for laser action to ensue

$$-\alpha l = \ln 1/\xi . \qquad 2.89$$

Therefore, the reflection loss is related by $\ln 1/r$,

the diffraction loss is related by $\ln 1/\xi$,

the scatter loss is related by Sl,

and the total loss of the cavity is

$$\ln \frac{1}{\xi} + \ln \frac{1}{r} + Sl \,, \qquad 2.90$$

or

$$\ln \frac{1}{\xi r} + Sl \,, \qquad 2.91$$

where $1-\xi$ is the diffraction loss per pass,

r is the mean reflectivity $= \sqrt{R_1 R_2}$,

S is the scatter loss per cm.

Aagard then gives α in terms of $\Delta\nu$, the fluorescent linewidth, τ_r the fluorescent decay time, g_1 and g_2 the statistical weights of the two atomic levels concerned, N_1 and N_2 the populations of each level, and λ_o the central wavelength of the resonance line;

$$\alpha = \frac{2}{\Delta\nu}\sqrt{\frac{\ln 2}{\pi}}\,\frac{\lambda_o^2}{8\pi}\,\frac{g_2}{g_1}\,\frac{(g_2/g_1)N_2 - N_1}{\tau_r}, \qquad 2.92$$

which reduces to

$$\alpha = \frac{(g_1/g_2)N_2 - N_1}{K_1 \Delta\nu} \qquad 2.93$$

if τ_r and λ_o are relatively independent of temperature. To adapt this equation to experiment, the further assumption is made that the population inversion is proportional to the pumping energy at threshold. This Aagard maintains is only possible at low temperatures and in a small temperature range. For these conditions, the assumption of τ_r and λ_o independent of temperature is particularly valid. Then

$$K_2\left[(g_1/g_2)N_2 - N_1\right] = E_{th} - C, \qquad 2.94$$

where C is the input energy required to equalize the populations of the upper and lower states. Substituting equations 2.94 and 2.93 into 2.85, Aagard derives

$$\frac{E_{th} - C}{K_1 K_2 \Delta\nu}\, l = \ln \frac{1}{\mathfrak{F} r} + S l , \qquad 2.95$$

and

$$E_{th} = K_3 \Delta\nu \left[\ln \frac{1}{\mathfrak{F} r} + S l \right] + C \qquad 2.96$$

$$= K_3 a_n \Delta\nu + C . \qquad 2.97$$

Here

$$a_1 = \ln \frac{1}{\mathfrak{F} r_1} + S l \qquad 2.98$$

and

$$a_2 = \frac{S_2}{S_1} a_1 = \ln \frac{1}{\mathfrak{F} r_2} + S l , \qquad 2.99$$

where r_1, r_2 are two different mean reflectivities and S_1, S_2 are the different slopes of the threshold - temperature characteristics for each reflectivity. Equations 2.98 and 2.99 may be solved for $\mathfrak{F}$ by Newton's Iterative Method commencing with $\mathfrak{F} = 1$.

2.10 The Modulation Period of a Ruby Laser:

With scatter and diffraction as well as transmission losses in a laser cavity, the cavity loss rate β_T may be given as

$$\beta_T = \frac{v}{l} \left[\ln \frac{1}{\mathfrak{F} r} + S l \right]. \qquad 2.100$$

To calculate τ' one must recalculate n_s/n_o. Now laser action commences only for

$$-\alpha l = \ln \frac{1}{\mathfrak{F} r} + S l. \qquad 2.86$$

Therefore,

$$\frac{n_s}{n_o} = \frac{\ln 1/\mathfrak{F} r + S l}{\alpha_o l} , \qquad 2.101$$

and

$$\frac{\tau}{\tau'} = \frac{n_o}{n_s} \left[\frac{1 + n_s/n_o}{1 - n_s/n_o} \cdot \frac{W}{W_{th}} - 1 \right]. \qquad \begin{matrix} 2.74 \\ 2.102 \end{matrix}$$

Then

$$T_M = 2\pi \sqrt{\frac{\tau'}{\beta_T}} . \qquad 2.103$$

CHAPTER III

EXPERIMENTAL TECHNIQUES

3.1 Metallic Film Deposition:

The thesis commenced in September, 1962, with an inquiry into the feasibility of silvering our own laser crystals. The problem encountered was that of deposition of a metal onto a crystalline substrate which can not tolerate a high temperature. The above restrictions reduce all the possible techniques to one - vacuum deposition. The drawbacks of this method are two-fold: good surface adhesion requires very clean surfaces, and pinholes are invariably left in the deposit.

The process involves the evaporation of a metal from a heater under vacuum. The metal atoms escaping from the heater travel unimpeded through an evacuated bell jar to a substrate onto which they condense on impact. The heater is made of some metal which will carry high electrical currents. The requirements on the heater material to be used are as follows: it must not combine chemically with the evaporant at high temperatures, its melting point must be higher than that of the evaporant, and, finally, the evaporant must, when it melts, adhere to or "wet" the heater surface. The heater may take the form of a filament heater such as a helical coil or a foil heater such as a boat. Holland (H2) gives a very useful table advising the best combination of heater and evaporant.

The vacuum system is required to maintain a long mean

free path for the metallic atoms. However, the evacuating unit also serves the purpose of removing gas molecules (mainly water vapour and hydrocarbons) from the system, preventing them from impinging on the surface of the substrate and forming impurities which would reduce the adhesion of the metal film. These gases are derived from back-streaming from the diffusion pump and desorption from the surfaces inside the bell jar as well as residual gases in the vacuum system, and to remove them effectively, high pumping speeds are necessary.

An Edwards 12E3 model Vacuum Coating Unit (figure 3.1) was acquired. The system employs a single stage rotary pump as a roughing pump and as a backing pump for the oil diffusion pump.

Characteristics of the Rotary Pump and Diffusion Pump:

Rotary Pump - model number 1SC150B:

ultimate vacuum: 0.005 torr,

displacement: 150 litres per minute with ballast.

Diffusion Pump - model number 403A:

three stages,

ultimate vacuum: less than 5×10^{-6} torr,

speed at the baffle-valve: 200 litres per second,

minimum backing speed: 150 litres per minute,

heater loading: 500 watts.

The system has a multi-filament turret assembly and high tension ionization cleaning equipment. The low tension transformer can drive up to sixty amperes through the heater but is

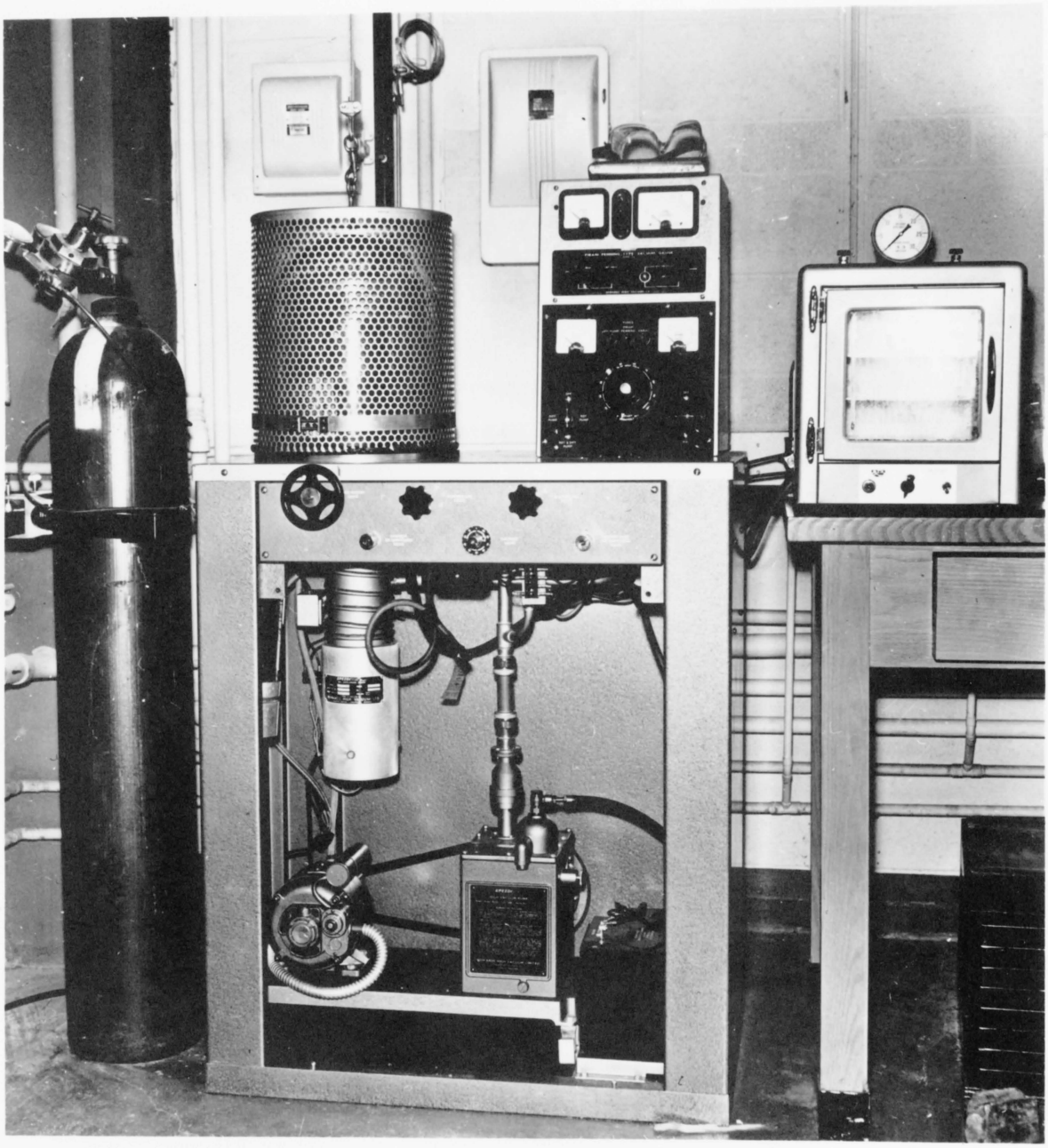

FIGURE 3.1

AN EDWARDS 12E3 VACUUM COATING UNIT

rated at forty amperes.

Many experiments were carried out to investigate the most suitable heater for silver, the best cleaning procedure for glass slides, and the best pump-down procedure. The heater found best for evaporating large quantities of silver (up to 150 milligrams) was a molybdenum boat. However, attempts to reproduce reflectivity under identical conditions were completely unsuccessful. Elaborate procedures for cleaning the glass slides were later revoked for the simple procedure of baking the slides in an Edwards Vacuum Oven (model 5830) for several hours, then scrubbing them with Ajax and distilled water until the "unbroken film of water" test was positive, and, finally, leaving them immersed in methanol until ready to be inserted into the vacuum system. This procedure gave acceptable results with regard to pinholes and adhesion. Finally, pump-down procedures were continuously revised until a final procedure evolved; only this will be described.

The bell jar was first evacuated by the rotary pump to a pressure of roughly 50 millitorr. The diffusion pump then took the pressure down to about 3×10^{-5} torr, and the system was continuously evacuated for an hour or two. Then, while liquid air was forced through a liquid air trap, the baffle valve leading to the vacuum pump was closed, helium gas was admitted to the bell jar, and the system was cleaned by the ionization bombardment technique. After ten minutes, the ion bombardment was turned off, the system was resealed,

and the diffusion pump again pumped on the system. The pressure rapidly dropped to less than 0.1×10^{-5} torr and the heater current was turned on. It has been pointed out (S1 and SS1) that higher reflectivities and less agglomeration of the deposit result from high evaporation rates. It is also evident that better adhesion is possible with a fast deposition rate as compared to a slow deposition rate. Hence, a current of sixty amperes was used to evaporate the metal and evaporation was completed in roughly twenty seconds. The system was then allowed to cool for fifteen minutes before air was admitted and the slides removed.

With regard to silvering the laser crystal, the end surfaces were carefully cleaned with dilute sodium hydroxide, which effectively removed any previously deposited silver. The crystal was mounted in close proximity to a comparator glass slide. To silver one end of the laser as close to 100% reflectivity as possible, 100 milligrams of silver were placed on each of the four heaters on the multi-filament assembly and all were evaporated in quick succession. For the partially transmitting end-face, amounts of silver varying from 10 to 50 milligrams were used. The reflectivity of the glass slide was taken to be the reflectivity of the laser end-face.

3.2 Reflectivity Measurements:

What is now the reflectivity of these silver films? As evidenced in the theory, a knowledge of the reflectivity

of the end-faces of the laser cavity is necessary to determine the loss rate of coherent photons. Further, since reflectivity is, in general, a function of frequency, one is only interested in the reflectivity of light at 6940Å.

Initial experiments demonstrated the need for a sophisticated design and measurement procedure. A design was drawn (figure 3.2) along the principles of a Strong-type reflectometer (S2). R_1 and R_2 refer to the reflectivities of two aluminized mirrors whose reflectivities are made the same by depositing both aluminum films simultaneously. Note that aluminum-coated mirrors are preferable to silver since they retain their reflectivity over a longer period of time. R refers to the reflectivity of the freshly-silvered comparator plate to be measured. With the comparator plate out of the system, chopped, monochromatic light entering at A is reflected off R_2 and leaves the system at B. A photometer placed at B detects the light, producing a signal V_1 proportional to $V_o R_2$, where V_o represents the intensity of light entering at A. Now the comparator plate is inserted into the system and intercepts the light beam travelling from A to R_2. The light is reflected onto R_1, back to R, and out again through B to be detected. The signal now, V_2, is proportional to $V_o R_1 R^2$. Hence, R is found to be

$$R = \sqrt{V_2/V_1}. \qquad 3.1$$

The major advantage of this system is that with two reflections from R, the errors in the calculation of R are

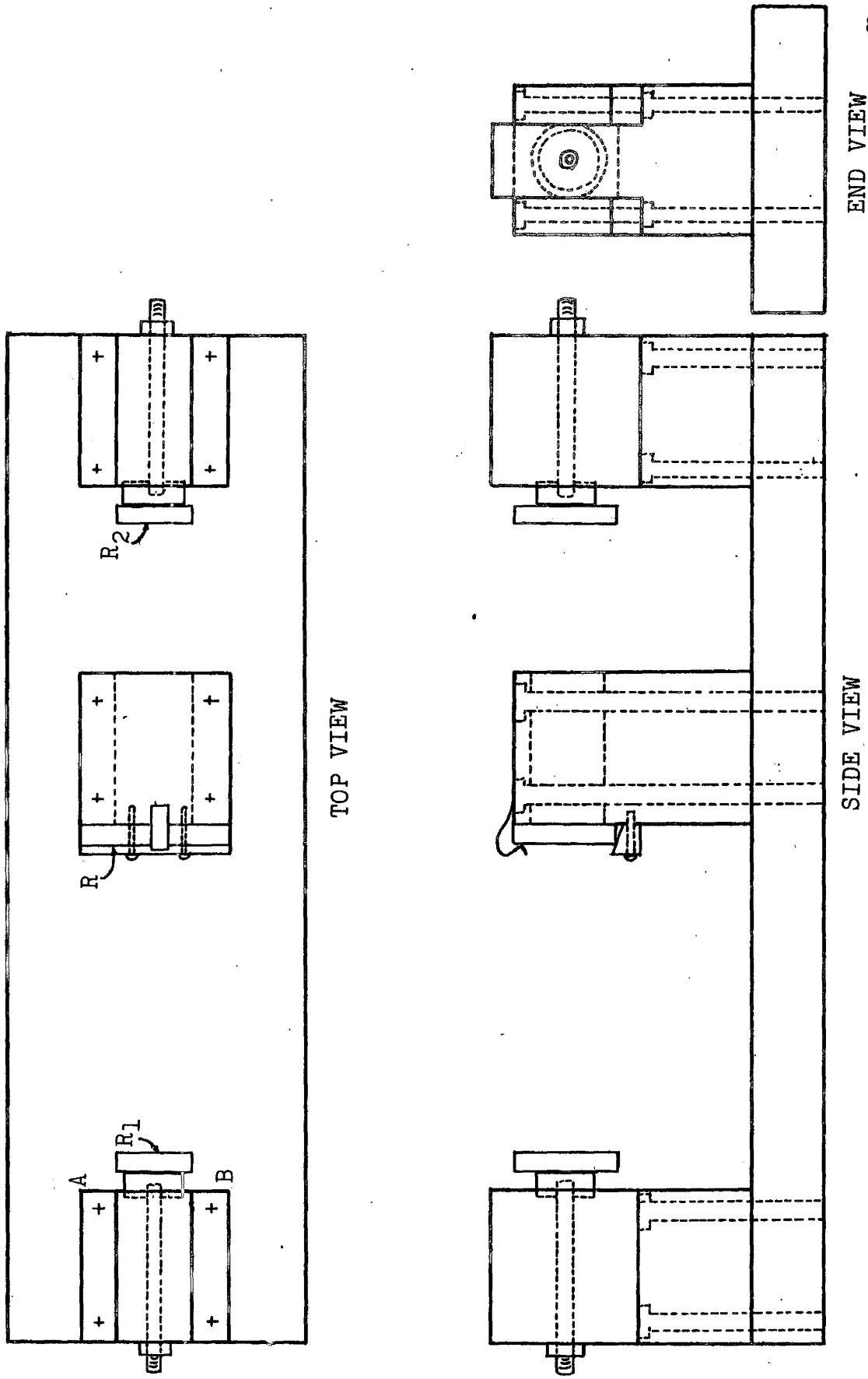

FIGURE 3.2 Scale $\frac{1}{2}$

A STRONG-TYPE REFLECTOMETER

halved. If V_1 and V_2 have relative errors ΔV_1 and ΔV_2, then the error in R is $\frac{1}{2}(\Delta V_1 + \Delta V_2)$. If there were n reflections off R, the error would be reduced to $\frac{1}{n}(\Delta V_1 + \Delta V_2)$.

In designing a reflectometer as described above, one must consider the variation in the reflectivity of the surface with the angle of incidence. At angles of incidence of less than 8°, the reflectivity is constant; further, polarization effects are obviated for angles within the same limit. (JW1, L2) Hence, all angles of incidence on each mirror surface were held to within 5°. To minimize the length of the reflectometer, beam width and beam divergence were restricted by the use of stops and lenses. Tolerances were calculated to be about four thousandths of an inch on most surfaces for the dimensions shown.

Let us consider more carefully the procedure described above. With the comparator plate in the system, some light will be transmitted through it to the mirror of reflectivity R_2 and reflected back through R and out B. This light must not be recorded by the phototube if an accurate measure of R is to be attained. As a result, a light-absorbing material must be inserted into this light path to ensure absorption of light transmitted by the comparator plate.

A second consideration is the reflectivity of the glass substrate itself. With the silvered surface on the front side of the comparator with respect to the illuminating source, some light transmitted by this deposit will be reflected off the

front and back surfaces of the substrate. This would give an erroneous measure of the reflectivity of the silvered surface. Another approach is this: as a preliminary step, an unsilvered comparator plate is inserted into the system, and the resulting signal is designated as V_2'. Now, if the silvered comparator plate is inserted with the silvered side against the support, the same intensity will fall on both glass surfaces as in the case of the clear plate, and the effect of reflection off these surfaces can be subtracted out in the final result. Nevertheless, after some analysis, one can show that, even for low reflectivities, the former approach is the most accurate.

To complete the experimental system, a collimating slit, a focusing lens, and a mechanical chopper may be mounted at A and a lens, a collimating slit and the phototube may be mounted at B. The whole system should be enclosed in a light-tight box with a narrow band-pass filter at the entrance slit to the box.

A further method of measuring reflectivities afforded itself in the availability of a Beckman Spectrophotometer (Model DK-1). This apparatus works on the principle of detecting an unbalance between two light beams of variable wavelength, one transmitted by the silvered glass comparator and the other by an unsilvered glass comparator. Here one is considering transmission measurements and so one would expect that results with the least error would be attained for the silver deposit

to be on the back face of the comparator since the intensity reflected off the glass surfaces is the same in this case where a much reduced intensity would be reflected off the glass surfaces for the silver deposit on the front face.

The main problem arising from a transmission measurement is that of obviating an absorption measurement in order to derive a reflectivity measurement. This was achieved through the use of published data on thin silver films by Kuhn and Wilson (KW1). In their paper is found a graph of transmission versus reflectivity, reproduced in figure 3.3. Only a small error is introduced in applying this graph for light of wavelength 6800Å to laser light at 6940Å. With the above graph, this method was by far the more desirable for measuring reflectivities.

3.3 Laser Crystal Holders:

The next problem encountered was the actual support of the laser crystal in the pumping configuration. Coupled directly to this problem is a consideration of cooling methods, but this discussion will necessarily be deferred until the next section.

As mentioned in Chapter I, the crystal was to be positioned coaxially with respect to the FT-524 helical flashtube and cylindrical reflector. This could be achieved by the use of glass tubes. Available in the Fall, 1962, was a triple-jacket crystal holder (figure 3.4). The central jacket supported the laser crystal and was filled with helium gas, the

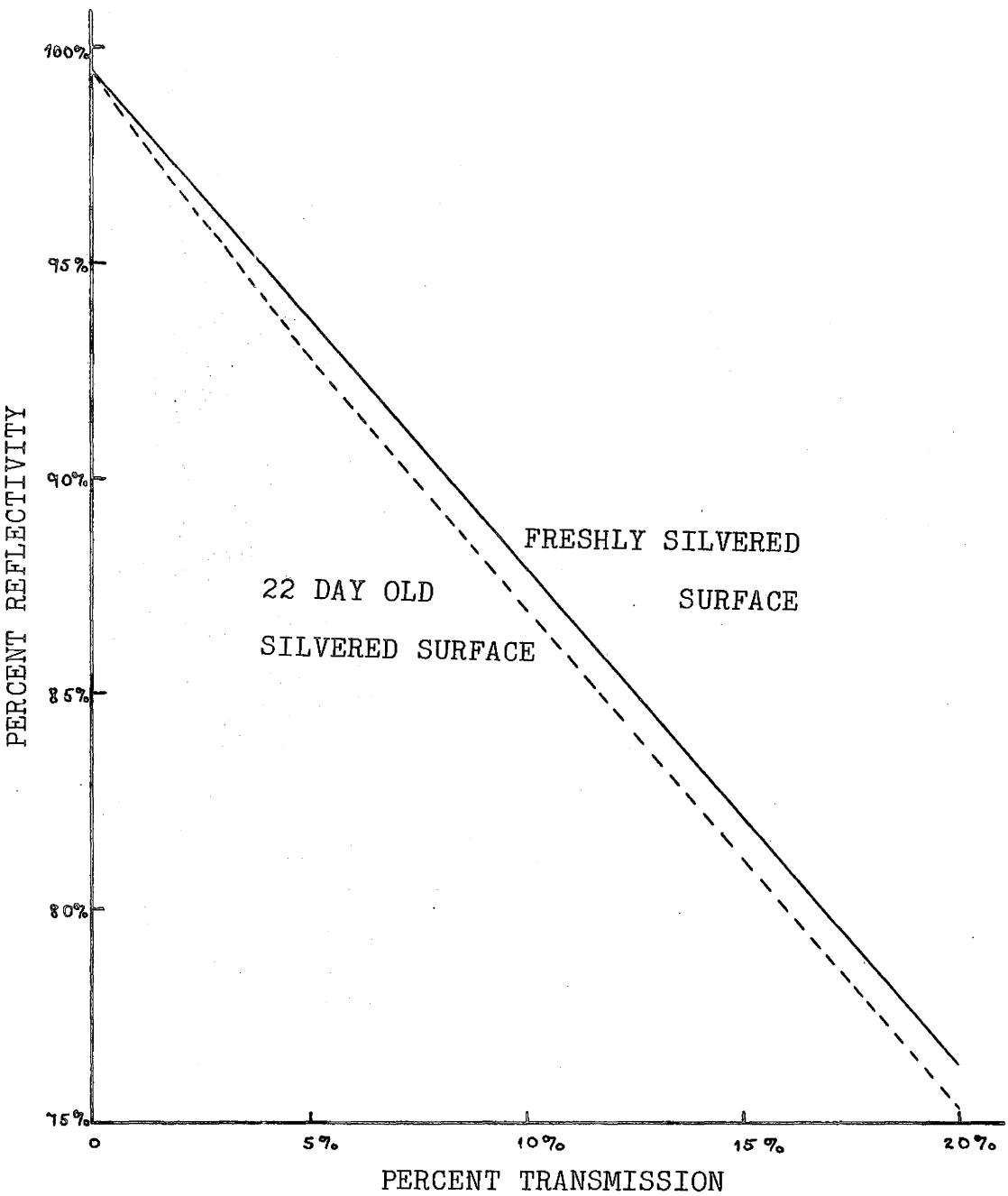

FIGURE 3.3

REFLECTIVITY VERSUS TRANSMISSION FOR SILVER, AFTER KUHN AND WILSON (KW1)

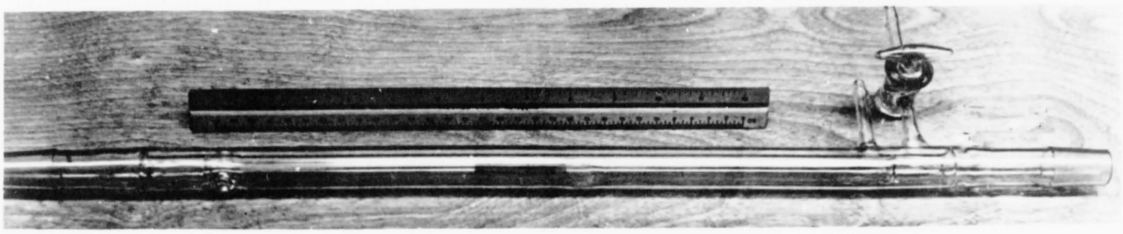

FIGURE 3.4

A TRIPLE-JACKET CRYSTAL HOLDER

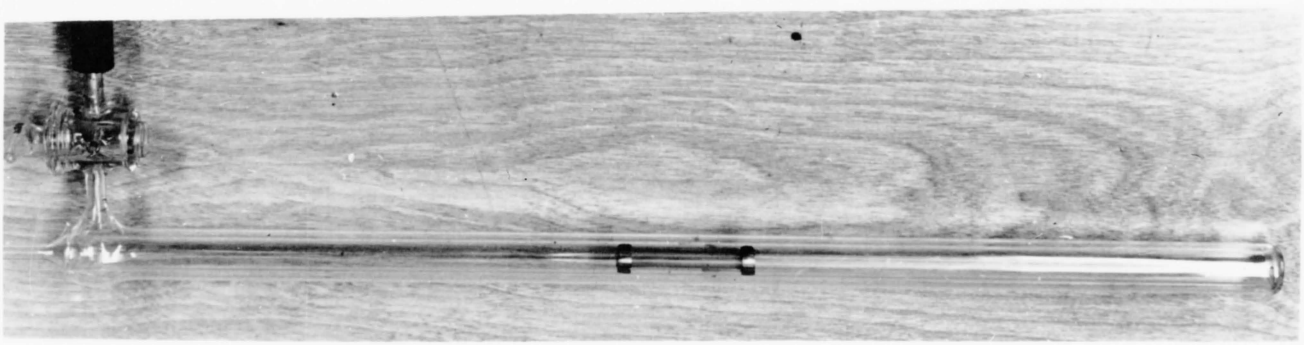

FIGURE 3.5

A DOUBLE-JACKET CRYSTAL HOLDER

purpose of which was to aid in heat transfer from the laser crystal to the second jacket and to eliminate any water vapour that might be frozen out at low temperatures. Cooling vapours were passed through the second jacket to cool the inner jacket and the laser crystal. The third jacket (the outermost) was continuously evacuated to avoid frosting on the cold glass surfaces of the second jacket. However, laser action could not be induced with this system. The reason, it was conjectured, was the reflection of the pump light by three layers of glass or the age of the flashtube.

With the acquisition of new flashtubes, a single-jacket crystal holder was employed and with this combination, laser action was detected at room temperatures and below. Cooling was employed by passing cool vapours through the jacket and around the crystal, and the glass walls around the crystal were kept defrosted by firing the flashtube every thirty seconds. Minimum temperatures achieved, as measured by a copper-constantan thermocouple, were in the vicinity of 182^{o}K.

To minimize reflection losses and maximize insulation to avoid frosting, a double-jacket crystal holder was constructed (figure 3.5). The crystal was supported in the central jacket by two spring-loaded brass rings with wide slots in the circumference to allow cool vapours to pass around the laser crystal and out the other end of the crystal holder. Surrounding this jacket was the second which was evacuated continuously to insulate the inner jacket and avoid frosting.

This was the system used for most of the experimental results quoted later in the thesis.

3.4 Temperature Control:

Another desirable feature of our experimental set-up was the facility of varying the temperature of the laser crystal from liquid nitrogen temperature (78°K) up to room temperature (300°K). To achieve this end, several methods were tested but the most versatile proved to be the following: a heater, immersed in the liquid air, contained in a liquid air dewar, was used to boil off vapours which were directed through a short length of rubber tubing to the crystal holder.

The first heater used was constructed in the Summer of 1962. It consisted of a long coil of nichrome wire which passed down the length of the heater element and back up again. The heater element, about one and one-half feet in length was enclosed in a one-half inch copper sheath and suspended by a long copper tube (one-quarter inch) so that the heater element was close to the bottom of the dewar. Asbestos matting and mica sheets served to electrically insulate the nichrome coil from the copper walls of the heater element and the return coil. Currents up to three amperes at seventy volts could be delivered to this heater. A large diameter rubber tube sealed off the neck of the dewar, forcing the vapours out of the dewar and through the crystal holder.

The temperatures attained were measured by a copper-

constantan thermocouple. The reference temperature was an ice bath ($0^{o}C$) and the potential difference was measured by means of a Honeywell Potentiometer (Model 2733). Using the double-jacket crystal holder and this heater, a minimum temperature of $135^{o}K$ was achieved.

Also available was another heater of much the same design but with a heater element only nine inches long. This heater was then lower in the liquid air and could therefore be used with less liquid air in the dewar.

However, both heaters had disadvantages. Because the process of boiling off the liquid air was indirect, the response time of the temperature in the crystal holder to a change in the current was long. That is, an increase in current increased the temperature of the copper sheath. This increased the boil-off rate of the liquid air with the result that the temperature decreased. This time delay involved in heat transfer made temperature stabilization difficult. The second problem was intermittent shorting to the copper sheath caused by overheating of the insulation.

As a result, a new heater (figure 3.6) was constructed which proved very satisfactory. A layer of Kyanex Refactory Cement (nine inches long) was moulded around one end of a one-quarter inch copper tube which electrically insulated the coil of nichrome wire, wrapped around the Kyanex, from the copper tube. Two insulated wires passed down the length of the copper tube: one passed out through a hole just above the heater

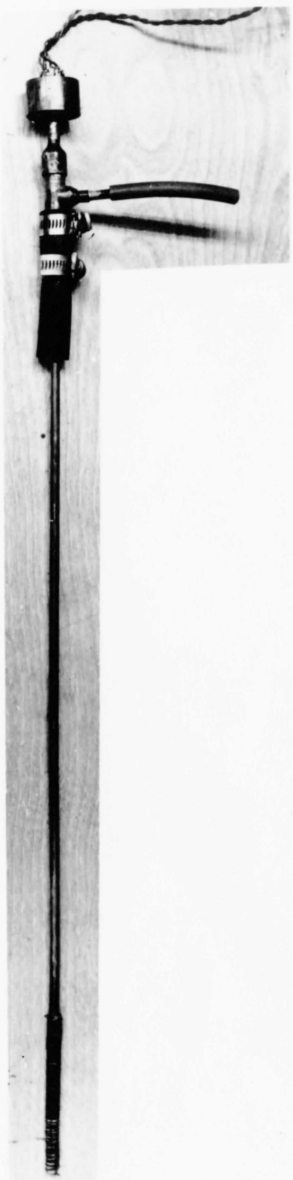

FIGURE 3.6

THE HEATER USED FOR COOLING THE LASER CRYSTAL

element and was connected to one end of the coil; the other passed out through the bottom of the copper tube and was connected to the other end of the heater coil. External electrical connections to a variac were made through a ten-lead Kovar seal, and the vapours were directed to the crystal holder as previously. The resistance of the coil was measured to be 14 ohms. With this heater, the coil itself heated the liquid air, ensuring a fast response time. At the same time, the liquid air kept the lead-in wires cool so that the chances of shorting or of burning out the coil were reduced.

To ensure that the level of the liquid air would not fall below the top of the heater, another copper-constantan thermocouple was inserted inside the copper tube with the junction just above the heater coil. An eight-ampere fuse was placed in the heater circuit. (The electrical circuit for the heater is shown in figure 3.7.) The double-pole, double-throw (DPDT) switch allows temperatures above and below $0^{o}C$ to be measured. The push-button switch enables the crystal temperature (button up) and the temperature just above the heater (button down) to be measured.

With this heater, the response time was much improved such that one could maintain the temperature at any desired value down as low as $95^{o}K$.

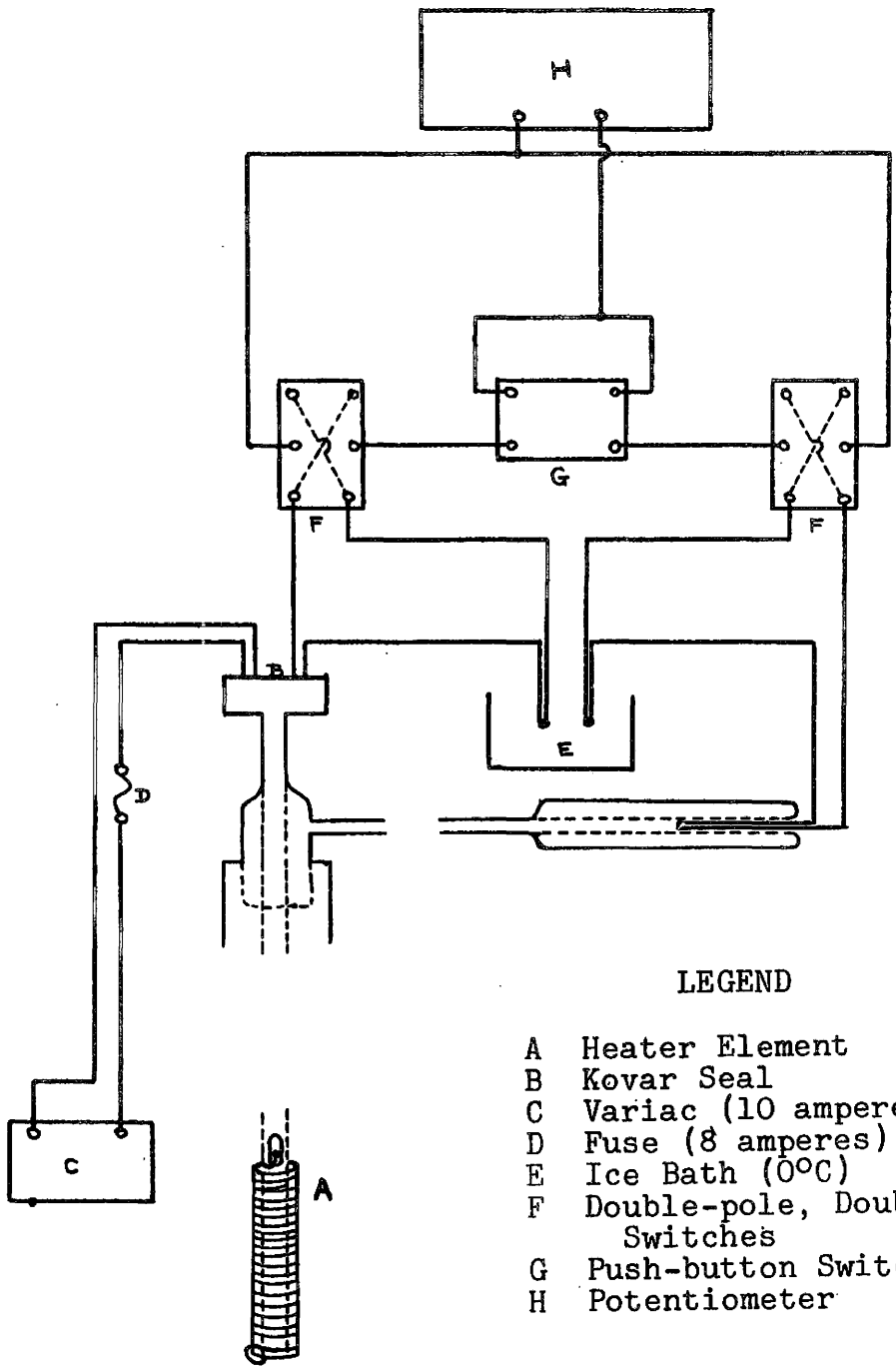

LEGEND

A Heater Element
B Kovar Seal
C Variac (10 amperes max)
D Fuse (8 amperes)
E Ice Bath (0°C)
F Double-pole, Double-throw Switches
G Push-button Switch
H Potentiometer

FIGURE 3.7

THE ELECTRICAL CIRCUIT ASSOCIATED WITH THE HEATER

3.5 Power Measurement:

With regard to the reading of the power supply voltages, it should be noted that the calculations of Statz and deMars (Sd1), Bostick and O'Connor (BO1), and all other papers discussed in Chapter I utilize the parameter of P/P_o, that is the power over the threshold power. Because the power is proportional to the square of the voltage, the error in power is twice the voltage error. Hence, the error in the ratio of P/P_o is four times the error in a voltage measurement. The problem is particularly acute in the analysis of Bostick and O'Connor where the term (P/P_o-1) occurs (equation 1.76). Since P/P_o is close to 1, the relative error associated with this term can easily be in the order of 1000%. An analogous problem occurs in considering the errors associated with the reflectivity where the term 1-R occurs (equation 1.47).

In an attempt to reduce this power measurement error, a resistor chain of five 4.02 megohm presistors (1%) was connected across the power supply output and a microammeter (200 microamperes full scale) measured the current through this chain. In a consideration of errors, the resistance of the chain was measured (accurate to three figures) to be 20.16 megohms. The heating effect due to current flow should produce no change in resistance. (The power dissipated across each one-half watt presistor at 200 microamperes is 0.16 watts.) A slight error was introduced by the heat due to the environs; after six hours the resistance was measured to decrease to 20.01 megohms, a drop of 0.75%

Concerning the microammeter, it has a class figure of 0.5% of full scale. Including the reading error and zero error, the maximum possible error on each current reading is ± 1.4 microamps or, for 3.1 kilovolts, ($\equiv 150$ microamperes) the relative maximum possible error is 0.93%. Hence, the error on a power measurement is roughly 2%. We have indications that these maximum possible errors are too high on two accounts: threshold can be duplicated to well within one microampere and the shape of threshold curves can be determined to be similar well within the experimental errors. (See, for example, figures 3.20 and 3.21.)

3.6 Detection of Laser Action:

A 925 S-1 response vacuum phototube, with a 90 volt supply and a one kilohm load resistor, was used to detect laser action. Taped to the front of the phototube was a narrow band-pass Baird-Atomic 730 multi-dielectric filter, necessary to filter out most of the pump light. The signal taken across the load resistor was fed directly to the Y-input on an oscilloscope. (The oscilloscope used was a Dual-Beam Tektronix Model 555 with a single sweep and a delay trigger function.) A Polaroid camera could be mounted on the oscilloscope screen to photograph the trace using a film with an ASA rating of 3000.

For low temperature experiments, it was necessary to protect the filter and phototube from the cold air jet emerging

from the crystal holder. The introduction of a glass plate in front of the phototube did not attenuate the oscilloscope signal and frosting was prevented by directing tap air or a fan at the back surface of the plate.

3.7 The Structure of the Laser Output:

(See figure 3.8 for the format adhered to in order to convey the experimental conditions under which a photograph is taken.)

Laser action was first detected on December 24, 1962, using the double-jacket crystal holder at a voltage of 3.3 kilovolts as measured on the power supply meter. Figure 3.9 shows laser action close to threshold pump-power at room temperature. Of interest was the initial time of laser action, its duration, and the light pulse on which laser action was superimposed. As mentioned in the theory, time is required to build up a population inversion which will sustain laser action. The time required in this case was roughly 0.6 milliseconds; the duration of laser action is, here, 0.4 milliseconds. The background light pulse of figure 3.9 has two possible sources: the pump light or fluorescence. The trace decays in about 2 milliseconds, and since the fluorescent decay time is about 3 milliseconds, one can conjecture that fluorescence does not contribute substantially to the light pulse. Figures 3.10a and 3.10b further demonstrate this fact. The former is the trace for no crystal in the crystal holder; the latter is

TEMPERATURE* °K	VOLTAGE INPUT (kilovolts)	DELAY SETTING
A TIME BASE Time/cm	Volts/cm	THRESHOLD VOLTAGE (kilovolts)
B TIME BASE Time/cm	Volts/cm	PERCENT POWER ABOVE THRESHOLD

*RT denotes room temperature.

FIGURE 3.8

FORMAT OF EXPERIMENTAL CONDITIONS ASSOCIATED WITH EACH PHOTOGRAPH

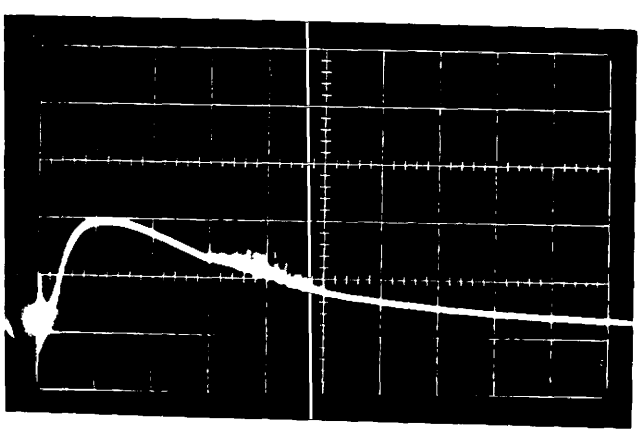

RT 3.3 Kv

.2ms/cm 1v/cm

FIGURE 3.9

LASER ACTION CLOSE TO THRESHOLD

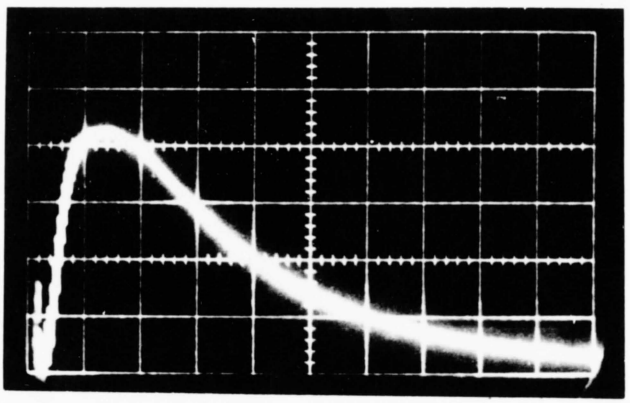

RT 3.5 Kv

.2ms/cm .5v/cm

FIGURE 3.10a

THE TRACE FOR THE LASER CRYSTAL OUT OF THE HOLDER

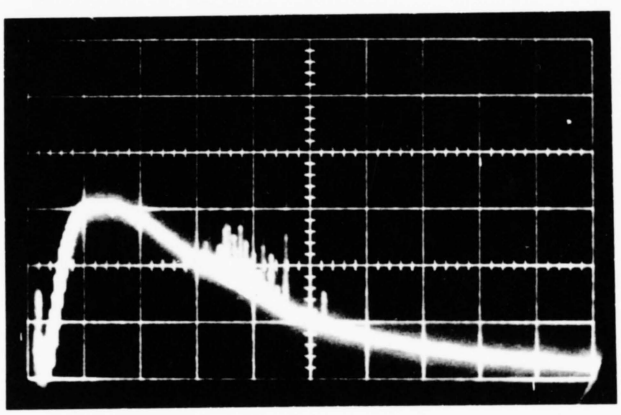

RT 3.5 Kv

.2ms/cm .5v/cm

FIGURE 3.10b

THE TRACE WITH THE LASER CRYSTAL IN THE HOLDER

the trace with the laser crystal in place. The reduced amplitude is probably due to the absorption by the crystal, but the decay time for both remains the same, indicating the light pulse is derived from the pump.

In order to study the laser output in more detail, one utilizes the time base B and the delay trigger on the Tektronix Oscilloscope. Time base A is usually set to 0.1 or 0.2 milliseconds per centimeter so that the whole laser pulse may be seen. The delay trigger can then be set to delay the triggering of the B trace until the beginning of the laser action so that the B trace can have a much faster sweep speed, down to one microsecond per centimeter. Using this function then, one can display the laser pulse on one trace and the expanded laser pulse on the second trace, as in figure 3.11. The third trace shows a bright-up pulse to indicate the area that has been expanded. (The arrows more clearly indicate the location of the bright-up pulse.) This picture was taken at room temperature with the single-jacket crystal holder.

Figure 3.12 shows the regular spiking period obtained at room temperature, close to threshold. Again the bright-up pulse indicates the area expanded. From this information, or using the setting on the delay and the A time base, one can calculate the initial time of laser action. In this case, it is 0.583($\pm$3%)milliseconds. Figure 3.13 was obtained under identical conditions from which one can see that the initial time of lasing and the period are quite reproducible. The period is

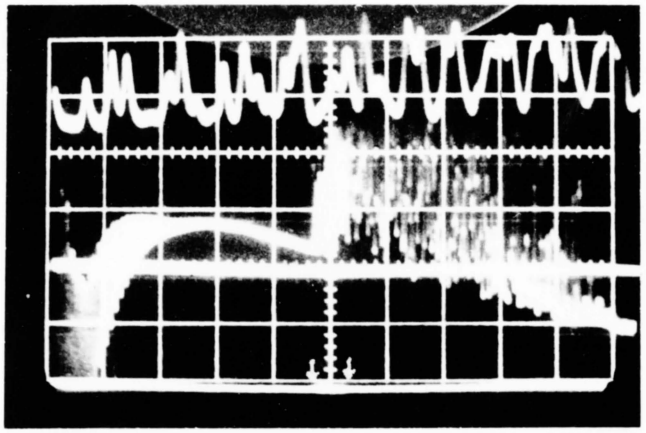

RT 3.4 Kv
.1ms/cm .1v/cm
5μs/cm .1v/cm

FIGURE 3.11

LASER OSCILLATIONS ON THE EXPANDED AND NORMAL SCALES

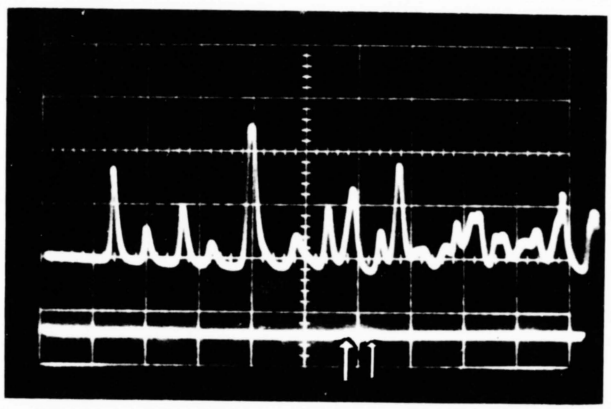

RT 3.2 Kv 5.76
.1ms/cm
5μs/cm .05v/cm

FIGURE 3.12

REGULAR SPIKES CLOSE TO THRESHOLD

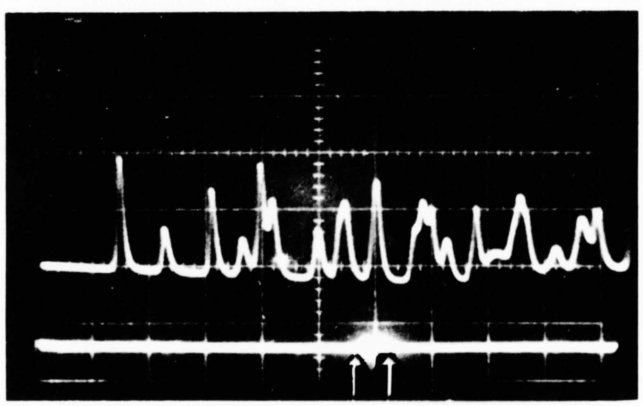

RT 3.2 Kv 5.76
.1ms/cm
5μs/cm .05v/cm

FIGURE 3.13

A TEST OF REPRODUCIBILITY OF INITIAL TIME OF LASER ACTION AND OF THE PERIOD

~ 4 microseconds which is roughly that reported by Statz et al. (SLSC1).

Figure 3.14 shows clearly the characteristics associated with high pumping powers. The regular spiking pattern is clearly upset almost as soon as oscillation begins with the onset of other modes. The initial time of laser action is earlier for higher powers; here for example, the first pulse occurs 0.396 milliseconds after the flashtube is triggered. Further, the baseline on which laser action occurs rises as the spikes occur more and more frequently. A comparison of figures 3.15, well above threshold, and 3.16, much closer to threshold, further demonstrate this feature. As is noted, for figure 3.15 the power is the same as for figure 3.16 but the temperature for the former is 155°K compared to 262°K for the latter. This observation indicates an increase in threshold with temperature, a result expected from the discussion of section 1.3. Note also the change in the Y sensitivity.

3.8 The Determination of Oscillation Threshold:

One phase of the research was to assess the validity of the approach and predictions of Bostick and O'Connor's theory to our ruby crystal. At this point our interest was focused on the initial time of laser oscillation as predicted by equation 1.77,

$$\frac{P}{P_0}\left[1 - \exp\left(-\frac{t}{\tau}\right)\right] = 1, \qquad 1.77$$

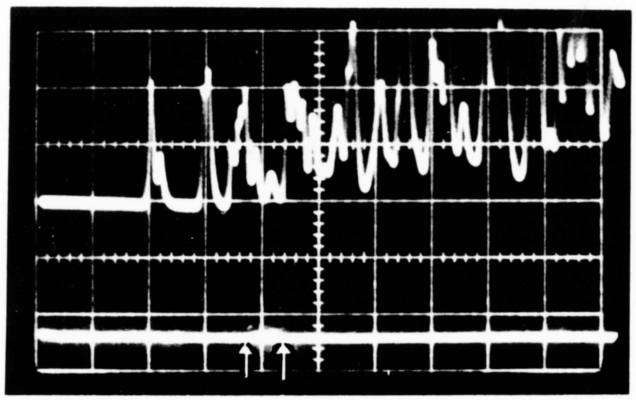

RT 3.6 Kv 3.86

.1ms/cm

5μs/cm .05v/cm

FIGURE 3.14

A TYPICAL SPIKING PATTERN WELL ABOVE THRESHOLD

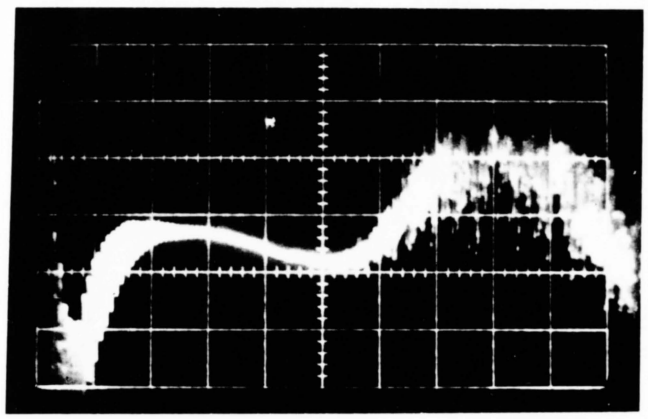

155°K 3.4 Kv

.1ms/cm .1v/cm

FIGURE 3.15

OVER-ALL LASER ACTION WELL ABOVE THRESHOLD

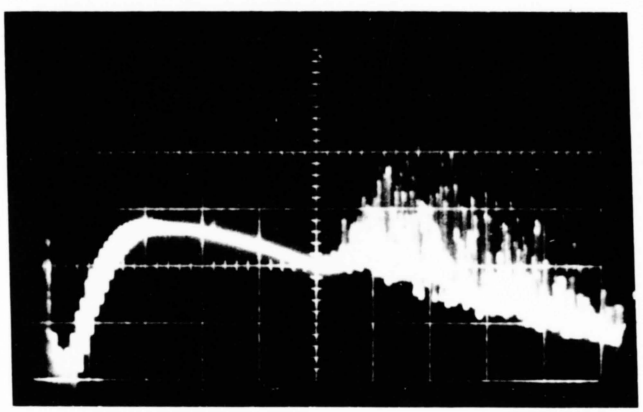

262°K 3.4 Kv

.1ms/cm .2v/cm

FIGURE 3.16

OVER-ALL LASER ACTION CLOSE TO THRESHOLD

and so, as a preliminary test of this theory, experimental parameters were substituted into equation 1.77 and the left hand side was compared with the value 1. (See Chapter IV.)

To apply this equation directly to our results, it was necessary to have a measure of P_o. The experimental difficulty here was that of seeing the first few spikes just at laser threshold on the oscilloscope screen. The first requirement was a large Y-plate sensitivity but recalling that laser oscillations were superimposed on a slowly decaying "DC" potential, the trace was greatly displaced vertically and had a large slope with a high Y-plate sensitivity. Also, to see the oscillation structure, the X-plate sensitivity had to be rather large, about five microseconds per centimeter. Recalling also that, as one approaches threshold, the initial time of laser action increases, one can see that the delay time was also a critical parameter. Further, the initial time of laser action varies with temperature. Hence, for every combination of temperature and power, the vertical position and the delay time must be adjusted by trial and error, and both these adjustments are interdependent. A typical result is shown in figure 3.17.

Thresholds were measured over the temperature range of 150°K to 223°K using the double-jacket crystal holder. The resulting plot is shown in figure 3.18. The results do not, even within maximum possible errors in the meter readings, form a smooth curve, particularly those points at higher tem-

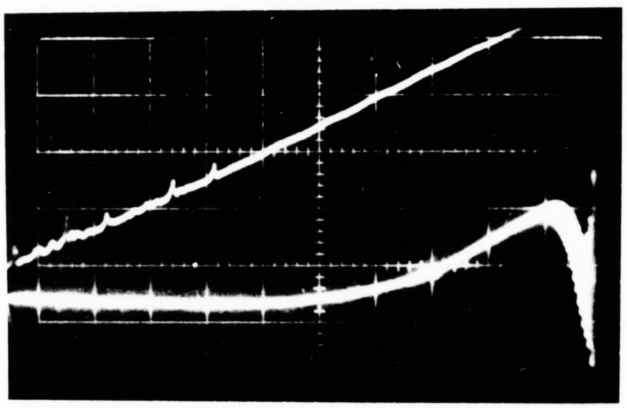

196°K 3.10 Kv 2.95

.2ms/cm .5v/cm 2.98 Kv

10μs/cm .02v/cm 8%

← TIME

FIGURE 3.17

AN ILLUSTRATION OF THE DIFFICULTY IN MEASURING THRESHOLD AT LOW TEMPERATURES

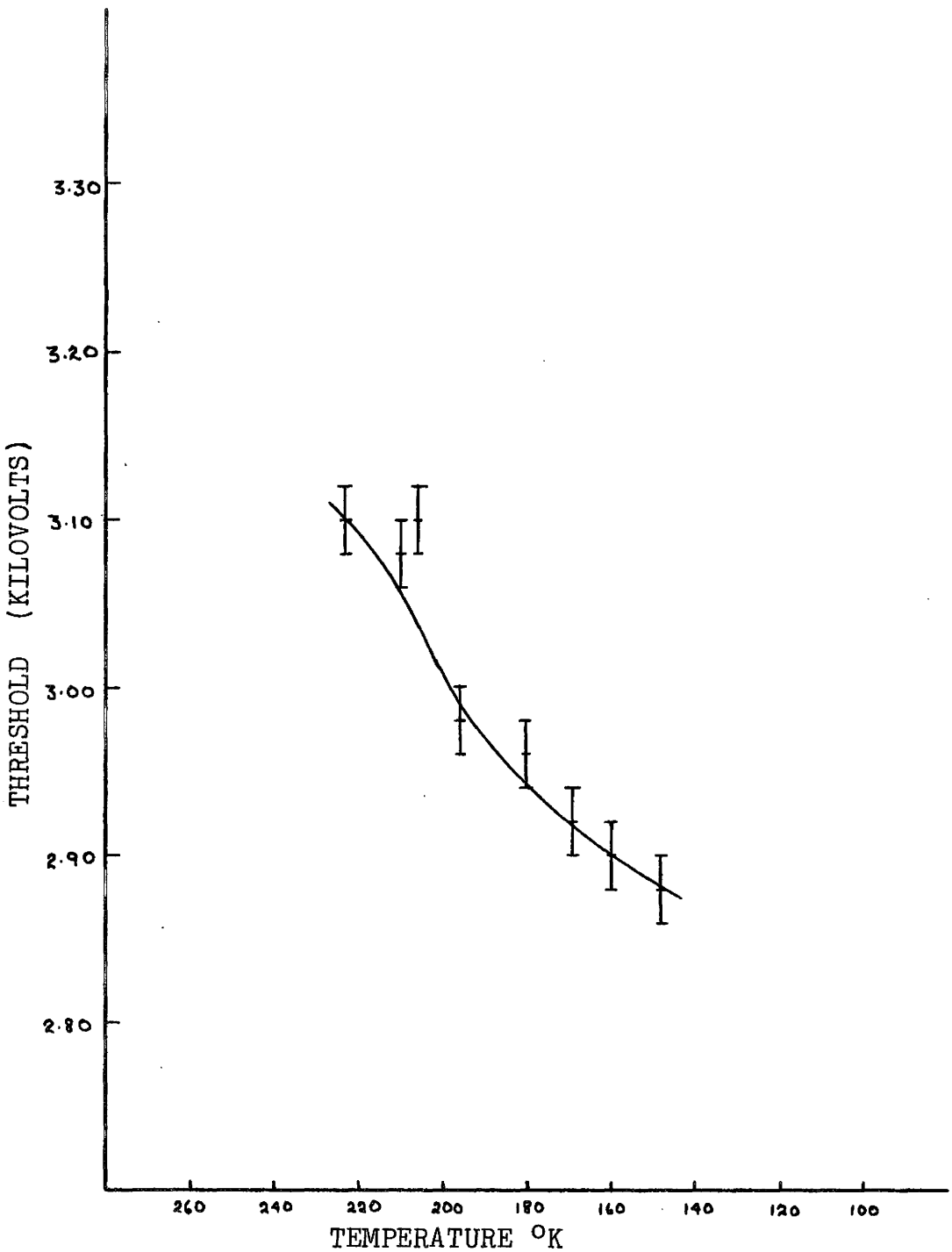

FIGURE 3.18

THE FIRST PLOT OF THRESHOLD VERSUS TEMPERATURE

peratures. The application of equation 1.77 is also seen to show very large disagreement. (See Chapter IV.)

Figure 3.18 illustrates the need to improve our measurements of threshold. To eliminate the vertical position adjustment, the phototube output was passed through a differentiating network (1000 picofarad capacitor and 3.0 kilohm resistor) which removed the pump pulse from the output but passed the laser spikes. The laser oscillations then typically resembled those of figure 3.19.

Further aid was sought in the use of a Technical Measurement Corporation Differential - Integral Pulse Height Selector and SG-3A Scalar. This scalar was observed to give out a count of 100 pulses or more well above threshold, but close to threshold, as few as three or four pulses were detected. However, close to threshold the counter was unreliable in that it would sometimes not detect any pulses, whereas a few pulses would be seen on the oscilloscope. The input to the pre-amplifier stage was required to have no DC component and only negative pulses. The trigger level was set just above the noise level.

The procedure used to plot threshold curves was this: if pulses were seen on the oscilloscope or detected by the Pulse Height Analyzer, the input power to the flashtube was above oscillation threshold. The voltage of the power supply was reduced in 20 volt steps (one microampere) until no pulses were seen or counted. Then laser threshold was taken

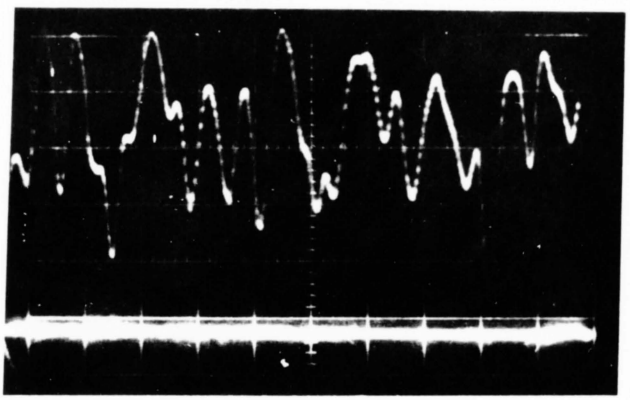

$140^{\circ}K$ 3.30 Kv 3.00

.2ms/cm

1μs/cm .005v/cm

- 10 counts on timer

FIGURE 3.19

LASER OSCILLATION ON AN EXPANDED SCALE WITH THE DIFFERENTIATING CIRCUIT

to be at the point halfway between these last two voltages. Graphs of threshold (kilovolts) versus temperature are shown in figures 3.20 and 3.21. Note the same general shape of each with a slight flattening tendency in the vicinity of 180°K. This shape is predicted by D'Haenens and Asawa (DA1) (figure 3.22) for high f values where

$$f = \frac{\ln 1/r}{\alpha_o l} = \frac{N_2 - N_1}{N_o}, \qquad 3.2$$

using equations 2.75 and 1.34. However, for the plot shown in figure 3.21, the reflectivity had been measured and f was calculated to be 0.004, a very low value. This apparent paradox will be resolved in Chapter IV.

A Beckman Universal E/Put and Timer (Model 7370) further facilitated threshold determinations. The frequency response was 10.5 megacycles (or 0.1 microseconds), well within the time resolution of the laser pulses. This counter has many functions but the most useful to us for threshold measurements was the E/B function. Here the signal was placed in the E terminal, while the square wave gate output from the oscilloscope (corresponding in time to the expanded scale) was placed in the B and A terminals, the on- and off-gate respectively. To measure thresholds, the E signal had to be attenuated by a factor of 10 to cut out the noise, and the B input was set to trigger on a positive slope, the A on a negative slope. A schematic of the laser detection system

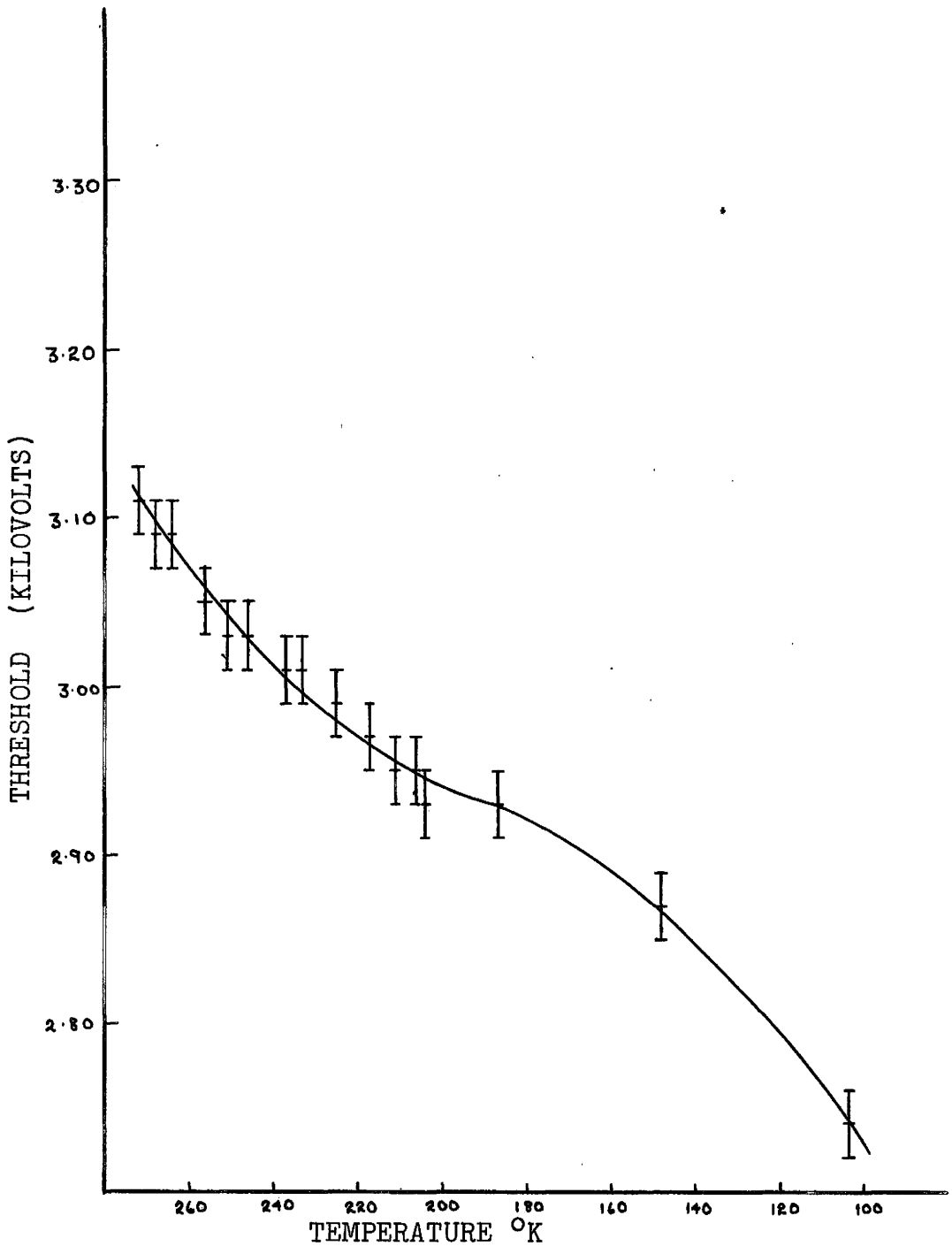

FIGURE 3.20

AN IMPROVED THRESHOLD CURVE, OBTAINED WITH THE AID OF A PULSE HEIGHT ANALYZER

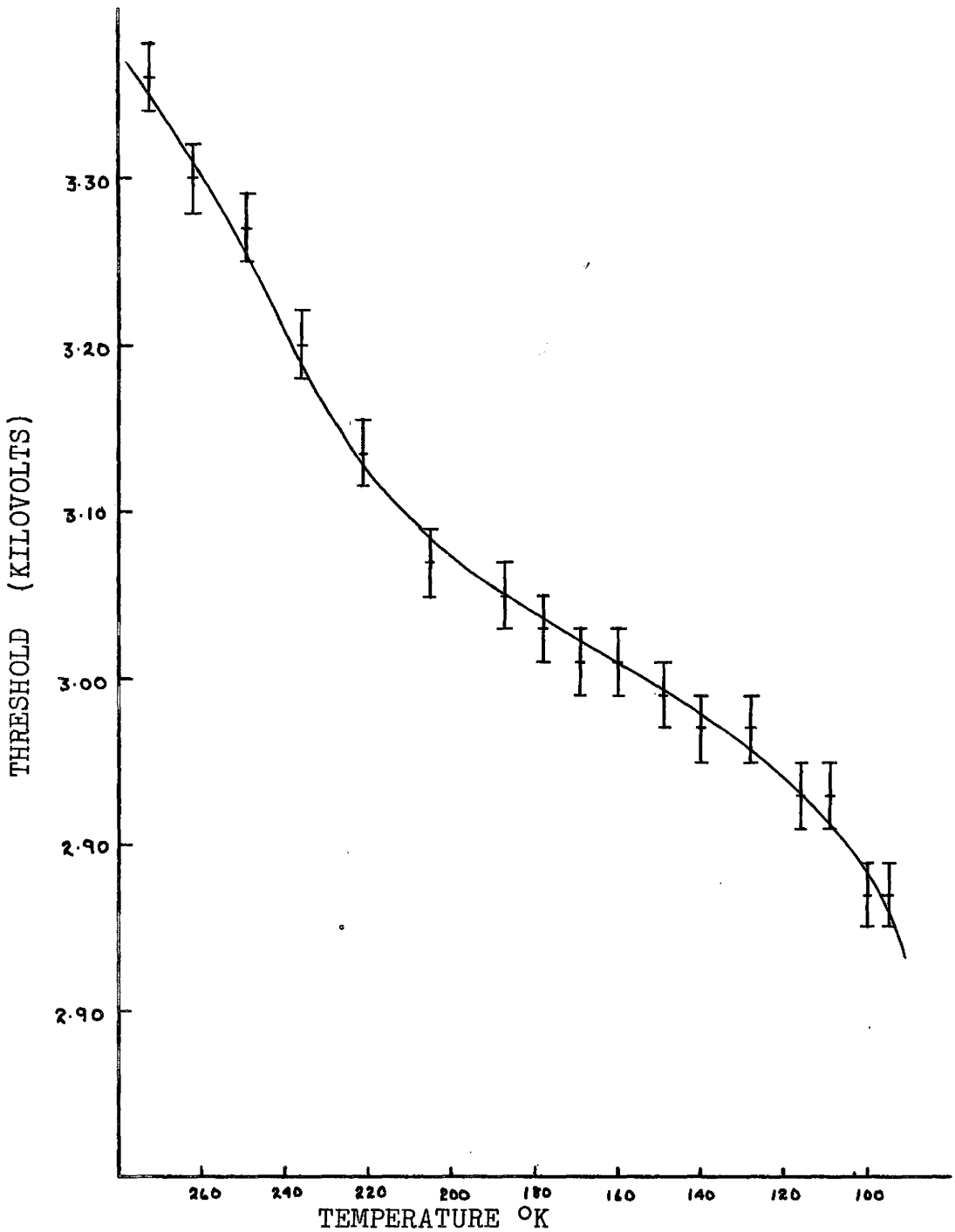

FIGURE 3.21

THRESHOLD CURVE FOR R_1 = 99.5%, R_2 = 98.7%

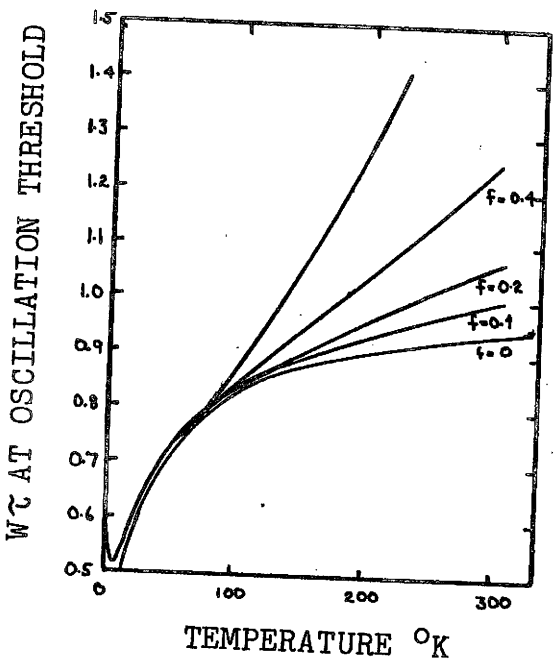

FIGURE 3.22

THEORETICAL THRESHOLD PLOTS FOR CERTAIN f VALUES, AFTER D'HAENENS AND ASAWA

described above appears in figure 3.23.

A much more consistent approach to threshold, as compared with the results of the Pulse Height Analyzer, was observed. A typical result is illustrated in the table below: for a temperature of 116°K., R_1=99.4%, R_2=97.8%, and a counting period of one millisecond,

Voltage	Number of Counts
3.02 Kv	101
2.98 Kv	70
2.94 Kv	20
2.92 Kv	6
2.90 Kv	1
2.88 Kv	0

Threshold was then taken to be 2.89 Kv for these conditions.

The threshold curve resulting from the use of the Beckman Counter is shown in figure 3.24. Note the tendency towards a more linear slope at high temperatures and a lower slope for a lower reflectivity (the reflectivity being reduced from its previous value (see figure 3.22) by aging.

These threshold curves are acceptable for our investigations and the procedure of using the Beckman Universal Timer and the oscilloscope was adopted throughout the remainder of the thesis.

3.9 Period Determination:

The analysis of photographs of the laser oscillations on an expanded scale was one approach to period determination. However, consideration was given to the feasibility of measuring the period with the Beckman Universal Timer. By the use

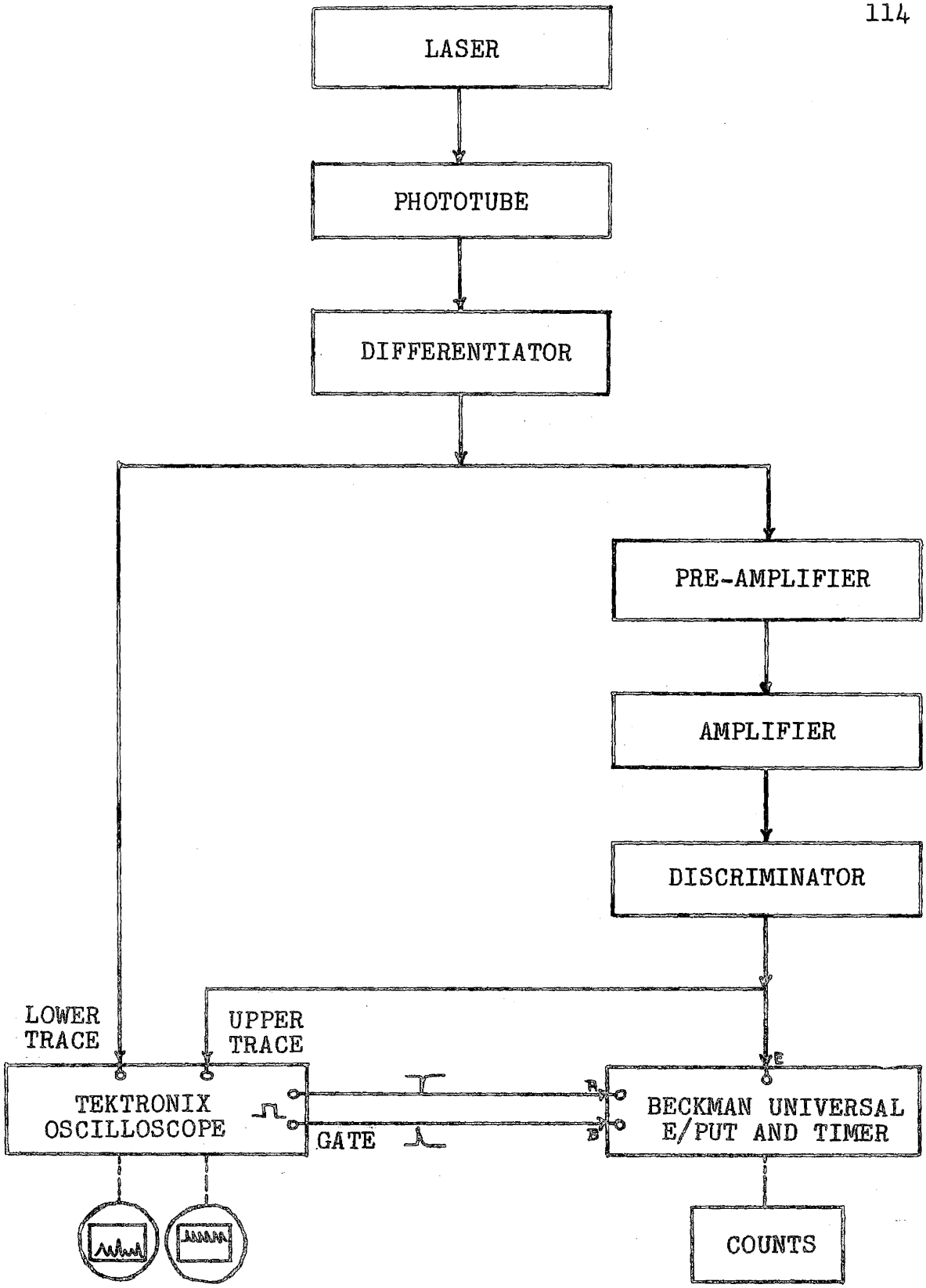

FIGURE 3.23

A SCHEMATIC OF THE LASER DETECTION SYSTEM

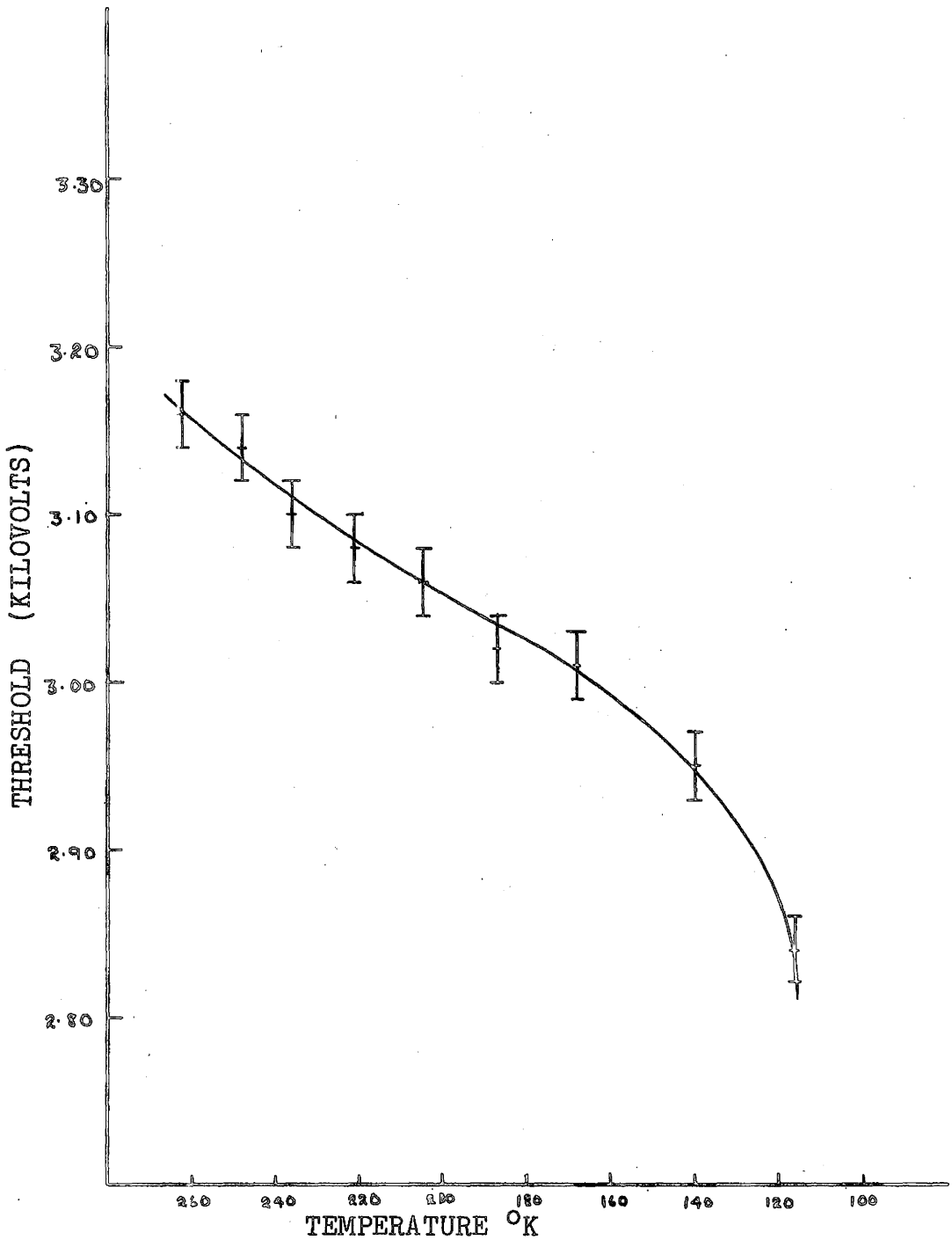

FIGURE 3.24

THRESHOLD CURVE USING A BECKMAN UNIVERSAL TIMER

of the on-off gates coupled to the expanded scale on the oscilloscope, one can determine the number of pulses counted in a certain time interval.

Because of the irregularity in the spiking period with the onset of multi-moding, it is desirable to expand only that region just after initial laser action where the pulses tend to be more regular. For powers a few percent above threshold, this is a very small region. Further, one must ensure visually on the oscilloscope that laser action has begun when the counter is triggered, otherwise the measured period will be longer than the actual period. Hence, the delay setting, the power setting and the temperature are all critical parameters. Using this technique a plot of the period versus the input voltage was made (figure 3.25). The errors shown are the maximum deviations observed for three or four measurements at the same temperature and power; the points shown are the averages of all the measurements made. One, therefore, expects a large error at powers close to threshold because of the extreme sensitivity of the period to the power in this range.

Let us investigate the validity of these results. The approach followed was to determine which laser spikes the counter saw. Figure 3.26 displays the discriminator output; the counter registered each of these forty pulses. The gaps, however, are a source of concern in that the pulses are irregular and the meaning of the term "period" loses some sig-

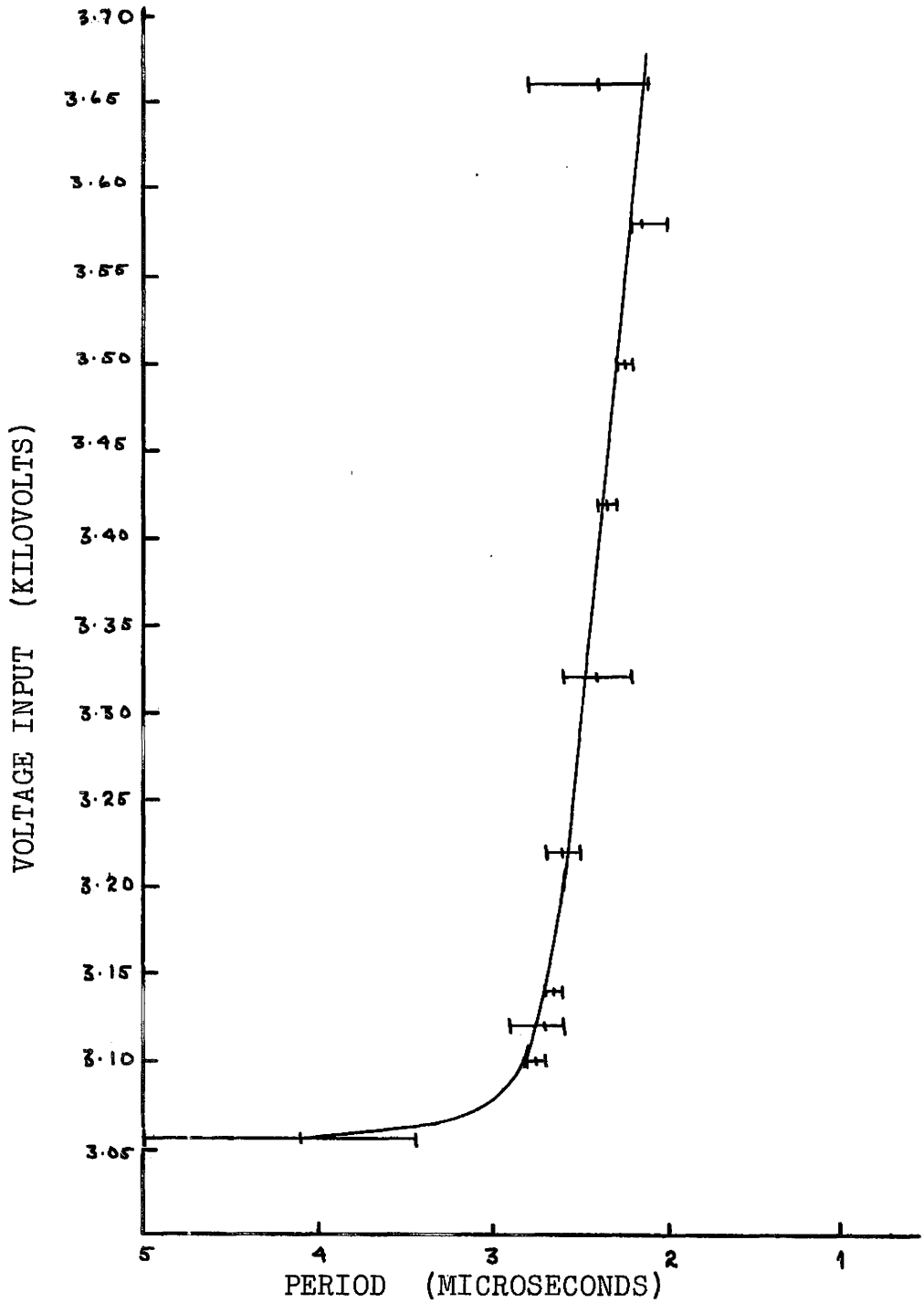

FIGURE 3.25

A PLOT OF PERIOD VERSUS VOLTAGE INPUT AT CONSTANT TEMPERATURE USING THE BECKMAN UNIVERSAL TIMER

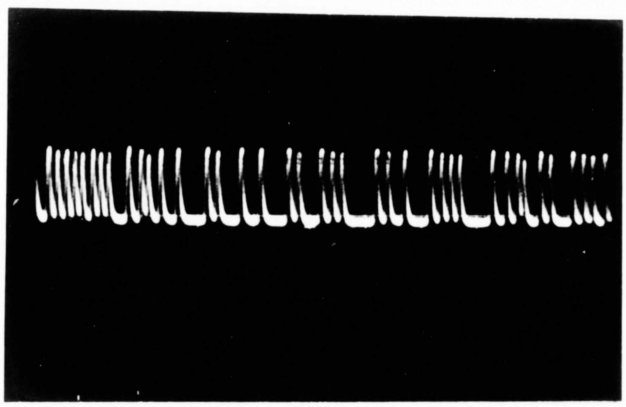

$140^{o}K$ 3.30 Kv 4.00

.2ms/cm

10μs/cm 20v/cm

FIGURE 3.26

THE OUTPUT FROM THE DISCRIMINATOR

nificance. In an attempt to discover which laser spikes were being detected, the laser output was photographed (figure 3.27), where full scale represents ten microseconds; the counter in this case registered six counts. The timer gives an oscillation period of 1.7 microseconds; the photograph gives a period of one microsecond. Figure 3.28 was obtained by placing both the upper and lower traces of the oscilloscope on the B time sweep of the Tektronix Oscilloscope, with the laser output on the lower and the discriminator output on the upper trace. Here, one can see that multi-moding on the first few laser spikes is not detected by the counter, but twenty microseconds later, this is not the case with the result that the period shortens considerably. The photograph in figure 3.29 illustrates the fallacy of relying solely on the timer for period determination. Despite the strong degree of multi-moding as expected at 11% power above threshold, in the first fifteen microseconds of laser oscillation, the discriminator sees only the regular spikes, giving a completely erroneous period.

On the basis of figures 3.27 and 3.29, the procedure used to determine the period was this: both the laser trace and the discriminator output were photographed and the former was used to help eliminate multi-moding effects.

Using a resilvered crystal (R_1=99.5%, R_2=86.2%), a threshold plot was made (figure 3.30) and the period was then measured for powers 1%, 3%, 5%, 7% and 9% above threshold,

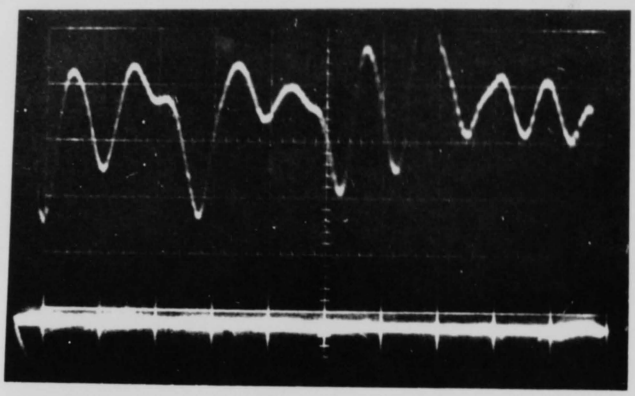

$140^{\circ}K$ 3.30 Kv 2.70

.2ms/cm

1μs/cm .005v/cm

- 6 counts registered on timer

FIGURE 3.27

A COMPARISON OF THE NUMBER OF LASER SPIKES AND THOSE COUNTED BY THE TIMER

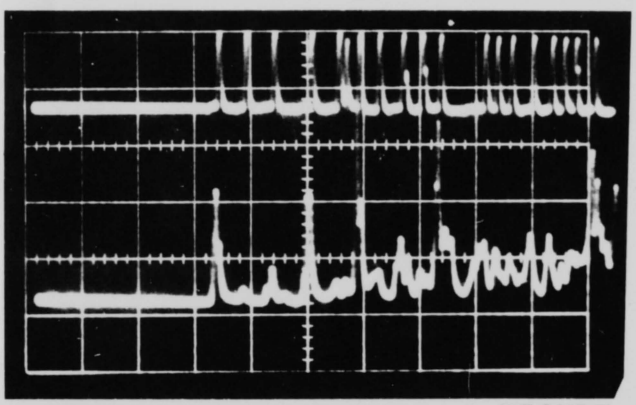

$180^{\circ}K$ 3.06 Kv 4.00

.1ms/cm 2.99 Kv

20v/cm

10μs/cm 5%

.1v/cm

FIGURE 3.28

A COMPARISON OF THE LASER OUTPUT AND THE COUNTER INPUT

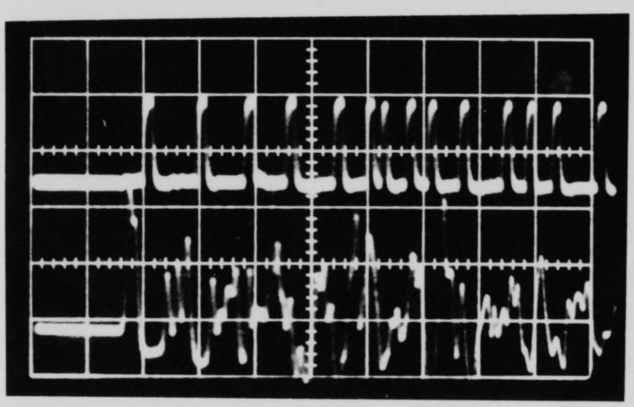

$187^{\circ}K$ 3.36 Kv 3.05

.1ms/cm 3.19 Kv

5μs/cm .5v/cm 11%

FIGURE 3.29

EVIDENCE OF AN ERRONEOUS PERIOD DETERMINATION AS CALCULATED FROM THE TIMER

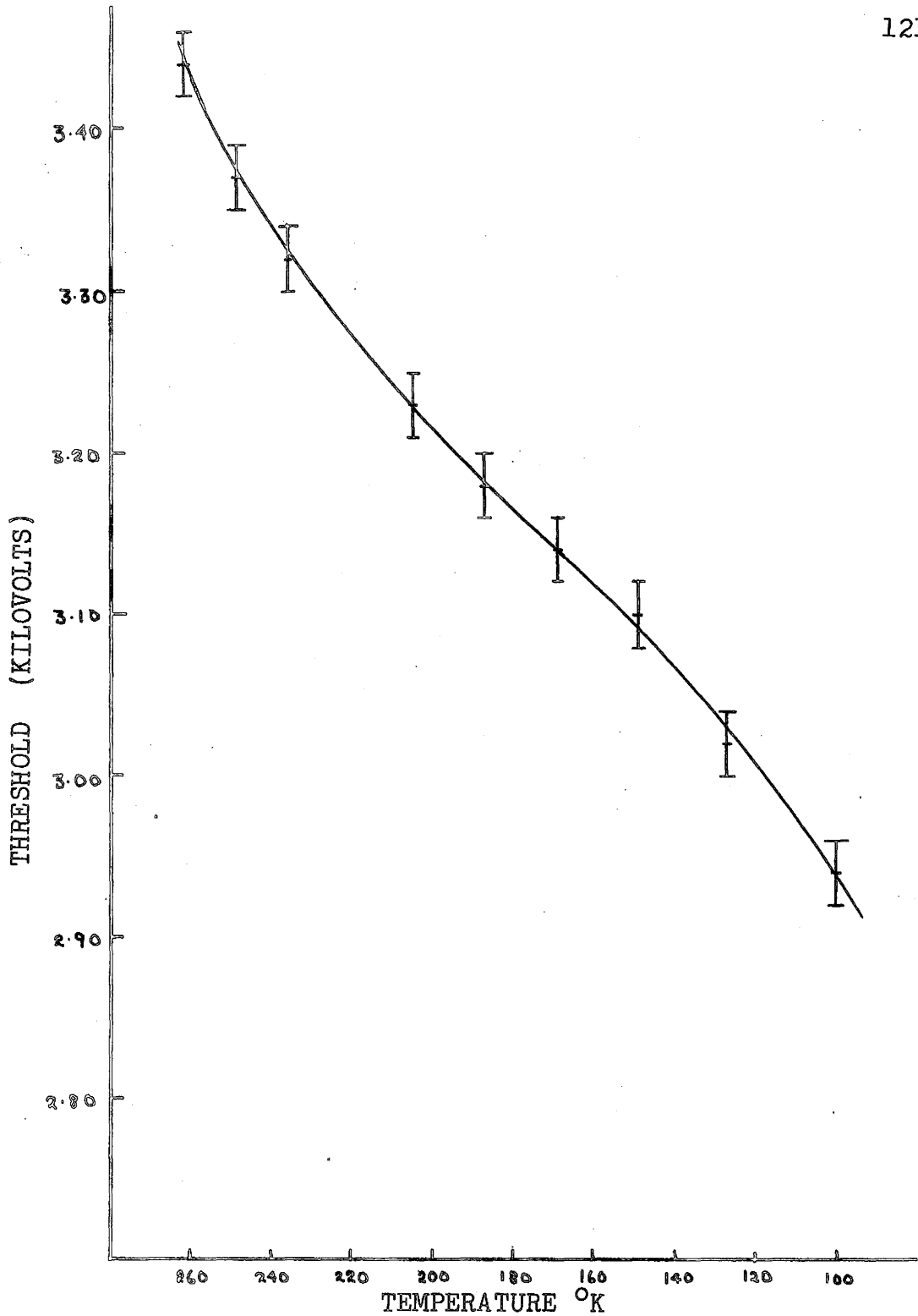

FIGURE 3.30

A THRESHOLD CURVE FOR R_1 = 99.3%, R_2 = 86.2%

and even higher where practical, at temperatures ranging from 100°K up to 262°K. Plots of the period versus power and the period versus temperature on the whole gave broken curves as illustrated in figures 3.31 and 3.32, as examples. We suspect the errors in these results are rather large as reproducibility was very difficult to achieve.

In summary we report that we can make measurements of these thresholds and periods at temperatures ranging between 100°K and 300°K. The error in the threshold curves is acceptable but the period determination is largely a matter of interpretation for our crystal, particularly at powers greater than 3% above threshold.

3.10 Measurements of the Scatter Loss for Our Ruby Crystal:

As indicated in Chapter II, scattering is an important loss parameter in laser analysis. Required for such a measurement is a powerful, monochromatic, collimated beam of light centred at a particular frequency. The frequency required must be chosen to avoid any absorption bands or lines in ruby and at the same time must be as close as possible to the laser frequency to avoid any complications with regard to scatter as a function of frequency. The light beam must be collimated so that no internal reflections are caused by the ruby crystal side-walls. The beam must be monochromatic in order to avoid absorption losses, as mentioned, and also must

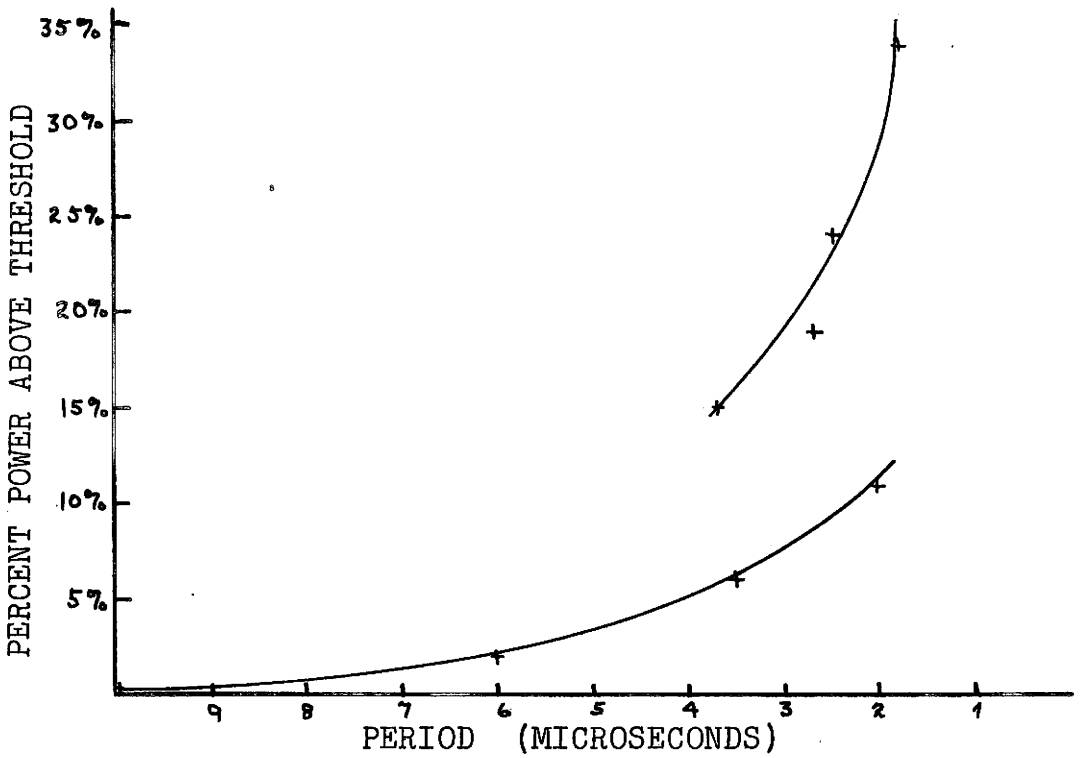

FIGURE 3.31

A TYPICAL PLOT OF THE PERIOD VERSUS THE POWER ABOVE THRESHOLD

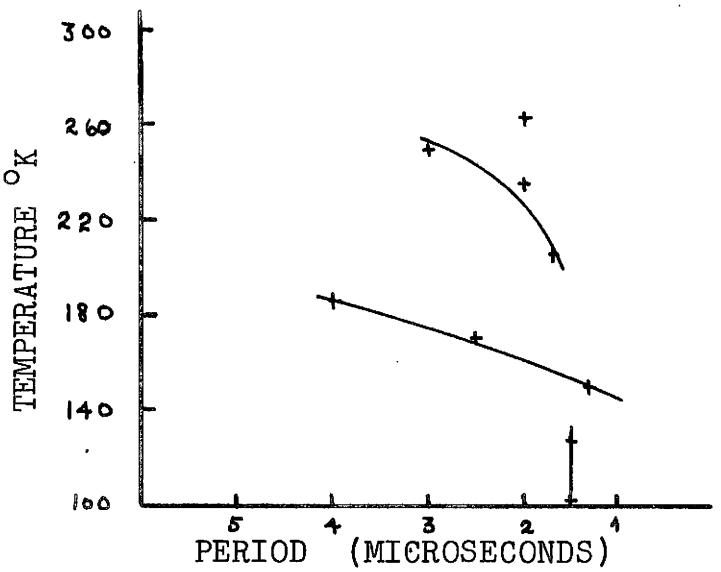

FIGURE 3.32

A TYPICAL PLOT OF THE PERIOD VERSUS THE TEMPERATURE

duplicate as closely as possible the scatter suffered by laser light. Finally, the most difficult requirement of all, experimentally, is sufficient power in a monochromatic, collimated beam of light to attain a detectable signal with a phototube.

The procedure used was to observe the loss of intensity due to the crystal in the light beam as compared with the intensity for the crystal out of the light beam. This loss of intensity is due to reflections from both end-faces of the laser crystal (a total loss of 15%) and due to scatter. Hence, scatter loss may be evaluated.

A crystal holder was machined from a steel block with a quarter-inch groove in the top surface, bored parallel to the bottom face, in which the crystal was placed. This crystal holder was then placed on an optical bench inside a grating spectograph (Bausch and Lomb Model No. 11-1.5 meters) the bench being shimmed until determined horizontal by a spirit level. A large stop was supported on the front face of the crystal holder and a variable diaphragm served as an entrance collimator. The whole system was painted black to reduce reflections. The signal was detected by the 925 S-1 type vacuum phototube, the signal being passed outside the spectograph to an amplifier (Maser Optics - Optical Pulse Detector Amplifier Model 361) through intercom wire. Grounding the outer casing of intercom wire to the spectograph and amplifier effectively reduced pickup in the signal. The

amplifier output was then placed on the oscilloscope.

Many different configurations were used in an attempt to satisfy the above requirements. Sources used for illumination included a carbon arc lamp, a cadmium arc lamp (6483A), and the xenon flashlamp, energized by the laser power supply. Narrowing of the spectral bandwidth was achieved with the aid of a monochromator, the spectograph diffraction grating and a Baird-Atomic multi-dielectric filter centred at 7300Å. (The transmittance of this filter as measured by the spectrophotometer, described in section 3.2, at 7000Å was effectively zero.)

The only combination powerful enough to produce a signal sufficiently far above the noise level was the system composed of the flashtube, the narrow band-pass filter and the diffraction grating. Light from the flashtube was focused on the filter which was placed over the entrance to the spectograph, with the entrance slit removed. The light passed through the spectograph and was reflected off the grating onto the crystal holder. The phototube was placed directly behind an exit hole close to the end of the laser crystal in order to reduce the possibility of stray light being detected. With no crystal in the system, a signal strength of about 30 millivolts was obtained. Surprisingly, though, with the crystal in, the signal increased to 68 millivolts.

The conclusion was that the crystal was itself collimating the light beam through internal reflections. To

avoid this source of error, three collimating holes were constructed. One was placed at the entrance of the light beam into the crystal, one at the exit end, and another two inches further back, directly behind which the phototube was placed. Alignment was achieved by looking through all three holes towards the red light reflected off the grating. With hole diameters 1/16 of an inch, no concern for diffraction existed, since the criterion for a geometrical image at a distance b from a hole of radius a is

$$\frac{a^2}{b\lambda} \gg 1, \qquad 3.3$$

and in our case this number was about 113.

However, the intensity was still insufficient and it was necessary to eliminate the diffraction grating and substitute a concave mirror to reflect the light to the crystal holder. The concave mirror had to be placed far enough from the collimator to defocus the light beam so that the light passed was almost parallel. The optics could then be easily and accurately aligned by passing white light through the whole system and positioning the two exit holes so that the image from the entrance hole just filled each of the other two collimating holes. All diameters of the collimating holes were 1/16 of an inch. Replacing the filter over the entrance to the spectograph, the flashtube was triggered at 3.5 kilovolts for succeeding measurements and the results are pictured in figure 3.33.

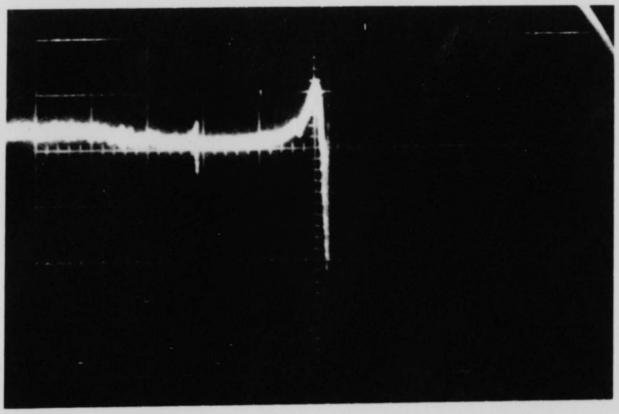

.01v/cm

12 millivolts

FIGURE 3.33a

NOISE

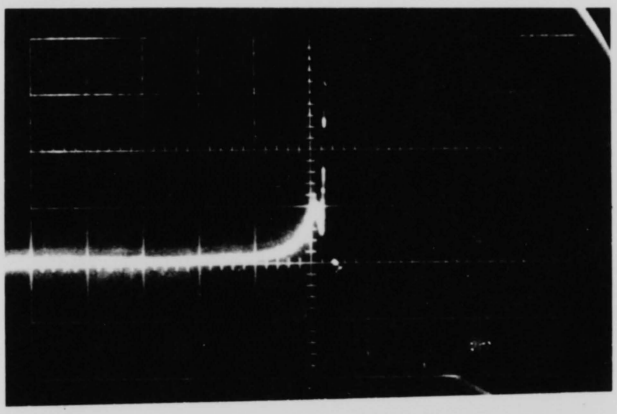

.05v/cm

55 millivolts

FIGURE 3.33b

CRYSTAL IN THE SYSTEM

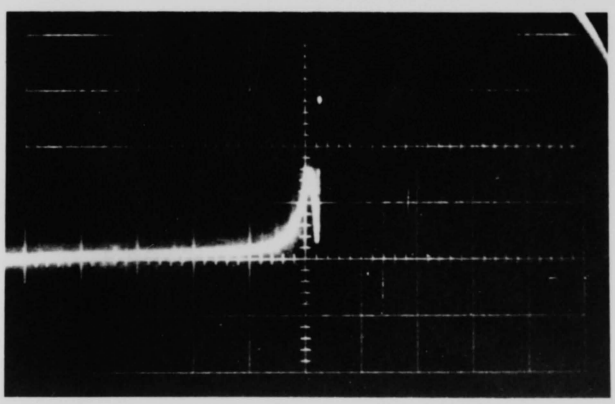

.05v/cm

80 millivolts

FIGURE 3.33c

CRYSTAL OUT OF THE SYSTEM
THE TRACES FROM WHICH SCATTER MAY BE MEASURED

Trace "a" of figure 3.33 shows the noise signal obtained by taping the first exit hole with black tape, and the signal strength was measured to be 12 millivolts. Trace "b" is that obtained for the laser crystal in the crystal holder and trace "c" for the laser crystal out of the crystal holder. Respectively the signal strengths were 55 millivolts and 80 millivolts. Subtracting the background signal of 12 millivolts, the total loss was found to be 25/68 or 37% so that the loss due to scatter was found to be 22%.

This result is in reasonable agreement with Kaiser and Keck (KK1), who quote a 17% extinction loss for ruby, and with Aagard (A1), who measured a scatter loss of 15% for his ruby laser crystal.

3.11 A Measurement of the Diffraction Loss:

The method of approach to this problem has been outlined in Chapter II; that is, threshold curves are drawn for different reflectivities and measurements of the slopes of the linear portion of the curves are made. The first threshold curve (see figure 3.34) was derived from reflectivities of R_1=99.3% and R_2=99.2% or r_1=0.993. Regarding the plot one can see clearly the deviations from a straight line over most of the temperature range are small. The departure from linearity at low and high temperatures is predicted by D'Haenens and Asawa (DA1). Resilvering the transmission end, a reflectivity R_2 of 80.4% was achieved by evaporating 17.6 milligrams

of silver, giving r_2 as 0.893. The threshold curve under these conditions is plotted in figure 3.35.

The measured slopes are calculated to be as follows:

$S_1 = 1.735$

$S_2 = 2.50.$

S was found to be, by Newton's Iterative Method, 0.806 and the diffraction loss per pass is hence 19.4%. This value is lower than that of Aagard (A1) who found a diffraction loss of 25%.

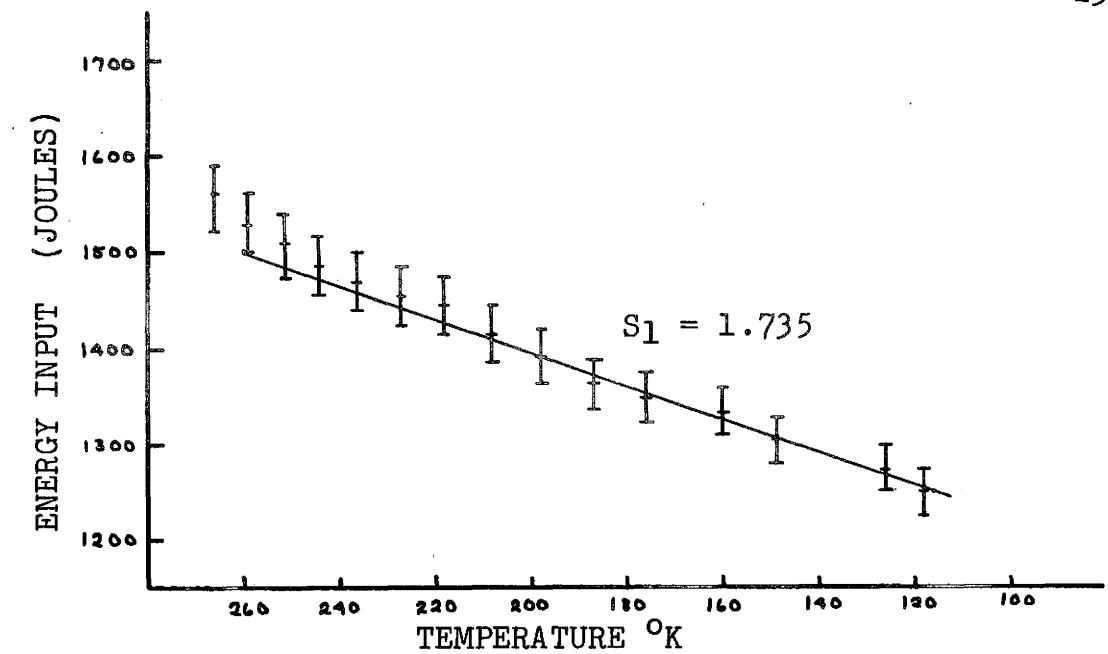

FIGURE 3.34

THRESHOLD CURVE TO DETERMINE THE DIFFRACTION LOSS
R_1 = 99.3%, R_2 = 99.2%, r_1 = 0.993

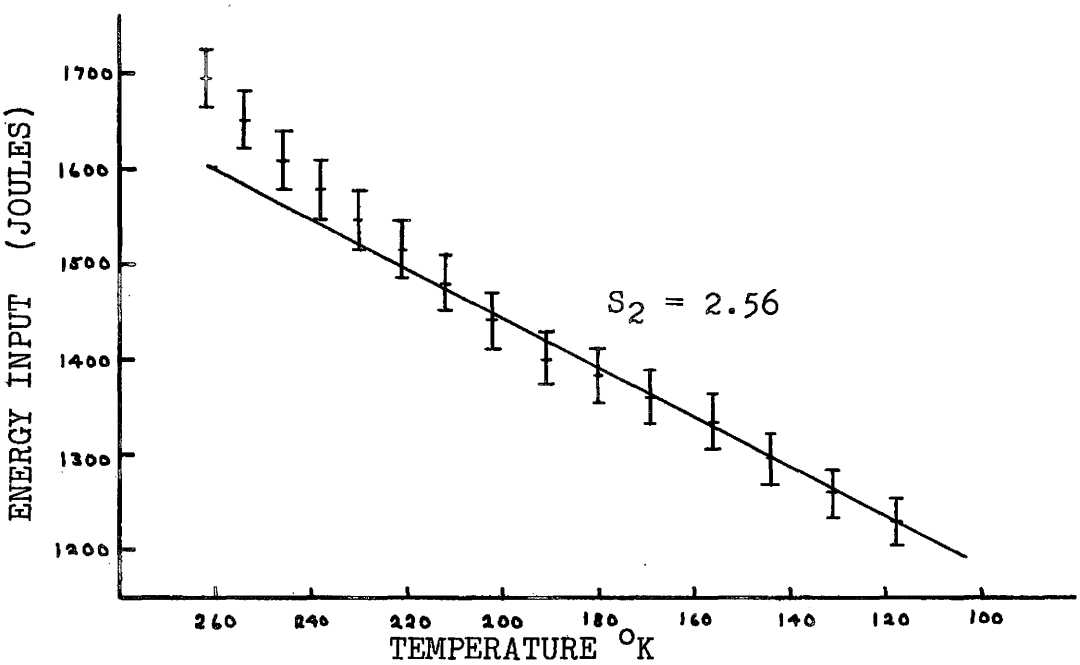

FIGURE 3.35

THRESHOLD CURVE TO DETERMINE THE DIFFRACTION LOSS
R_1 = 99.3%, R_2 = 80.4%, r_2 = 0.893

CHAPTER IV

CONCLUSIONS AND RECOMMENDATIONS

4.1 The Effect of Scatter and Diffraction on the Period Determination of Our Ruby Laser:

In the theory of period determination, we have followed through the assumption that optical maser oscillations are governed by the same equations as microwave masers. (See equations 1.53, 1.54 and 1.55.) That is, we have assumed that the oscillations are produced by the competing processes of the pump and stimulated emission.

Evidence that the theory and the equations proposed were valid as applied to a four-level optical maser, was first published by Bostick and O'Connor (BO1). As an example for $CaF_2:U^{3+}$, they predicted a modulation period of 7.2 microseconds and observed a period of 8.3 microseconds. However, as one would expect, the application of the equations as used by Bostick and O'Connor to ruby proved in error. As pointed out in Section 3.8, the first test was that of checking equation 1.77,

$$\frac{P}{P_o}\left[1-\exp\left(\frac{-t}{\tau}\right)\right]=1 \qquad 1.77$$

where t, it will be recalled, is the initial time of laser action. As an example (figure 3.29), t is 0.313 milliseconds. In order to calculate the relaxation time τ, a linear

relation, as a function of temperature (T), is assumed between the two values given by Maiman (M3) as

$T=300^{o}K$ $\qquad\qquad$ $\tau=3.0$ milliseconds

and $\qquad$ $T=78^{o}K$ $\qquad\qquad$ $\tau=4.3$ milliseconds.

Therefore

$$\tau = \frac{816-T}{172} \text{ milliseconds.} \qquad 4.1$$

In this case, the temperature was $187^{o}K$ so that τ was calculated to be 3.66 milliseconds. P/P_o was 1.12 and the left hand side of equation 1.77 took the value .092. This result was typical of many, giving an indication of how erroneous the application of a four-level theory to a three-level laser can be. We shall later calculate the period predicted by this theory as applied to our ruby laser.

The theory most accurately describing the three-level ruby laser is that proposed by Birnbaum et al. (BSW1). Here the dynamic equations are linearized and solved for the modulation period T_M. We have, as shown in section 2.7, revamped their treatment, and from equations 2.68, 2.67, 1.47 and 1.101, we can predict the oscillation period for pump powers close to the threshold condition.

As an example, consider figure 4.1. Here $r=\sqrt{.993x.862}=0.925$, so that using equation 2.86, $n_s/n_o=0.037$. Using equation 4.1, for $T=249^{o}K$, $\tau=3.30$ milliseconds; β is 1.24×10^{8} sec^{-1} using equation 1.47, and finally T_M is found to be 20 microseconds.

The period observed is seen to be ~ 5 microseconds.

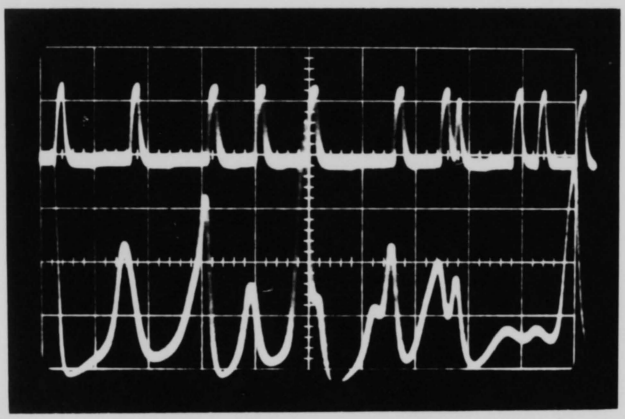

249°K 3.40 Kv

.1ms/cm 3.37 Kv

5 s/cm .1v/cm 2%

FIGURE 4.1

THE EXPERIMENTAL PERIOD FOR OUR RUBY LASER 2% ABOVE THRESHOLD, r = 0.925

Often, a longer period was observed between the first few spikes than for succeeding spikes, which assumed a regular period until multi-moding began. The period, as a result, was taken to be that measured once the spiking period became regular, the irregularity of the first few spikes being considered as a transient phenomenon.

The problem now is one which seems to be common both to microwave and optical masers: that of accounting for a period much less than is predicted theoretically. (See, as examples, sections 1.9 and 1.10.) In the microwave case, Statz and deMars (Sd1) resolved the problem by recourse to the mechanism of cross-relaxation. (See section 1.9). In the optical case, Statz et al. (SLSC1) reasoned that the presence of "extra spikes", arising from outer filaments, circumvented the difficulty. As pointed out in section 2.3, we find that alternatives are not ruled out by their observations and, in turn, we propose the following: the transmission loss mechanism is augmented by scatter loss and diffraction loss.

From Chapter III scatter loss for the ruby crystal under investigation was measured to be 22% per pass or $S=0.043\ cm^{-1}$. Diffraction loss was measured to be 19.4% per pass or $\zeta=0.806$. (These values are to be compared with those of Aagard: a scatter loss of 15% and a diffraction loss of 25% per pass for his ruby crystal.) Applying the parameters of figure 4.1 to the theory summarized in section

2.10, we obtain the following results:

Case 1: for r = 0.925, S = 0, $\mathfrak{F}$ = 1,

T_M = 13.7 microseconds.

Case 2: for r = 0.925, S = 0.043 cm^{-1}, $\mathfrak{F}$ = 1,

T_M = 6.38 microseconds.

Case 3: for r = 0.925, S = 0.043 cm^{-1}, $\mathfrak{F}$ = 0.806,

T_M = 5.2 microseconds.

Hence, with the measured values of scatter loss and diffraction loss for our crystal and the inclusion of these losses in the theory, the predicted value of 5.2 microseconds is seen to compare very well with the experimental period of ~5 microseconds.

As applied to the theory of Bostick and O'Connor, these values of parameters were used by us to predict a period of 62 microseconds, using equation 1.76 and substituting β_T for β.

Recall the oscillation threshold curves, after D'Haenens and Asawa (DA1) (figure 3.22). It was noted throughout Chapter III that the oscillation threshold curves resembled those for high f values. We now see that f, as given (equation 3.2), must be revamped to include these additional loss terms such that

$$f = \frac{\ln 1/\mathfrak{F}r + Sl}{\alpha_0 l} \qquad 4.2$$

Now f takes on a value in the order of 0.25 rather than 0.04 for a mean reflectivity r=0.925. The threshold curves obtained in Chapter III are now characterized by those predicted by D'Haenens and Asawa for high f values and the apparent paradox mentioned in section 3.8 is resolved.

It should be noted that close to oscillation threshold, where our theory applies, the modulation period varies rapidly with power, as seen in figure 3.25. The errors in the power setting are rather large so that reproducibility of results is very difficult. Such attempts resulted in observed periods varying from 6 to 3.5 microseconds. The average of about 5 microseconds was, therefore, felt to be the experimental period for a pumping power 2% above threshold. The theoretical period, on the other hand, is almost unaffected by changes in power. (For our system this value was 5.31 microseconds at threshold.) Experimentally, the period was found to be about 9 microseconds, but rapidly decreased to about 6 microseconds for powers 1% above threshold.

Secondly, the period predicted by our theory is rather insensitive to temperature variations. Again the errors in power settings are large enough that no quantitative evaluation can be made regarding the variation of period with temperature. (See figure 3.32.)

In conclusion, it is worthy of note that no other

existing theory predicts such close agreement with the oscillation period obtained from our crystal. Birnbaum et al. predicted a modulation period of 10 microseconds, to be compared with an observed period of 13 microseconds and they considered this agreement good. Secondly, we would like to point out that our theory indicates that the results of Birnbaum et al. were obtained from a relatively scatter-free, diffraction-free crystal, as is confirmed by their rather long observed oscillation period of 13 microseconds at 1% above threshold (CV1).

4.2 Recommendations:

Two suggestions as to further research present themselves, one of which is the further investigation of the period of oscillation (section 2.3). A study of the mode structure in each filament would yield decisive information as to the mechanism by which the same oscillation pattern is observed from different filaments. We feel confident that such an analysis will demonstrate modes derived from outer filaments will contribute to spikes observed from inner filaments, lending support to our postulate of scatter as the cause for the same time-resolved spiking structure of the light output being observed from different portions of the laser end-face. Such information would also shed more light on the relation of the spiking pattern to the mode structure.

A further realm of research is suggested by this thesis, that of investigating the period variation as a function of temperature and power. For this purpose, one would require a flash-tube voltage supply with a small drift and a voltage measuring device accurate to about one part in eight hundred. Such accurate investigations could lead to a further refinement in the theory to predict the period variation as a function of temperature and power, a factor not, as yet, investigated quantitatively on a theoretical basis.

REFERENCES

A1 R. L. Aagard, "Losses in a Pulsed Ruby Laser", J. Opt. Soc. Am., 53 (Aug '63) pp 911.

AT1 I. P. Abella and C. H. Townes, "Mode Characteristics and Coherence in Optical Ruby Masers", Nature 192 (Oct-Dec '61) pp 957.

B1 N. G. Basov, O. N. Krokhin and Yu. M. Popov, "Generation, Amplification, and Detection of Infrared and Optical Radiation by Quantum-Mechanical Systems, Soviet Physics Uspekhi 3 (Mar-Apr '61) pp 702.

BO1 H. A. Bostick and J. R. O'Connor, "Infrared Oscillations from $CaF_2:U^{3+}$ and $BaF_2:U^{3+}$ Masers", Proc. IRE 50 (Feb '62) pp 219 (Correspondence).

BSPA1 N. Bloembergen, S. Shapiro, P. S. Pershan and J. O. Artman, "Cross-Relaxation in Spin Systems", Phys. Rev. 114 (Apr '59) pp 445.

BSW1 M. Birnbaum, T. Stocker and S. J. Welles, "Pulsed Oscillations in Ruby Lasers", Proc. IEEE 51 (May '63) pp 854 (Correspondence).

CN1 R. J. Collins and D. F. Nelson, "The Pulsed Ruby Optical Maser", Proc. Conference on Optical Instruments, 1961, Chapman and Hall Ltd., London, 1962, pp 441.

CV1 C. K. Campbell and J. P. Van Nest, "The Effects of Scatter and Diffraction on the Spiking Period of a Ruby Laser", Proc. IEEE 52 (Feb '64) pp 210 (Correspondence).

D1 R. Dunsmuir, "Theory of Relaxation Oscillations in Optical Masers", J. Electr. and Control, 10 (Jun '61) pp 453.

DA1 I. J. D'Haenens and C. K. Asawa, "Stimulated and Fluorescent Optical Emission in Ruby from 4.2° to $300^{\circ}K$: Zero-Field Splitting and Mode Structure", J. Applied Physics 33 (Nov '62) pp 3201.

REFERENCES (CONTINUED)

EN1 V. Evtuhov and J. K. Neeland, "Observations Relating to the Transverse and Longitudinal Modes of a Ruber Laser", App. Opt. 1 (Jul '62) pp 517.

GLSC1 M. D. Galanin, A. M. Leontovich, Z. A. Sviridenkov, Z. A. Chizhikova, "Pulsations in the Emission from a Ruby Laser", Optics and Spect. 14 (Jan '63) pp 86.

H1 O. S. Heavens, "Optical Masers", Supplement on Optical Masers, App. Opt. 1962, pp 4.

H2 L. Holland, Vacuum Deposition of Thin Films, John Wiley and Sons Inc., New York; 1961.

JW2 F. A. Jenkins and H. E. White, Fundamentals of Optics, McGraw-Hill Book Co. Inc., Toronto; 1957.

KGW1 W. Kaiser, C. G. B. Garrett and D. L. Wood, "Fluorescence and Optical Maser Effects in $CaF_2:Sm^{2+}$", Phys. Rev. 123 (Aug '61) pp 766.

KK1 W. Kaiser and M. K. Keck, "Scattering Losses in Optical Maser Crystals", J. App. Phys. 33 (Feb '62) pp 762 (Correspondence).

KW1 H. Kuhn and B. A. Wilson, "Reflectivity of Thin Silver Films and Use in Interferometry", Proc. Phy. Soc. Section B 63 (1950) pp 750.

KZ1 J. I. Kaplan and R. Zier, "Model for Transient Oscillations in a Three-Level Optical Maser", J. App. Phys 33 (Jul '62) pp 2372.

L1 W. Low, "Optical Spectra of Paramagnetic Solids", Advances in Quantum Electronics, Columbia University Press, New York; 1961.

L2 R. V. Langmuir, Electromagnetic Fields and Waves, McGraw-Hill Book Company, Inc., Toronto; 1961.

M1 T. H. Maiman, "Optical and Microwave - Optical Experiments in Ruby", Phys. Rev. Letters, 4 (1960) pp 564.

M2 T. H. Maiman, "Stimulated Optical Emission in Fluorescent Solids. I. Theoretical Considerations", Phys. Rev. 123 (Aug '61) pp 1145.

REFERENCES (CONTINUED)

M3 T. H. Maiman, R. H. Hoskins, I. J. D'Haenens, C. K. Asawa and V. Evtuhov, "Stimulated Optical Emission in Fluorescent Solids. II. Spectroscopy and Stimulated Emission in Ruby", Phys. Rev. 123 (Aug '61) pp 1151.

McM1 B. J. McMurtry, "Investigation of Ruby Optical Maser Characteristics Using Microwave Phototubes", App. Opt. 2 (Aug '63) pp 767.

MZ1 A. C. G. Mitchell and M. W. Zemansky, Resonance Radiation and Excited Atoms, University Press, Cambridge; 1961.

PC1 J. L. Powell and B. Craseman, Quantum Mechanics, Addison-Wesley Publishing Company, Inc., London; 1961.

R1 J. F. Ready, "Correlation of Output Spikes from Different Portions of a Ruby Laser", App. Opt. 2 (Feb '63) pp 151 (Correspondence).

RH1 J. F. Ready and D. L. Hardwick, "Effect of Mirror Alignment in Laser Operation", Proc. IRE 50 (Dec '62) pp 2483 (Correspondence).

S1 H. Schwartz, "Relation of Rate and Duration of Evaporation to Background Pressure for the Deposition of Thin Films in Vacuum", J. App. Phys. 34 (Jul '63) pp 2053.

S2 J. Strong, H. V. Neher, A. E. Whitford, C. H. Cartwright and R. Hayward, Procedures in Experimental Physics, Prentice-Hall, Inc., New York; 1938.

Sd1 H. Statz and G. deMars, "Transients and Oscillation Pulses in Masers", Quantum Electronics, Columbia University Press, New York, 1960; pp 530.

SLSC1 H. Statz, C. Luck, C. Shafer and M. Ciftan, "Observations on Oscillation Spikes in Multimode Lasers", Advances in Quantum Electronics, Columbia University Press, New York, 1961; pp 342.

SS1 R. S. Sennet and G. D. Scott, "The Structure of Evaporated Metal Films and Their Optical Properties", J. Opt. Soc. Am 40 (1950) pp 203.

REFERENCES (CONTINUED)

STl A. L. Schawlow and C. H. Townes, "Infrared and Optical Masers", Phys. Rev. 112 (1958) pp 1940.

Tl G. Troup, Masers, John Wiley and Sons Inc., New York; 1959.

TSdl C. L. Tang, H. Statz and G. deMars, "Spectral Output and Spiking Behaviour of Solid State Lasers", J. App. Phys. 34 (Aug '63) pp 2289.

Vl A. A. Vuylsteke, Elements of Maser Theory, D. Van Nostrand Company, Inc., Princeton, New Jersey; 1960.